THE EFFECT OF INJECTION MOLDING CONDITIONS ON THE NEAR-SURFACE RUBBER MORPHOLOGY, SURFACE CHEMISTRY, AND ADHESION PERFORMANCE OF SEMI-CRYSTALLINE AND AMORPHOUS POLYMERS

by

Shannon Christine Weakley-Bollin

A dissertation submitted in partial fulfillment
of the requirements for the degree of
Doctor of Philosophy
(Materials Science and Engineering)
in the University of Michigan
2010

Doctoral Committee:

Professor J. Wayne Jones, Co-Chair
Professor David C. Martin, Co-Chair
Professor Ronald G. Larson
Deborah F. Mielewski, Ford Motor Company

"Anyone who stops learning is old, whether at twenty or eighty.
Anyone who keeps learning stays young.
The greatest thing in life is to keep your mind young."

Henry Ford

Acknowledgments

I'd like to thank all of the people in the Materials and Processes department at Ford Motor Company's Research and Innovation Lab for their help and support, especially: Debbie Mielewski for volunteering to be on my committee and guiding me the entire way of my thesis; Patti Tibbenham for teaching me from her vast knowledge of polymer processing and helping me with just about every part of this thesis including designing and running the DOE in Chapter 4; Matt Zaluzec and James Boileau, my manager and supervisor who supported my pursuit of this degree; Ann Straccia and Larry Haack for teaching me how to use the XPS and helping me interpret the data; Mark Nichols for some helpful (and not so helpful) discussions about polymers and graduate school in general; Kevin Ellwood for insight in to the foreign world of modeling for this experimentalist; Tony Godlewski for conducting the impact testing in Chapter 2.

I'd also like to thank Professor Dave Martin for taking on a student who had a full-time job and being supportive and acknowledging of that fact. Thanks are also due to members of Dave's research group at UM, including Jihua Chen for his TEM imaging in Chapter 3 and Brenda Vyletel and Jinghang Wu for their work on the adhesion testing done for Chapters 3 and 4.

Thank you to Ford Motor Company and the Detroit Chapter of the Society of Plastic Engineers, since without their financial support this degree would not be possible.

Finally I'd like to thank my family, including: my husband, Rob, for all of his love and support along the way; my Dad for all of his help with my homework and my Mom for appreciating my thesis title – not to mention all of their help supporting me financially throughout my schooling; my sister-in-law Tracy for thesis commiseration and my brother Ryan for his motivation by never failing to ask "aren't you done with that yet?". And finally, Charlie - his "wiggle-butt" greetings never failed to brighten even the longest day of writing.

Table of Contents

List of Figures

List of Tables

Chapter 1

Introduction

Rapidly climbing gasoline prices in 2008 led many customers to reconsider their automotive purchases and driving behavior (Effects of Gasoline Prices on Driving Behavior and Vehicle Markets, 2008). A historical look at the price of gasoline ("Retail Gasoline Historical Prices," 2009) compared to purchases of cars and trucks ("U.S. Sales, 1980 - 2008," 2009) in the U.S. shows that rising fuel prices, starting in 2005, changed a long standing trend of customers preferring trucks (including sport utility and cross-over vehicles) over cars at a rate of 1.5% since 1990 (Figure 1-1). Surveys in early 2008 found that fuel economy had become the number one factor to shoppers considering a new car, even above make and model, safety features, performance, seating capacity and technology features ("AAA Survey Measures Effect Of High Gas Prices On Members," 2008). These changing preferences resulted in a nearly 10% increase in the number of cars purchased between 2007 and 2008.

Despite current lower gas prices compared to 2008, fuel economy is still a major issue for the automotive industry. In March 2009, the Corporate Average Fuel Economy (CAFE) standards were raised for the first time in 25 years, requiring a fleet-wide average of 27.3 miles per gallon (mpg), 8% percent above the 2010 model year requirement of 25.3 mpg. The new standards break out to passenger cars averaging 30.2 mpg and light trucks averaging 24.1 mpg. This is just a step toward the goal of a fleet-wide average of 35.5 mpg that was moved ahead to 2016 from 2020 in May 2009 (Power, 2009; Shepardson, 2009).

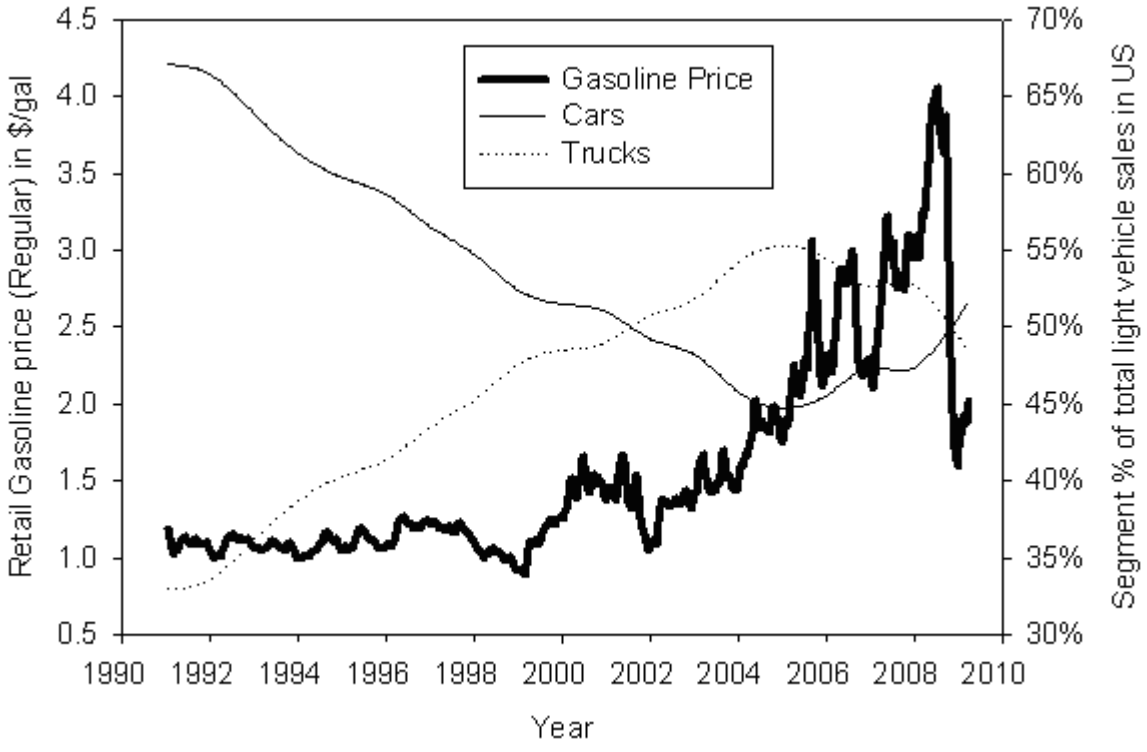

Figure 1-1: Comparison of gasoline prices and customer vehicle purchases

In addition to changing CAFE regulations, in April 2009 the Environmental Protection Agency (EPA) declared Carbon Dioxide (CO_2) a threat to public health and welfare ("EPA Finds Greenhouse Gases Pose Threat to Public Health, Welfare / Proposed Finding Comes in Response to 2007 Supreme Court Ruling " 2009). This ruling could lead to new standards in the United States governing CO_2 emissions under the Clean Air Act, and are a step closer to committing to the Kyoto climate treaty followed by the European Union. Since transportation makes up 28% of the CO_2 emissions in the U.S. (Figure 1-2), the automotive industry would likely be a target for any type of CO_2 legislation/regulation (Weisman, 2009). One possible result could be the nationwide adaptation of California's legislation to reduce tailpipe emissions 18% by 2020 ("Frequently Asked Questions - Climate Change Emissions Standards for Vehicles," 2007).

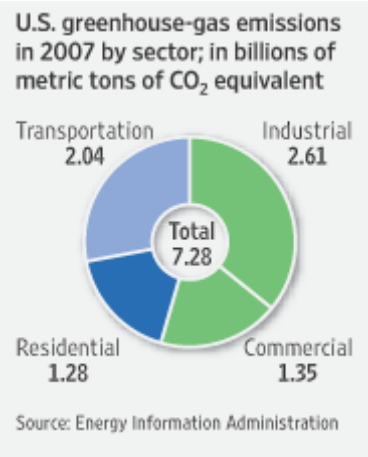

Figure 1-2: Sources of CO_2 emissions in United States (Weisman, 2009)

While there are numerous pathways to improved fuel economy and reduced CO_2 emissions, vehicle lightweighting will always be a factor. It is estimated that 75% of a vehicle's gas (energy) consumption is directly related to factors associated with its weight ("Lightweight Materials Program," 2010). Studies have found that a 10% reduction in weight will result in 5-8% greater fuel efficiency (Brooke, 2009). A rule of thumb used in the automotive industry is that removing 150 lbs (68 kg) of vehicle weight will improve fuel economy by 1 mpg. Carbon emissions are also affected by vehicle weight; removing 220 lbs (100 kg) from the vehicle will result in a 20 g/mile reduction in CO_2 (Brooke, 2009).

Plastics are often considered for lightweighting opportunities because of their low density compared to traditional steels and aluminums (Table 1-1). However, these lightweighting technologies typically don't come without a cost. For example, propene (C_3H_6), the monomer from which polypropylene is made, is made from distilling or cracking fossil fuels, so the price of polypropylene resin tracks very closely with the price of gasoline (Figure 1-3) (Monthly Petrochemical and Plastics Analysis, April 2009). With rapidly fluctuating global economies, fuel, and commodity pricing, it is difficult to predict how much a customer would

be willing to pay for improved fuel economy. The cost of lightweighting must be balanced with the cost of penalties for not meeting current or new governmental fuel economy standards. But even if there are future advances in energy technology moving us away from the gasoline powered internal combustion engine, plastics will continue to be an important, and increasing, part of automotive manufacturing.

Table 1-1: Average density of common automotive materials

Material	Average Density (g/cm^3)
Polypropylene	0.85
ABS	1.05
PC/ABS	1.15
Carbon Fiber Reinforced Composites	1.58
Aluminum	2.7
Steel	7.9

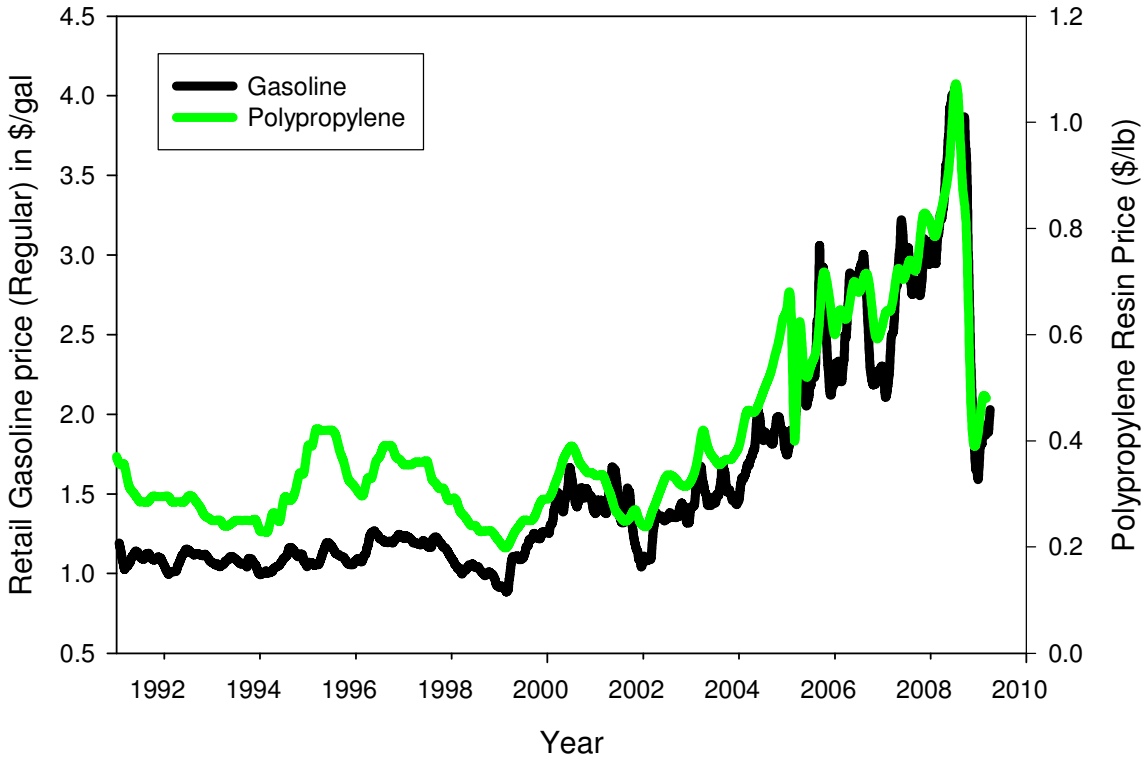

Figure 1-3: Price of gasoline (retail) compared to the price of new polypropylene resin

1.1 Materials

The amount of plastic in vehicles has increased over the past several decades (Figure 1-4) and is used throughout the vehicle in applications such as exterior and interior panels and trim, bumper fascia, window encapsulation, headlamp housings, manifolds and valve covers, electronic/electric parts and components, wiring harnesses, steering wheels, insulation, dampening and deadeners, upholstery, mechanical parts and components, and safety glass (Smith, 2008).

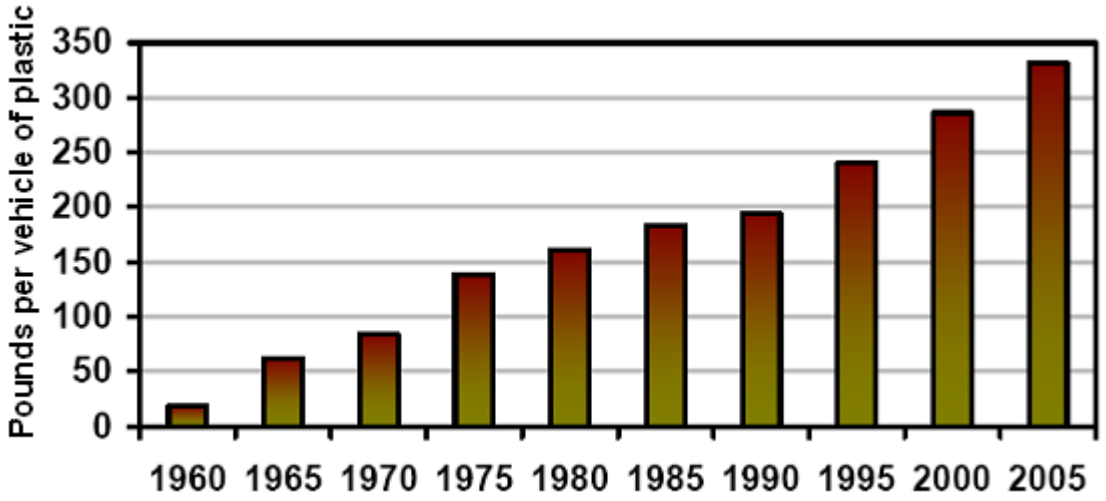

Figure 1-4: Average vehicle composition by weight of plastic materials (Smith, 2008)

PolyPropylene (PP) and ThermoPlastic Olefins (TPO, a polypropylene matrix with rubber modifiers and other fillers) are one type of polymer studied in this work. These materials are attractive due to their low cost, good impact resistance even at low temperatures, light weight and recyclablity. These materials make up almost a quarter of the total weight of polymers used in automotive applications (Figure 1-5). Their use in the automotive industry is predicted to continue rising to a projected value of 82.4 pounds (37 kg) in 2013 (Automotive Plastics Report, 2003). PP and TPO are commonly used for interior trim applications and exterior bumper fascia, and are frequently painted.

Acrylonitrile-Butadiene-Styrene (ABS), and its blend with PolyCarbonate (PC/ABS), are also major contributors to automotive applications. While the amount of ABS used in interior trim applications is shrinking (and being taken up by polypropylene and TPO), the use of ABS and PC/ABS in structural applications and exterior trim is increasing. PC/ABS is especially attractive for substitution with metal components in structural applications due to its good impact toughness and relatively high thermal stability. The use of PC/ABS is

projected to increase 26% from 2003 to 2013 (Automotive Plastics Report, 2003). These parts can either be painted or metalized.

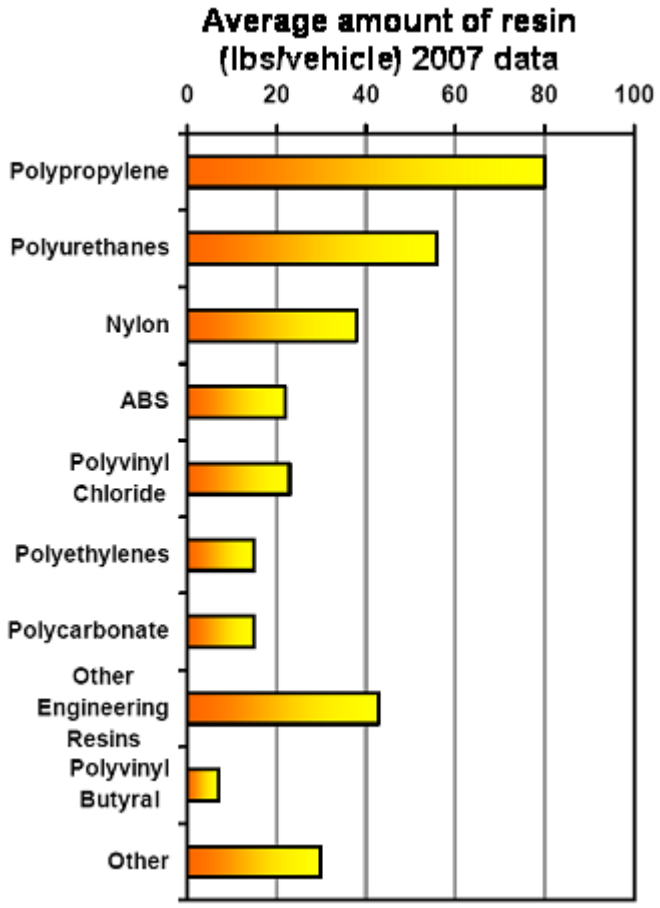

Figure 1-5: Average amounts of plastic in 2007 vehicles by resin type (Smith, 2008)

1.2 Processing

In the plastics industry, injection molding makes up approximately 32 wt % of all plastic processing methods, second only to extrusion (36% wt) (Rosato, 2000). Injection molding is a cost-effective way to produce complex, three dimensional shapes at high volumes (Kennedy, 1995; Pasquini, 2005). However, due to the high costs associated with the mold and machine operation, injection molding is only economically practical for large volumes of parts.

1.3 Injection Molding Equipment

There are three basic components to any injection molding machine: the injection unit, the mold, and the clamping system (Figure 1-6). The injection unit, also called the plasticator, melts the plastic and injects it into the mold. The clamping system closes and opens the mold and ejects the finished part.

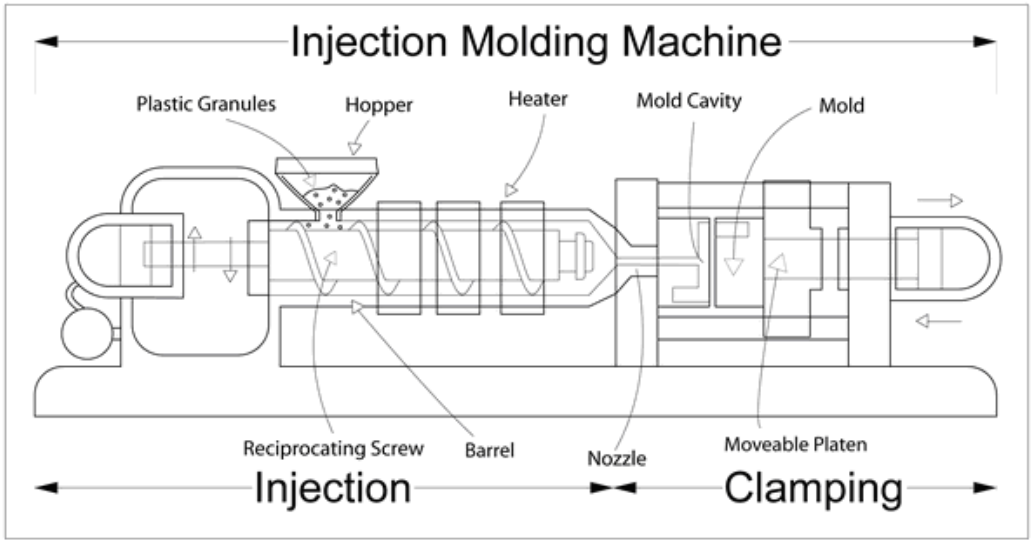

Figure 1-6: Diagram of injection molding machine (Rockey, 2009)

1.3.A Injection Unit

The most common type of injection unit is a reciprocating screw (Figure 1-7). It consists of a hopper, feed throat, barrel, screw, screw drive motor, and nozzle. Plastic pellets are fed from the hopper onto the screw and melted by the shear of the rotating screw and by conduction through the heated barrel. The melt temperature is controlled by as many as 5 different stages that can be programmed along the barrel. During injection, the screw is driven forward by a hydraulic piston or electric motor forcing the melted polymer through the nozzle into the mold. The shot size is determined by the travel length of the screw.

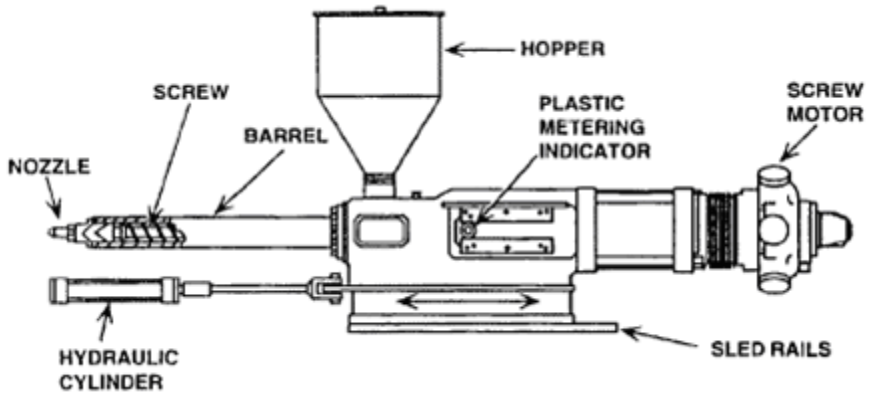

Figure 1-7: Diagram of a reciprocating screw injection unit (Harper, 2000)

1.3.B Mold

Injection molds are designed to give final desired shape to the part(s). They must be designed to adequately distribute the melt, cool the part(s) evenly with water lines if needed, and be able to withstand the forces of closing, melt injection and part ejection. Typically, molds consist of two halves: the stationary "A" or cavity side and the movable "B" or core side. The division between these halves is called the parting line. Depending on the part, these molds can be simple or complex with many moving parts.

Injection molds for high volume applications are typically made of tool steel, which can be hardened or plated with chromium or nickel if needed. Cast aluminum can be used for low volume (<1000 shots) or prototype molds, but due to its porosity and low hardness, it is not applicable for typical injection molding applications. Recently, forged aluminum alloys, originally developed for the aerospace industry, have been attracting attention for high volume injection molding tools (Bank, 2008). Forging eliminates the porosity and hardness concerns associated with cast aluminum, extending the tool life considerably. Since aluminum offers 4-5 times the thermal conductivity of typical tool steel (~150 vs. ~30 W/m•K), cycle time can be reduced by as much as 20%, saving processing costs. Aluminum tools are also quicker to machine, saving tooling

costs, and require less energy to move because of their lighter weight. The effect of aluminum's rapid cooling on the morphology and mechanical properties of polymers is not yet understood, but will be investigated here for the first time.

1.3.C Clamping Unit

The clamping unit closes the mold and holds it closed during injection, and then opens it and ejects the part (Figure 1-8). The primary specification for a clamping unit is the maximum clamp force, or the force needed to keep the mold closed during injection and packing. If the clamp force is not greater than the injection and packing forces, the mold can be forced open during injection or packing. This results in leakage of the molten polymer or "flash".

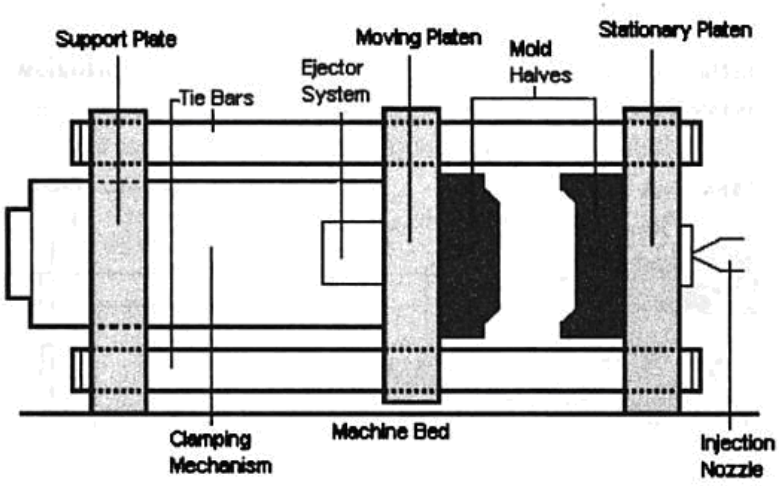

Figure 1-8: Diagram of clamping unit with ejection system (Olmsted, 2001)

1.4 Injection Molding Process

An injection molding cycle starts with the mold closing in preparation for the first step, which is the filling stage. The screw forces molten plastic through the nozzle and into mold. Important processing parameters in the filling stage are:

melt temperature (controlled by the barrel), the injection pressure (which determines the fill time), and the shot size.

After the mold is filled, the pack and hold stage begins. Here, additional material flows into the mold to compensate for shrinkage of the cooling melt and apply pressure to the melt until the mold gates solidify. During packing and holding, movement of the plastic melt is determined by melt viscosity, which is determined by the material properties. Important processing parameters in the pack and hold phase are: packing pressure, clamping pressure and hold time.

Once pack and hold is completed, the cooling stage is entered. The plastic in the mold is cooled until the part can be ejected. Important processing parameters in the cooling stage are: cooling time and mold temperature. During the cooling stage, the screw rotates and melt is built up for the next molding cycle.

1.5 Effect of processing on performance

Injection molding processing parameters such as melt and mold temperatures, mold geometry, injection speed, filling, packing and cooling hold times and pressures all affect the resulting microstructure of the polymer, which changes throughout the part. The quality of the surface finish, dimensional stability and mechanical properties are all determined by the microstructure (Kennedy, 1995), which can vary by orders of magnitude depending on processing conditions (Katti, 1982). General recommendations based on trial and error experience have been summarized for troubleshooting (Table 1-2).

Table 1-2: Effect of injection molding parameters on finished product quality (adapted from DuPont, 2010)

Poor surface finish	Increase shot size
	Increase injection pressure and/or speed
	Increase melt temperature
	Increase mold temperature
	Increase cycle time
Flash	Decrease melt temperature
	Decrease injection pressure
	Decrease cycle time
	Improve mold venting
	Increase clamp pressure
Weld Lines	Increase injection pressure
	Increase packing time and pressure
	Increase melt temperature
	Increase mold temperature
Sinks or Voids	Increase injection pressure
	Increase packing time and pressure
	Increase melt temperature (sinks)
	Decrease mold temperature (voids)
Warping	Increase mold temperature
	Increase injection pressure and/or speed
	Increase packing time and pressure

Despite advances in understanding of fluid dynamics and computer aided simulations, the complexity of the process and variation in material properties

even within the same polymer class prevents a detailed, qualitative understanding and modeling of the morphology and properties of these polymers as a function of structure and processing. A diagram illustrating some of the variables involved and the relationships between structure, processing, morphology and end-use properties is shown in Figure 1-9.

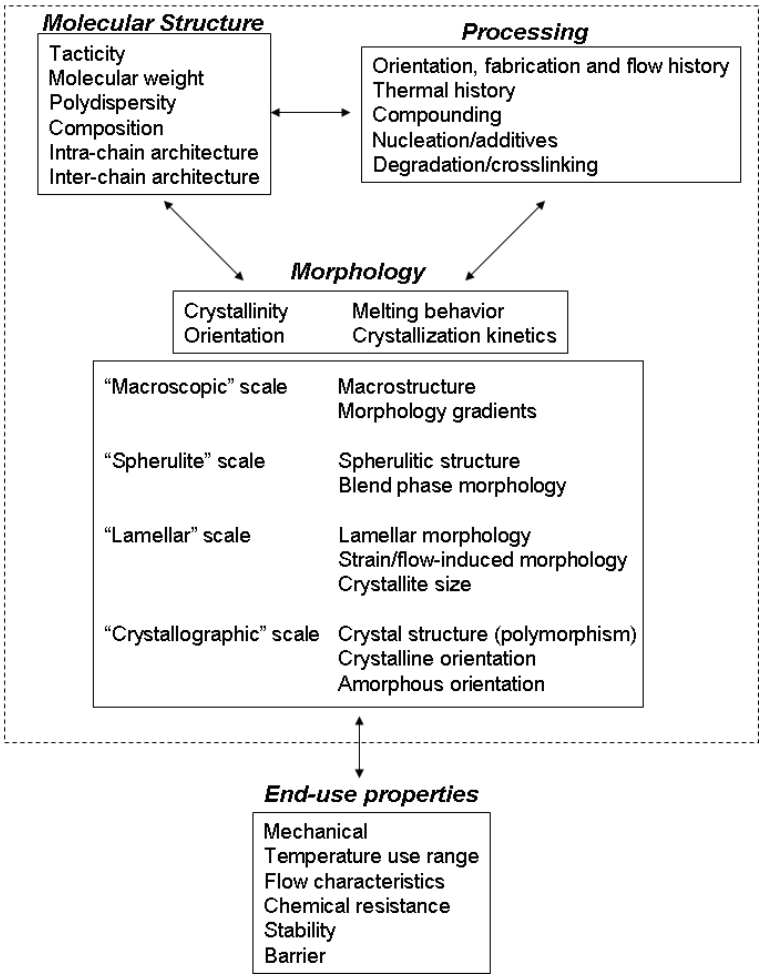

Figure 1-9: Diagram of relationships between molecular structure, processing, morphology (Pasquini, 2005)

1.6 Adhesion

Adhesion performance is particularly important in the automotive industry, considering that about 30% of the plastic used in automobiles is coated in some fashion (Ryntz, 2005). Polypropylene has a low surface energy (~30 mJ/m^2),

lacks polar functionality, and has good resistance to solvents, all of which prevent good paint adhesion (Ryntz, 2005). The addition of amorphous elastomeric rubbers (as in the case of TPO) can improve adhesion slightly, but typically surface modifications such as flame or plasma treatment, ultraviolet irradiation (Nie, 1999), or chlorinated polyolefin (CPO) adhesion promoter primers are still needed for acceptable paint adhesion performance (Morris, 1998).

The morphology of the rubbery phase in TPO at the surface has been studied by several authors. Some authors have found a thin (≤ 5 μm) layer of pure polypropylene at the surface (Ryntz, 1996; Morris, 1998; Tomasetti, 1998; Tomasetti, 1999; Tang, 2002; Tang, 2003; Ryntz, 2005), while others have found rubber nodules at the surface (Mirabella, 2000; Tomasetti, 2000). Thin (nm) layers of concentrate heat stabilizer additives (thio-esters) have been found preferentially covering the surface of an injection molded industrial polypropylene (Mielewski, 1998). These differences are all due to processing, material, and geometry differences and could have an impact on adhesion performance.

Chrome plated ABS and PC/ABS pieces are often focal points on the vehicle. Parts such as grilles, badges and emblems, wheel covers and knobs are not only highly visible, but are often in places that involve a lot of contact from the user or from road debris. That contact, plus the thermal and mechanical mismatch between the plastic substrate and the plated metal layers demonstrates the need for good adhesion on these parts.

Historically, automotive standards have relied on qualitative cross-hatch adhesion tests as a measure of adhesion (Standard Practice for Qualitative Adhesion Testing of Metallic Coatings, 2008; Standard Test Methods for

Measuring Adhesion by Tape Test, 2008). These tests have many variables, and per ASTM:

> *"…are used to establish whether the adhesion of a coating to a substrate is at a generally adequate level. They do not distinguish between higher levels of adhesion for which more sophisticated methods of measurement are required."*

Other ASTM adhesion test methods standards for coated plastics include mandrel or bend testing (Standard Practice for Qualitative Adhesion Testing of Metallic Coatings, 2008; Standard Test Methods for Mandrel Bend Test of Attached Organic Coatings, 2008), saw testing (Standard Practice for Qualitative Adhesion Testing of Metallic Coatings, 2008), peel testing (Standard Practice for Qualitative Adhesion Testing of Metallic Coatings, 2008), pull-off testing (Standard Test Method for Measuring Adhesion of Organic Coatings to Plastic Substrates by Direct Tensile Testing, 2008). Of these tests, only the pull-off test provides a quantitative measure of adhesion, but there are still variables introduced by the aluminum stub that must be adhered to the surface as the pull-off anchor point. Some authors have adapted the peel test with an Instron to obtain a quantitative number for that test, but there are still many variables (Ellis, 1967; Matsunaga, 1971; Villamizar, 1981).

The Martin group at University of Michigan developed a quantitative method to measure the adhesion of brittle coatings on ductile substrates, such as automotive paint on PP or TPO (Tang, 2001). The method involved using an Instron tensile test or a mandrel bend to generate a shear stress between the paint and polymer layers due to their different moduli (Figure 1-10). The crack spacing can then be used as a quantitative measure of adhesion strength. This test method will be described in more detail in the applicable chapters.

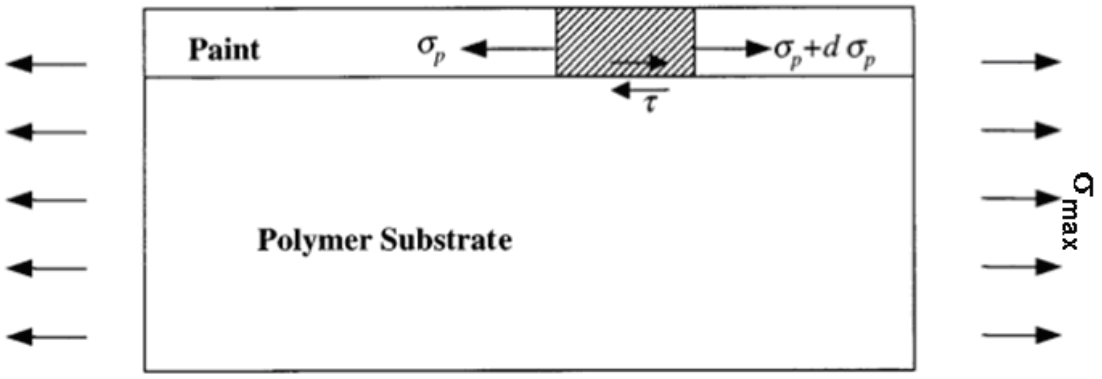

Figure 1-10: Schematic of applied tensile stress generating shear stress between the paint and polymer (Tang, 2001)

1.7 Problem Statement

Tying together processing, morphology and properties of polymers is the "Holy Grail" of manufacturing, but the enormous complexity of the interactions makes this feat incredibly challenging. However, the considerable potential cost savings and quality improvement achieved through optimization of processing conditions and mechanical properties is enough motivation to try to gain a greater understanding of these relationships.

Despite years of anecdotal evidence and the increasing use of plastics in the automotive industry, there is still an incomplete fundamental understanding of the relationship between material, processing conditions, morphology and performance. Predictive software, such as Moldflow, attempts to model some aspects of this, but treats morphology as a black box. As an example, the amount of molded in stress in an injection molded ABS automotive component was measured and found to be 14 MPa compared to the < 1 MPa predicted by current modeling software. A better understanding of the effect of material formulations, processing and geometry on morphology will help the industry

design parts and optimize processing conditions to achieve improved adhesion and mechanical performance.

While the existing literature pertaining to the subject of polymer morphology is extensive, it is not complete. In fact, in the numerous references reviewed for this work, the processing conditions and sample location are treated as an afterthought rather than a variable, and often not even included in the report! Part geometry and flow length are often neglected factors in the literature, and in this study, were found to have a large impact on morphology.

The goal of this work was to provide more insight on the material composition-processing-morphology-performance mystery and use it to improve part design, material selection, and processing conditions, thereby saving time and money, and improving part quality. The materials (polypropylene based and ABS based) and coating systems (paint and chrome) chosen for this work were quite different, which is why the chapters were split up by material and therefore detailed literature reviews and discussions of each material will be given in the appropriate chapters rather than in this introduction. Despite these profound differences, the overarching theme that processing conditions and geometry affect surface morphology, which in turn affects adhesion performance, applies to both systems and ties this work together.

Neat isotactic polypropylene is the focus of Chapter 2. The study of neat polypropylene serves as a foundation for further studies on TPO in Chapter 3. Neat polypropylene removes many of the variables that are present in TPO (filler type/amount, rubber type/amount, other additives, etc.), and the morphology can also be more easily studied with optical microscopy.

In Chapter 2, the effect of injection speed, flow length, and heat transfer rate between the melt and the mold were studied. Usually, heat transfer rate could only be adjusted by changing the mold and melt temperatures, offering a narrow window of ΔT before negatively affecting the filling of the part. We imparted a much more drastic change in heat transfer rate by changing the mold material from typical tool steel to a new forged aluminum tool, which has a large increase in thermal conductivity (35 W/m•K for tool steel and 157 W/m•K for aluminum). Aluminum tools are attractive for the cost saving opportunity in cycle time reduction and tooling costs, but the effect on morphology of the change in heat transfer rate must be understood to assure good adhesion of coatings and mechanical performance.

Chapter 3 builds on the knowledge of polypropylene in Chapter 2 and applies it to two different, but both industrially relevant, types of TPO. In this chapter, we studied the effect of injection speed, cooling rate, and geometry on both a compounded TPO with talc, and a reactor grade TPO without talc. Atomic Force Microscopy (AFM) was used in this chapter to study the near surface morphology that was no longer detectable using optical microscopy methods. Transmission Electron Microscopy (TEM) and X-Ray Photoelectron Spectroscopy (XPS) were also used to study the effect of heat transfer rate and flow length on the surface. The effect of processing on adhesion was studied using ASTM standard methods and a quantitative test involving measurements of crack spacing in the more brittle painted layer.

Chapter 4 studied the effect of processing conditions on surface morphology and adhesion of metal-plated ABS materials. While Chapters 2 and 3 focused on plaques for an in-depth understanding of the effect of flow length, Chapter 4 looked at the effect of processing on the performance of a materials system used in real-world automotive parts. The bonding of the metal layers to the ABS is a

mechanical process rather than the predominantly chemical adhesion mechanism seen in painted TPO, but there is still a strong dependence on surface morphology that was studied using Scanning Electron Microscopy (SEM). Again, the effect of processing on adhesion was studied using a variety of different testing methods.

Chapter 5 concludes with a summary of findings and suggestions for future work.

1.8 References

"AAA Survey Measures Effect Of High Gas Prices On Members."(2008). from http://media.aaamichigan.com/article_display.cfm?article_id=2.

Automotive Plastics Report (2003). Toledo, Market Search Inc.

Bank, D., D. Klafhen, et al. (2008). "Why Plastic Flows Better in Aluminum Injection Molds." from http://www.alcoa.com/mold/en/pdf/spiral_report.pdf.

Brooke, L. and H. Evans (2009). "Lighten Up!" Automotive Engineering International (March): 16-22.

DuPont "Injection Moulding" from http://plastics.dupont.com/plastics/pdflit/europe/design/L12565_2.pdf.

Effects of Gasoline Prices on Driving Behavior and Vehicle Markets (2008). The Congress of the United States - Congressional Budget Office.

Ellis, P. A. M. (1967). "The importance of moulding conditions to the quality of electroplated ABS plastics." Trans. J. Plastics. Inst. **June**: 537-542.

"EPA Finds Greenhouse Gases Pose Threat to Public Health, Welfare / Proposed Finding Comes in Response to 2007 Supreme Court Ruling "(2009). from http://yosemite.epa.gov/opa/admpress.nsf/0/0EF7DF675805295D8525759B00566924.

"Frequently Asked Questions - Climate Change Emissions Standards for Vehicles."(2007). from http://www.arb.ca.gov/cc/factsheets/ccfaq.pdf.

Harper, C. A. (2000). Modern Plastics Handbook, McGraw-Hill

Katti, S. S. and M. Schultz (1982). "The microstructure of injection-molded semicrystalline polymers: A review." Polymer Engineering & Science **22**(16): 1001-1017.

Kennedy, P. (1995). Flow Analysis of Injection Molds. Cincinatti, Hanser/Gardner Publications.

"Lightweight Materials Program."(2010). 2010, from http://www.ornl.gov/sci/lightmat/Lightweight.html.

Matsunaga, M. and Y. Hagiuda (1971). "Mechanical properties of electroplated ABS plastics." Metal Finishing **69**(4): 36-40.

Mielewski, D. (1998). Weld Line Morphology of Injection Molded Polypropylene. Department of Chemical Engineering. Ann Arbor, University of Michigan. **Ph.D.:** 137.

Mirabella, F. M., N. Dioh, et al. (2000). "Theoretical analysis and experimental characterization of the TPO/adhesion promoter/paint interface of painted thermoplastic polyolefins (TPO)." Polymer Engineering & Science **40**(9): 2000-2006.

Monthly Petrochemical and Plastics Analysis (April 2009). Houston, TX. , Chemical Data (CDI).

Morris, H. R., B. Munroe, et al. (1998). "Fluorescence and Raman Chemical Imaging of Thermoplastic Olefin (TPO) Adhesion Promotion." Langmuir **14**(9): 2426-2434.

Nie, H. Y., M. J. Walzak, et al. (1999). "Atomic force microscopy study of polypropylene surfaces treated by UV and ozone exposure: modification of morphology and adhesion force." Applied Surface Science **144-145**: 627-632.

Olmsted, B. A. and M. E. Davis (2001). Practical injection molding, CRC Press.

Pasquini, N., Ed. (2005). Polypropylene Handbook. Munich, Hanser.

Power, S. and C. Conkey (2009) U.S. Orders Stricter Fuel Goals for Autos. Wall Street Journal **Volume**, DOI:

"Retail Gasoline Historical Prices."(2009). 2009, from http://www.eia.doe.gov/oil_gas/petroleum/data_publications/wrgp/mogas_history.html.

Rockey, B. (2009). Injection Molding Machine. Creative Commons Attribution 3.0 I. molding.png.

Rosato, D. V., D. V. Rosato, et al. (2000). Injection Molding Handbook, Springer - Verlag.

Ryntz, R. A. (1996). "The effects of thermoplastic poly(olefin) (TPO) morphology on subsequent paintability and thermal shock performance." Progress in Organic Coatings **27**(1-4): 241-254.

Ryntz, R. A. (2005). "Attaining Durable Painted Plastic Components." JCT Research **2**(5): 351-360.

Ryntz, R. A. (2005). Real World Performance of Painted Plastic Components, Federation of Societies for Coatings Technology, 492 Norristown Rd , Blue Bell, PA, 19422-2350, USA,.

Shepardson, D. (2009). "Average mpg to increase 8%." Detroit News Retrieved March 27, 2009 from http://www.detnews.com/article/20090327/AUTO01/903270399/Average+mpg+to+increase+8+.

Smith, T. K. (2008). Changing Customer Dynamics: Chemistry and Light Vehicles, American Chemistry Council**:** 12.

Standard Practice for Qualitative Adhesion Testing of Metallic Coatings (2008). ASTM Standard B 571, ASTM. **ASTM Standard B 571**.

Standard Test Method for Measuring Adhesion of Organic Coatings to Plastic Substrates by Direct Tensile Testing (2008). ASTM. **D5179:** 7.

Standard Test Methods for Mandrel Bend Test of Attached Organic Coatings (2008). ASTM. **D522:** 4.

Standard Test Methods for Measuring Adhesion by Tape Test (2008). ASTM Standard D3359, ASTM. **D3359:** 7.

Tang, H., B. Foran, et al. (2001). "Quantitative measurement of adhesion between polypropylene blends and paints by tensile mechanical testing." Polymer Engineering & Science **41**(3): 440-448.

Tang, H. and D. C. Martin (2002). "Microstructural studies of interfacial deformation in painted thermoplastic polyolefins (TPOs)." Journal of Materials Science **37**(22): 4783-4791.

Tang, H. and D. C. Martin (2003). "Near-surface deformation under scratches in polypropylene blends Part I Microscopic characterization of deformation." Journal of Materials Science **38**(4): 803-815.

Tomasetti, E., R. Legras, et al. (2000). "Plastic deformation in polypropylene/(ethylene-propylene) copolymer blend during paint debonding." Polymer **41**(17): 6597-6602.

Tomasetti, E., R. Legras, et al. (1998). "Quantitative approach towards the measurement of polypropylene/(ethylene-propylene) copolymer blends surface elastic properties by AFM." Nanotechnology **9**: 305-315.

Tomasetti, E., B. Nysten, et al. (1999). "Surface characterization of polypropylene/(ethylene-propylene) copolymer blends (PP/EP): application to injection-moulded systems." Surface and Interface Analysis **27**(8): 735-742.

"U.S. Sales, 1980 - 2008."(2009). from: http://subscribers.wardsauto.com/refcenter/.

Villamizar, C. A., J. Rojas, et al. (1981). "Chemical Etching Versus Plasma Etching in Electroplating ABS Resin Surfaces." Metal Finishing **79**(3): 27-33.

Weisman, J. and S. Hughes (2009). U.S. in Historic Shift on CO2. The Wall Street Journal**:** A1.

Chapter 2

Anisotropic Structure and Molded-in Stress in Injection-Molded Neat Polypropylene

2.1 Introduction

Neat isotactic polypropylene (iPP) is rarely used in automotive applications. Typically, multiple fillers and additives are used to improve low temperature impact performance (rubber) (Jang, 1984; Tanem, 2003), lower cost (talc and other mineral fillers) (Guerrica-Echevarria, 1998), or affect appearance (colorants). Each of these additions can drastically change the resulting morphology because they alter nucleation and crystallization behavior. For example, less than 1 wt% of a dye in iPP has been shown to dramatically affect the melt properties (viscosity, transition temperatures) as well as the properties of the resulting part (morphology, shrinkage) (Kennedy, 2008). In addition to talc, rubber and colorants, other additives may be included to improve processing, performance and durability such as lubricants, and heat and UV stabilizers.

While it is not frequently used in practical applications in its neat state, iPP has been more intensely studied than commercial polypropylene products and blends due to minimization of variables, formulation secrecy, and the ability to use optical microscopy to observe the resulting microstructure. Even with numerous studies done by multitudes of authors, there are still many questions about the effect of processing variables on resulting properties that have not been addressed, since only one set of conditions is typically studied.

Despite overwhelming industrial experience proving the effect of processing and geometry can have on the properties and performance of injection molded polymers, very little of the public literature addresses these issues. Most of the published literature focuses on a single molding condition for simple, small plaque geometries, as opposed to the variability in processing and complex geometries found in most "real-world" parts. Because the effects of these variables are not fully understood, this leads to a "trial and error" approach to molding.

Of the more than 100 references reviewed on polypropylene morphology for this work, almost half were on samples that had cooled from a melt, eliminating the shearing effects of injection molding, known to have a large effect on crystallization behavior (Kumaraswamy, 1999; Kumaraswamy, 2000; Kumaraswamy, 2002). Of the studies that were conducted on injection molded samples, fewer than 30 addressed the effect of processing conditions on morphology or properties. A summary of references, comparing the part geometry, molding conditions and types of evaluations was conducted by Fujiyama *et. al.* (Fujiyama, 1991). However, most of those studies examined only small samples, such as molded tensile bars, discs or plaques (<120 mm in length or diameter). Only 6 references that were found examined the effect of processing conditions on large plaques that could begin to be representative of real-world automotive parts. Mencik and Fitchmun studied larger 76 mm x 203 mm plaques and used a variety of molding conditions (Fitchmun, 1973; Mencik, 1973). However, the morphology was only examined at one spot in that large plaque. The orientation of the gates made it impossible to determine the orientation of their sample to the flow direction. Wenig et. al. studied the morphology using X-ray scattering on different locations along larger tensile bars, however the only processing effect they studied was mold wall temperature, which they found to have little influence on the resulting morphology (Wenig, 1993). Liu et. al. studied the morphology of end gated plaques, such as in this

work, and also found that the shear zone disappeared at the end of his flow length (~200 cm) (Liu, 2001). However, the processing conditions are not divulged, or presumably varied, and there is no investigation of orientation to flow. Zipper et. al. studied a layout very similar to that done in this work on a 70 mm x 230 mm plaque (Zipper, 1996). They varied cavity pressure and molecular weight of the material, and studied the morphology as a function of distance from the gate and orientation to the flow. Our work will expand on that, by also investigating variable injections speed and melt cooling rates. Phillips et. al. also studied the effect of flow length and orientation on morphology of different polypropylenes (Phillips, 1994). The melt temperature was varied, but other processing variables were held constant. The wrinkling in the shear zone that was discovered in this work was also apparent in their samples; however the authors did not comment on or explain its presence.

This work is the first to systematically investigate the effects of molding parameters, flow length and orientation on the surface and near surface morphology and properties of injection molded polypropylene. This information can be used to improve the molding and performance of large parts in the future, saving time and money in production. With the ever increasing prices of the raw material, the only real opportunities for cost savings are in improved part and mold design or optimized processing, especially in the automotive where savings of mere pennies a part can translate into millions in savings due to part volumes.

This is also the first investigation of the effect of considerable changes in the heat transfer rate from the melt to the mold, through the use of aluminum tooling, on the morphology and properties of injection-molded polypropylene. The use of aluminum tools is increasing in the automotive industry, due to the improvement on the through-thickness hardness and durability of the aluminum alloys used for the mold, combined with the smaller quantity of parts being made on a given tool

due to more frequent product cycle changes (Miel, 2009, 2009). The effect of the dramatic change in cooling rate on the surface microstructure will be important to understand for part performance, especially for coating adhesion.

This chapter is intended to serve as the foundation for the following chapter on TPO. Fully understanding the effects of molding and geometry on the morphology of iPP directed the research done on the more complex, commercially important TPO blends. This chapter begins with a literature review and background discussion of the morphology of polypropylene and the effect of molding conditions on morphology and properties. First, optical microscopy and XPS is used to investigate the effect of flow length, fill speed, orientation to flow and cooling rate (determined by aluminum or steel mold material) on the surface microstructure and chemistry. The effect of these same variables is studied on molded-in stress using coefficient of thermal expansion (CLTE) measurements and optical profilometry of cross-sections as a function of part temperature. These findings will be correlated to mechanical performance using automotive test methods for high speed (2.2 m/s) impact testing at cold temperatures (-40°C).

2.2 Literature Review

2.2.A Micro (Spherulitic) Morphology

The structure of iPP is shown schematically in Figure 2-1. Isotactic polypropylene is most commonly found in the monoclinic α-form, but polymorphs in hexagonal β-form, triclinic γ-form, and smectic forms have also been demonstrated, depending on processing conditions (Mencik, 1973; Kalay, 1997; Brucato, 2002; Janeschitz-Kriegl, 2005). The spherulites of the α-form of iPP crystallize into three types which can be differentiated using optical microscopy. Type I and Type II α -spherulites both have a Maltese cross pattern under cross-

polarized light, but the Type I spherulites have weak positive birefringence whereas Type II spherulites have weak negative birefringence. Mixed spherulites do not have a Maltese cross pattern. Type I α -spherulites are typically formed at low temperature or high undercoolings and have more a third of the chains lying parallel to the spherulite radius, causing the positive birefringence. Type II α -spherulites are typically formed at higher temperatures and have more chains lying perpendicular to the spherulite radius (Padden, 1959; Pasquini, 2005).

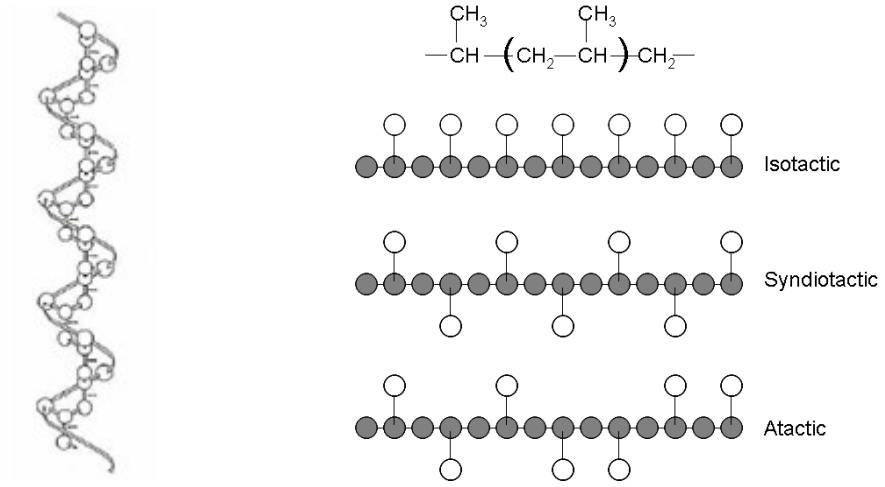

Figure 2-1: Schematic 3_1-helical conformation of iPP and stereochemistry configurations (Pasquini, 2005)

Hexagonal β spherulites are not cross-hatched like α-type spherulites, but are instead composed of radially distributed arrays of parallel lamellae. The β -form can be induced by nucleators (Grein, 2002) or certain processing conditions such as large amounts of shear in the melt, slow growth rates and high temperature gradients (Turner-Jones, 1964). The β -form spherulites grow more quickly than the α-form, but they are not as stable (Keith, 1959; Turner-Jones, 1964), and are

differentiated using optical microscopy because they appear uniformly bright under polarized light compared to the α-spherulites (Kadota, 1999; Park, 2002).

The γ phase is not typically found in industrially relevant injection moldings (Pasquini, 2005) because it requires low molecular weight material, high pressures and is associated with high degrees of molecular alignment (Kalay, 1997). The mesomorphic, or smectic form is typically found in commercially fabricated pieces due to their rapid cooling and is an intermediate form between the amorphous and crystalline phases (Pasquini, 2005).

2.2.B Macro Morphology

Using optical microscopy and x-ray diffraction, authors have defined the "skin-core" structure of injection molded iPP into three (Kantz, 1972; Katti, 1982; Chen, 2000), four (Fitchmun, 1973; Mencik, 1973; Trotignon, 1987), or as many as six (Karger-Kocsis, 1989) different layers each having different degrees of orientation and crystallinity as well as different morphologies. The outer skin layer is generally agreed to be non-crystalline and non-spherulitic, and most authors report thicknesses of approximately 25 μm. The degree of orientation of this layer has been reported as both poorly oriented (Mencik, 1973; Trotignon, 1987) and highly oriented (parallel to injection direction) (Kantz, 1972; Katti, 1982). The inner-most core layer is agreed to be spherulitic, with little to no net orientation (Kantz, 1972; Mencik, 1973; Katti, 1982; Trotignon, 1987; Fujiyama, 1991).

The area between the skin and the core, typically called the shear or transition zone, is the region where the number of layers can vary depending on the authors definition. Authors who define this region as one layer describe it as a row-oriented shear structure, or shish-kebab (Fujiyama, 1988). Fitchmun and

Mencik state that there are two layers between the skin and the core, but they are indistinguishable optically, and are only different in their orientation as determined by XRD (Fitchmun, 1973; Mencik, 1973). The layer closer to the skin is found to have a preferred orientation of the a-axis with the flow direction, whereas the layer closer to core has both a-axis and c-axis orientation, and is not always present, depending upon molding conditions. Trotignon and Verdu define two layers between the skin and the core, and do distinguish them using optical microscopy (Trotignon, 1987). The layer closer to the skin has a fine but distinguishable spherulitic structure, but the layer closer to the core has no visible crystalline structure. Karger-Kocsis and Friedrich break the shear zone into four layers, each optically distinguishable. The layer closest to the skin has a fine spherulitic structure similar to that described by Trotignon and Verdu, grown by transcrystallization on the skin layer. The next layer is a fine-grained section, followed by a layer composed of type III β-form spherulites. The final layer before the core is defined as a highly elongated fibrillar structure, assumed to be formed during the packing phase (Karger-Kocsis, 1989).

2.2.C Effect of Processing on Morphology

The morphology of injection molded iPP has been demonstrated to be a function of injection molding parameters such as mold and melt temperatures, fill times and pressures. Changes in these parameters impact the temperature gradient and shear rate, which each have an effect on crystallization (Fitchmun, 1973). There are varying opinions on the impact of each of these molding parameters on morphological characteristics such as layer thickness, degree of crystallinity and orientation, amount and location of β-phase, and spherulite size, but summaries of multiple works have been attempted (Katti, 1982; Fujiyama, 1991).

The temperature of the mold wall is said to affect both the crystallization as well as the heat transfer rate (Katti, 1982). Increasing the mold temperature has been

shown to decrease the skin thickness (Katti, 1982; Wright, 1988; Cermak, 2005), and increase the bulk spherulite size, degree of crystallinity (Wright, 1988; Cermak, 2005), and amount of β-phase present (Cermak, 2005). Other authors contend that the mold temperature is of minor importance when compared to the melt temperature and injection pressure (Fitchmun, 1973; Wenig, 1993). The melt temperature is said to only affect the heat transfer, and increasing the melt temperature has been shown to decrease the skin thickness (Kantz, 1972; Fitchmun, 1973; Katti, 1982; Fujiyama, 1991; Phillips, 1994; Schrauwen, 2004), degree of orientation (Fujiyama, 1991), amount of β-phase present (Cermak, 2005), and spherulite size (Wright, 1988), while increasing the crystallinity (Fujiyama, 1991). While one author showed that injection pressure does not affect the skin thickness (Kantz, 1972), others have shown that increasing the flow rate will decrease the skin thickness (Fitchmun, 1973; Fujiyama, 1991; Schrauwen, 2004) and increase the degree of crystallinity (Trotignon, 1982).

The effect of mold geometry on morphology has not been studied as well as the effect of molding parameters. Typically, authors pick a single location and orientation to the flow for their samples (Fitchmun, 1973; Mencik, 1973; Wright, 1988; Karger-Kocsis, 1989; Dai, 2003; Cermak, 2005). The few studies done on the effect of location from the gate have found in general that the skin thickness (Fujiyama, 1991; Phillips, 1994) and overall degree of crystallinity (Trotignon, 1982; Phillips, 1994) decrease with increasing distance from the gate. The amount of the β-phase is independent of distance from the gate (Fujiyama, 1991).

2.2.D Effect of Morphology on Properties

For injection molded, neat i-PP, the molding conditions, crystal phase and sample orientation with respect to melt flow direction all affect morphology, and therefore all showed effects on the mechanical behavior. The elastic modulus

and yield strength of i-PP was found to increase and the elongation at break was found to decrease with increasing mold temperature due to increased crystallinity and order. This effect was found to be independent of crystal phase at normal processing conditions (Kantz, 1972; Fujiyama, 1988; Wright, 1988; Phillips, 1994; Cermak, 2006). Holding pressure was found to have little effect on the elastic modulus of iPP (Cermak, 2006).

The predominant phase of polypropylene present in the sample was also found to affect mechanical behavior. The toughness of β–nucleated iPP both above and below the glass transition temperature was found to be higher than that of predominately α-iPP. This is likely due to the arrangement of the microstructure and the β- to α–phase transition under stress (Grein, 2002; Cermak, 2006). However, the yield stress and elastic modulus of the α-iPP was found to be higher than that of the β-phase (Kalay, 1997; Cermak, 2006). The γ-phase, which has been reported in some injection moldings, has a higher modulus and tensile strength due to its high molecular alignment and orientation, as long as its presence is not a result of degradation (Kalay, 1997). With respect to sample geometry, increases in tensile yield stress and strain hardening, as well as flexural modulus, were found when the sample was oriented parallel to the flow direction compared to perpendicular to the flow direction (Kantz, 1972; Fujiyama, 1977; Fujiyama, 1988; Phillips, 1994; Schrauwen, 2004; Pasquini, 2005). Impact toughness was also found to be as much as 4.5 times higher in samples taken oriented parallel to the flow direction than in those perpendicular to flow (Schrauwen, 2004).

2.3 Experimental

Plaques (100 mm x 300 mm x 3.5 mm) with a 100 mm fan end gate were molded on a 350 ton Van Dorn press out of Pro-fax 6523 natural polypropylene homopolymer (LyondellBasell, USA), which is a standard injection molding grade

material with a low concentration of additives. Various combinations of processing conditions were used and are shown in Table 2-1. End gated plaques were chosen to study the effect of orientation to flow. Identical molds were made out of both P20 grade tool steel and a QC-10 forged aluminum alloy (Alcoa, USA). The nozzle temperature was 221°C, and both halves of the mold were set at 21°C. Actual mold temperatures after start-up ranged from 54-63°C depending on mold material and injection speed (aluminum tool and slower injection speeds were cooler). The injection pressure was 500 bars. The injection molding machine used to make the plaques did not have a quantitative measure of injection speed, but two different speeds were examined with the "Fast" injection speed being representative of typical industrial processing speeds (~90 mm/s) and approximately 5 times faster than the "Slow" injection speed (~10 mm/s).

2.3.A Optical Microscopy

Samples taken in the plaque were chosen in two different orientations to the flow, parallel to (Flow Direction (FD)) and perpendicular to (Transverse Direction (TD)), as shown schematically in Figure 2-2. The effect of flow length was also studied by taking samples at three different locations with respect to the gate location (Table 2-1). The "Near" samples were taken approximately 50 mm from the gate, "Mid" samples were taken approximately 150 mm from the gate and "Far" samples were taken approximately 250 mm from the gate. The location and orientation of the samples is shown on a plaque in Figure 2-3. Samples were taken within 1 cm of each other from plaque to plaque.

Table 2-1: DOE of Process Variables for Injection Molding of Neat PP Samples

Mold Material	Sample Location (Distance from Gate ± 1 cm)	Flow Rate*
Steel	Near (~50 mm)	Slow
		Fast
	Middle (~150 mm)	Slow
		Fast
	End (~250 mm)	Slow
		Fast
Aluminum	Near (~50 mm)	Slow
		Fast
	Middle (~150 mm)	Slow
		Fast
	End (~250 mm)	Slow
		Fast

*Flow rate could only be measured qualitatively on the injection molding machine, but Fast ≈ 5 * Slow

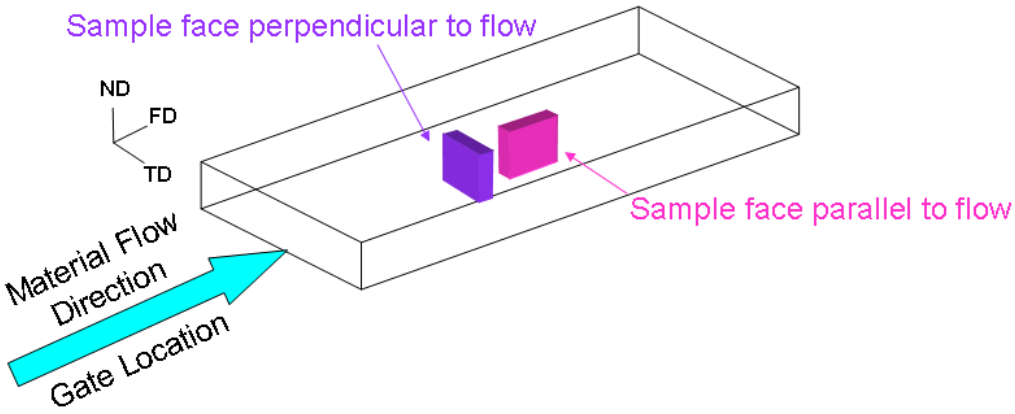

Figure 2-2: Schematic of sample orientation with respect to flow direction. ND = Normal direction, FD = Flow Direction, TD = Transverse Direction.

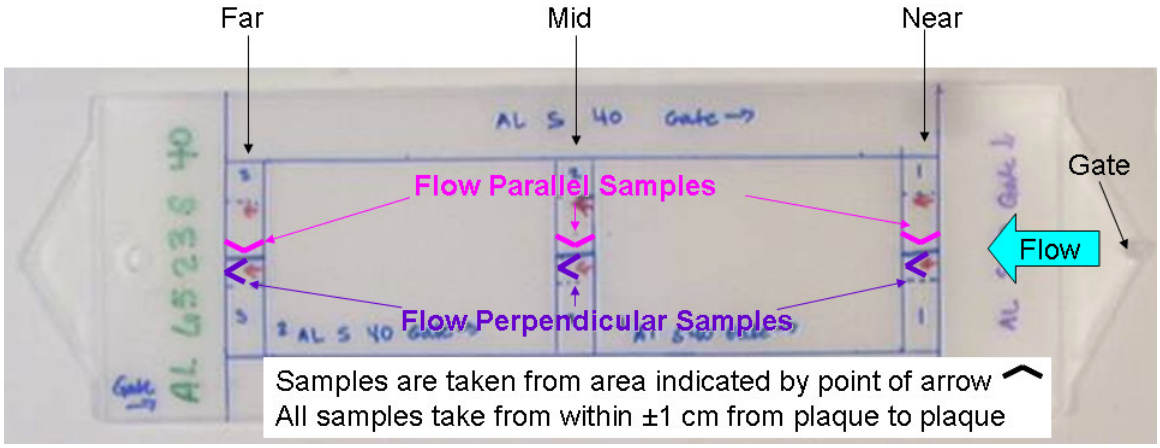

Figure 2-3: Sample geometry layout of plaque

Thin sections (5 μm) were cryomicrotomed using a glass knife at 5°C. This temperature was chosen to make the block sufficiently hard to cut smoothly without stretching the sample, but without becoming brittle (below T_g). Samples were microtomed parallel to the plaque thickness in order to prevent sample compression, which had been found to change the measured layer thicknesses

by almost 20%. The thin slices were sandwiched between a glass slide and coverslip using immersion oil (Cargille Type A), and examined under crossed polars in an optical transmission light microscope.

2.3.B Molded-in stress measurements

Measurements of molded-in or residual stresses of injection molded polymers has been studied by other authors using a layer removal method (Treuting, 1951; Coxon, 1980; Siegmann, 1982; Chiu, 1987; Pham, 1993) or a stress relaxation method, which involves thermally relieving the part while measuring stresses (Coxon, 1980). A new technique was developed to study the residual molded-in stress less destructively than the layer removal method, and at a smaller scale than the bulk relaxation method.

A sample cross-section was polished flat to a 0.3 μm finish using alumina suspensions. The surface profile of the cross-sections was measured using a Wyko NT3300 optical profilometer (Veeco Instruments, USA) as a function of temperature using a programmable INSTEC HCS402 hot stage. Samples were equilibrated at a given temperature for at least 10 minutes (until the profile had stabilized) before the measurements were taken. All of the scans were filtered using the Wyko software to remove any sample tilt. Background (room temperature) scans were subtracted from the elevated temperature measurements and results were averaged across the area of the sample for the resulting line scan data.

2.3.C Coefficient of Linear Thermal Expansion (CLTE)

The coefficient of linear thermal expansion (CLTE) was measured using a dual pushrod Dilatronic dilatometer (Theta Industries, Inc., USA) with 50 mm X 8 mm

full thickness samples. The samples were run from 30℃ to 100℃ at a rate of 0.5℃ per minute and compared to a NIST fused silica reference (SRM 739).

2.3.D Low Temperature Impact Testing

Samples from the plaques were cut to an approximate size of 76.2 mm x 25.4 mm at different locations and orientations with respect to the gate using a band saw. The plaque layout is shown in Figure 2-4. The edges of the samples were sanded to a 600 grit finish to avoid crack initiation.

For impact testing, ASTM test method D790 (Standard Test Methods for Flexural Properties of Unreinforced and Reinforced Plastics and Electrical Insulating Materials 2008) was followed with a modification to the test speed, using 2.2 m/s in place of the quasi-static speeds (10^{-4} – 10^{-6} m/s) defined by the method. An Instron Dynatup 9250HV drop tower ("Impact Test System Model 9250HV," 2002) was configured for three point loading and a drop weight of 24 kg was used (Figure 2-5). The tup has a 12.7mm diameter cylindrical nose that is 30mm wide, a load capacity of 0.5 kN and a load impact error of ±2% ("Tup 3B-SRL," 2000). Load measurements were obtained from strain gages located 13 mm away from the tup impact area. The three-point bend supports were 6.4 mm in diameter with a span of 50 mm and samples were allowed to sit freely with no lubrication. Impact velocity was measured using a photo-electric diode and a flag system. Tup velocity during impact and consequently specimen deflection were calculated from the instantaneous velocity at impact using standard equations of motion (Impact Test System Model 9250HV Manual, 2002). The samples were allowed to equilibrate to -40℃ for 30 minutes prior to testing.

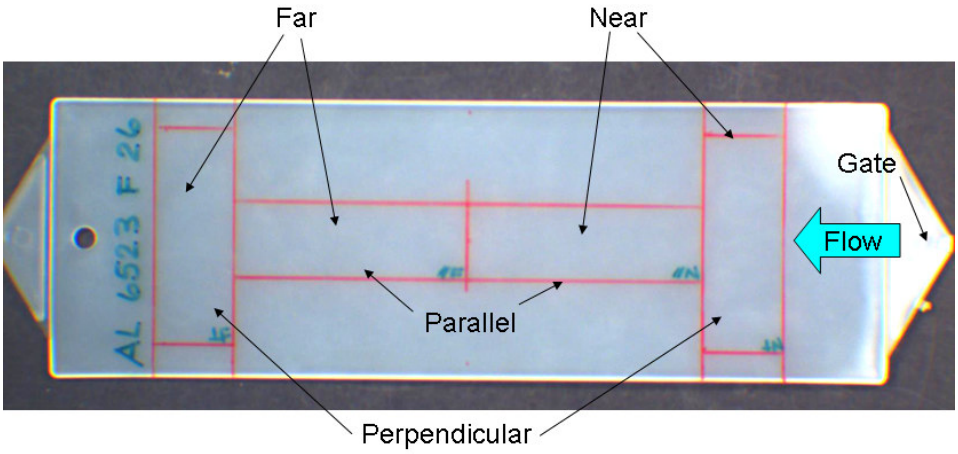

Figure 2-4: Layout for impact testing samples both parallel and perpendicular to flow, and near and far from gate

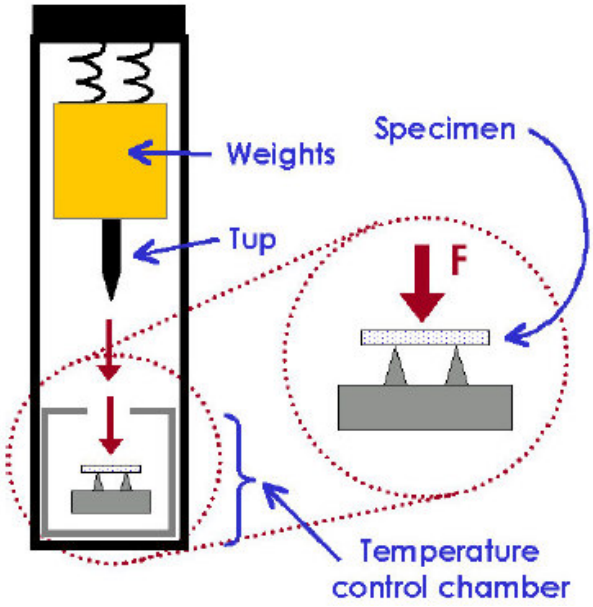

Figure 2-5: Schematic of Instron Dynatup 9250HV impact test setup

2.3.E X-Ray Photoelectron Spectroscopy (XPS)

X-ray Photoelectron Spectroscopy (XPS) was done on a Kratos AXIS 165 Electron Spectrometer (Kratos Analytical, England) using monochromatic aluminum Kα (1486.6 eV) source operated at 12 kV, 20 mA and collected using hybrid mode magnification. A 20 eV pass energy was used for high resolution

spectra, and an 80 eV pass energy was used for surveys. Data analysis was completed using manufacturer provided software. Binding energies were referenced to the aliphatic carbon 1s line at 284.6 eV.

2.4 Results and Discussion

2.4.A Optical Microscopy

The effect of flow length on near-surface morphology is shown for steel molded samples in Figure 2-6 and aluminum molded samples in Figure 2-7. For both, there appears to be a large effect of flow length on the surface to core morphology. The "Near" and "Middle" samples both show a thin outer skin followed by a spherulitic zone, a shear band and the core. The definition of these zones as used in this publication is shown in Figure 2-8. The "Far" samples only appear to show the outer skin and the core. The thickness of these zones was measured and the average of three measurements is reported in Table 2-2.

It should be noted there are a number of possible sources of error in these measurements. The boundaries between the zones are not clear, so where to take the measurements is a personal judgment. To minimize some of the variables, however, the spherulitic zone measurement was started from where the skin measurement ended, and the shear zone measurement was started from where the spherulitic zone ended. The values reported were measured on the samples taken parallel to the flow, because they were not wrinkled in the shear zone like the samples taken perpendicular to the flow (discussed later), reducing measurement error. Theoretically, the orientation of the sample should not affect the location of the physical boundaries of the layers, but the appearance of the layer may differ with different orientations.

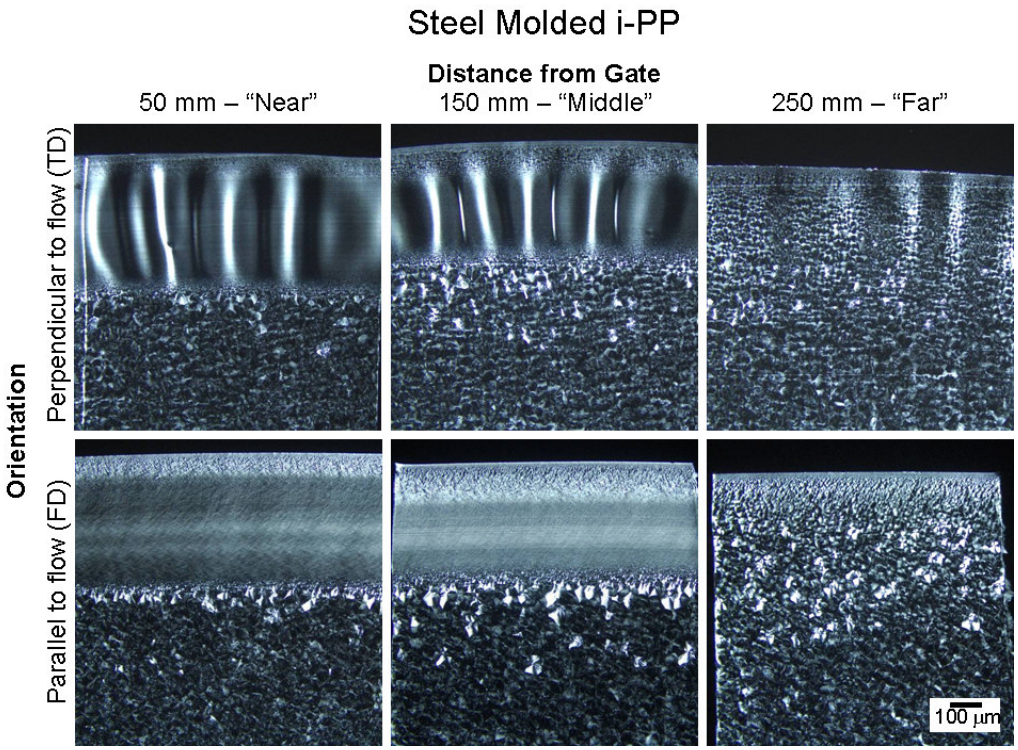

Figure 2-6: Steel mold, slow injection speed

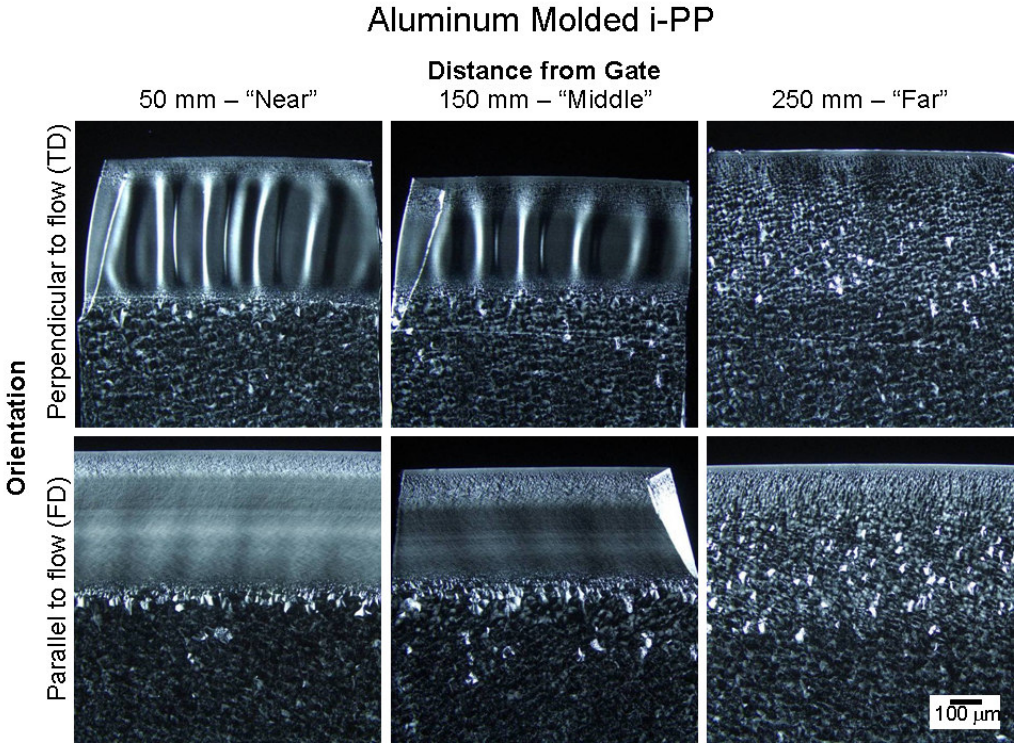

Figure 2-7: Aluminum mold, slow injection speed

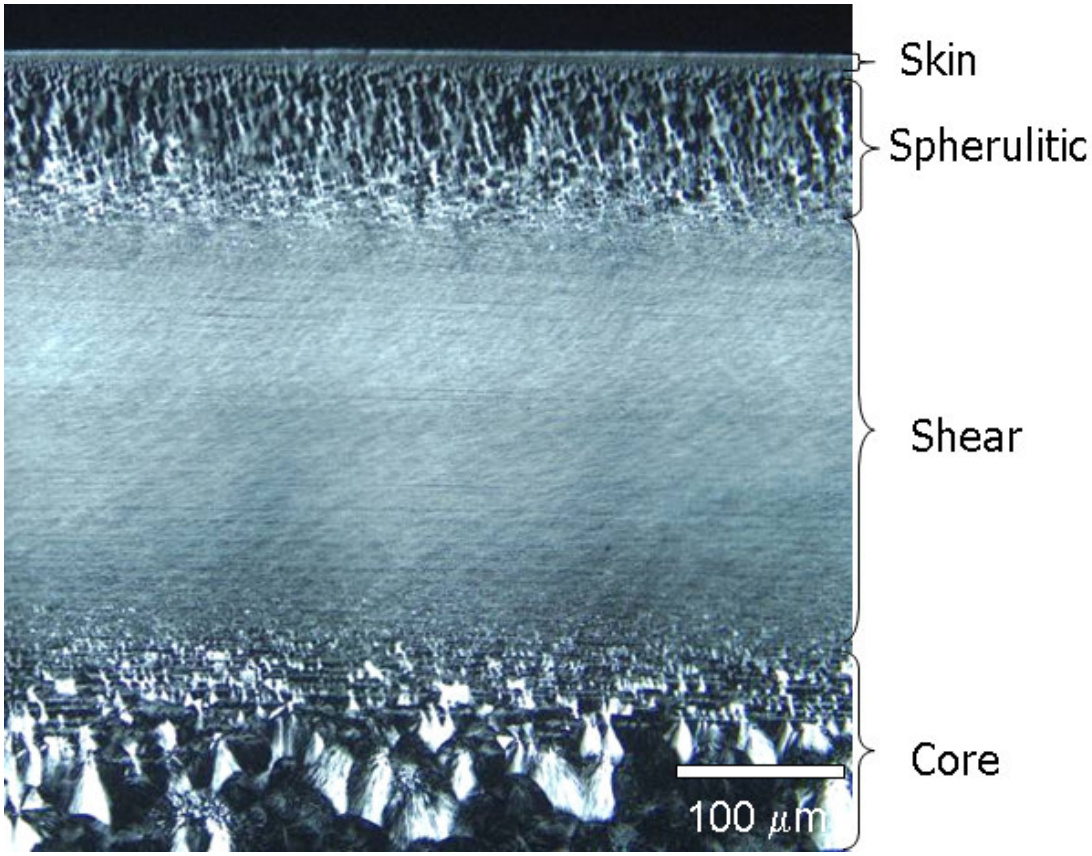

Figure 2-8: Definition of zones of optical microscopy of i-PP

Table 2-2: Measurements from PP Optical Microscopy

		Layer Thickness in μm		
Sample	Distance from Gate	Skin	Spherulitic	Shear
Steel Slow	50 mm - Near	2.0 ± 0.3	72.5 ± 0.8	342.5 ± 4.5
	150 mm - Middle	8.4 ± 1.8	107.1 ± 2.4	249.8 ± 9.5
	200 mm - Far	3.6 ± 0.9		
Steel Fast	50 mm - Near	2.6 ± 0.4	65.2 ± 0.3	331.0 ± 0.4
	150 mm - Middle	3.9 ± 0.4	101.6 ± 5.5	229.5 ± 7.5
	200 mm - Far	3.3 ± 0.9		
Aluminum Slow	50 mm - Near	2.9 ± 0.7	85.0 ± 2.1	330.6 ± 3.1
	150 mm - Middle	4.5 ± 1.4	110.2 ± 2.0	232.8 ± 7.0
	200 mm - Far	3.2 ± 1.4		
Aluminum Fast	50 mm - Near	4.2 ± 0.9	69.0 ± 3.3	356.5 ± 4.4
	150 mm - Middle	5.1 ± 0.7	97.2 ± 4.2	276.9 ± 7.6
	200 mm - Far	7.0 ± 0.8		

The measured values confirm the observation made from the optical images that the shear band found in the "Near" and "Middle" samples appears to be shrinking from both sides as one moves further from the gate. The non-linear shrinking of the shear zone is more evident in Figure 2-9, the graphical representation of Table 2-2. The shear zone shrinks approximately 100 μm in the 100 mm between the samples near the gate and in the middle of the plaque. If it had continued shrinking at the same rate, there should be at least 100 μm left of the shear band in the sample at the end of the plaque, but the shear zone is completely absent.

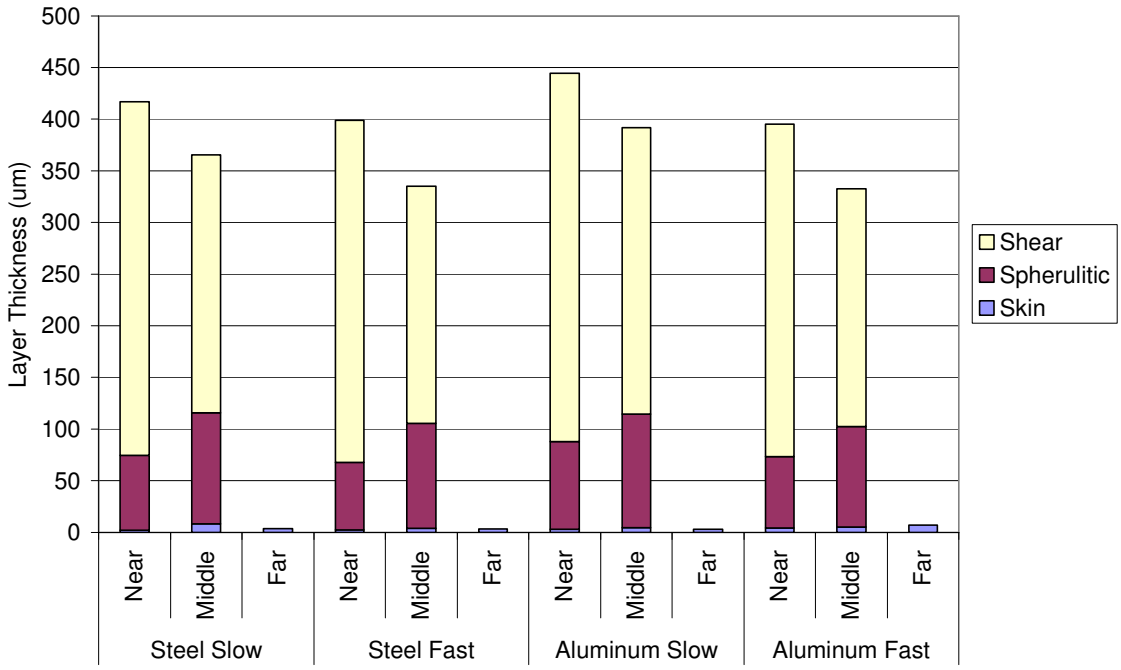

Figure 2-9: Measurement of morphological zones in Neat PP from optical microscopy

To confirm the behavior of the shear zone, more samples were taken between the "Middle" and "Far" points in the slow aluminum and steel molded samples. The results are shown visually in Figure 2-10 and graphically in Figure 2-11. The shrinking of the shear zone with increasing distance from the gate correlates with the findings of Phillips et. al. (Phillips, 1994), but because only small sample sizes have been examined in other literature, it had been unknown how far the shear zone would extend from the gate.

No previous studies have shown a non-linear decrease in the shear zone size with increasing distance from the gate. The fact that there is no dependence of fill speed or cooling rate suggests that this non-linear behavior is geometry driven. Knowledge of the variation and extent of the shear zone would be important for mechanical modeling due to the role of the shear zone in resisting crack propagation during failure (Karger-Kocsis, 1989), as well as the effect of the shear zone on molded-in stress, as discussed later.

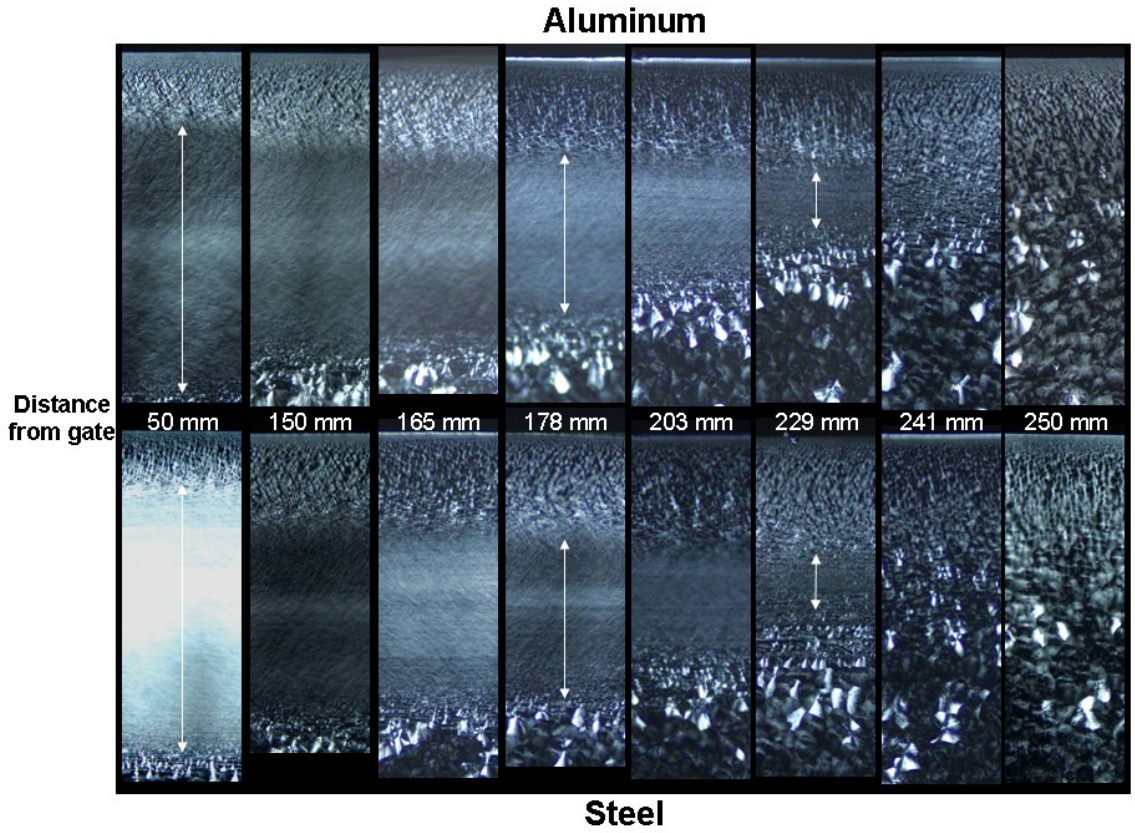

Figure 2-10: Optical microscopy of i-PP of slow molded samples parallel to flow taken at varying distances from the gate showing non-linear shrinking of the shear zone

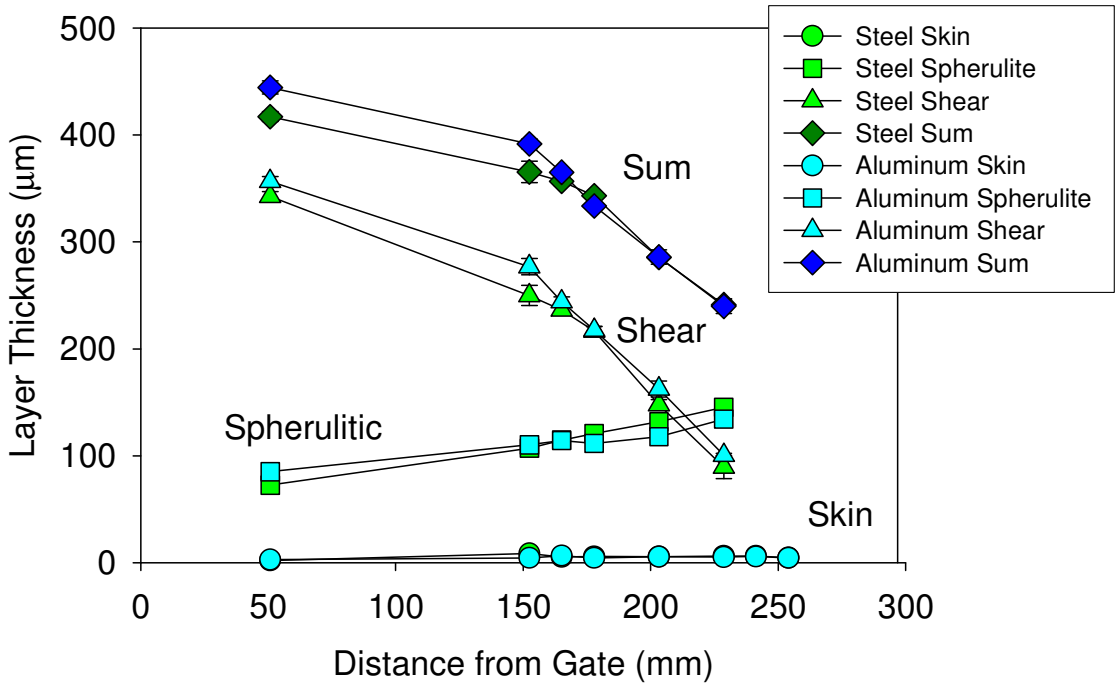

Figure 2-11: Layer thickness as a function of flow length for steel and aluminum samples

It appears that the effect of using an aluminum or steel mold on the optically observable morphology is negligible. There is a small increase in the size of the shear zone in the slowly molded sample on the aluminum mold, but there is little difference otherwise.

In Figure 2-6 and Figure 2-7, there appears to be slightly more β-phase in the steel molded samples, as indicated by the number of brighter spherulites. The distinction between the α and β spherulites in optical micrographs is shown in the example in Figure 2-12. This observation was confirmed by WAXS (Figure 2-13). The greater amount of the β-phase in the steel molded sample could be due to the slower growth rates because of the lower heat transfer rate in the steel compared to the aluminum (Turner-Jones, 1964).

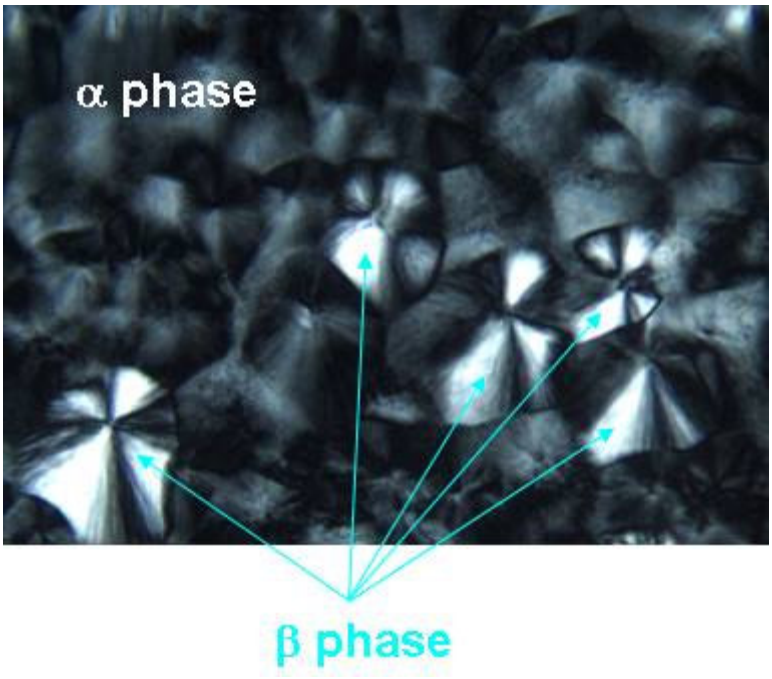

Figure 2-12: Example of α and β phase spherulites in optical microscopy of i-PP

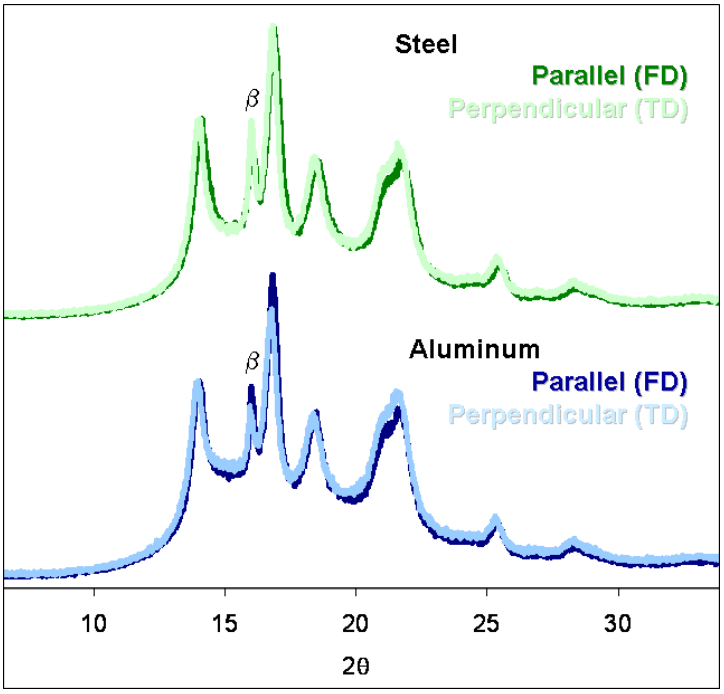

Figure 2-13: WAXS of core

Also noticeable in the optical images (Figure 2-6 and Figure 2-7), is considerable wrinkling in the shear band of the samples taken perpendicular to the melt flow (TD) which is not present in the shear zone of the samples parallel to the melt flow (FD). This behavior can be observed in the pictures presented by other authors, but no explanation or discussion of the phenomenon was given (Wright, 1988; Phillips, 1994; Schrauwen, 2004).

The first assumption for this "wrinkling" behavior was molded-in stress that was relieved during microtoming. To test this theory, full plaques as well as small sample blocks were placed in an oven at 80°C for 18 hours to relieve stress. Relief of the stress was noticeable by the increased curvature of the full plaque, but thin sections removed from the relaxed parts still showed the same wrinkling in the perpendicular to flow samples (Figure 2-14). This was repeated at 110°C for 18 hours and similar results were found (Figure 2-15).

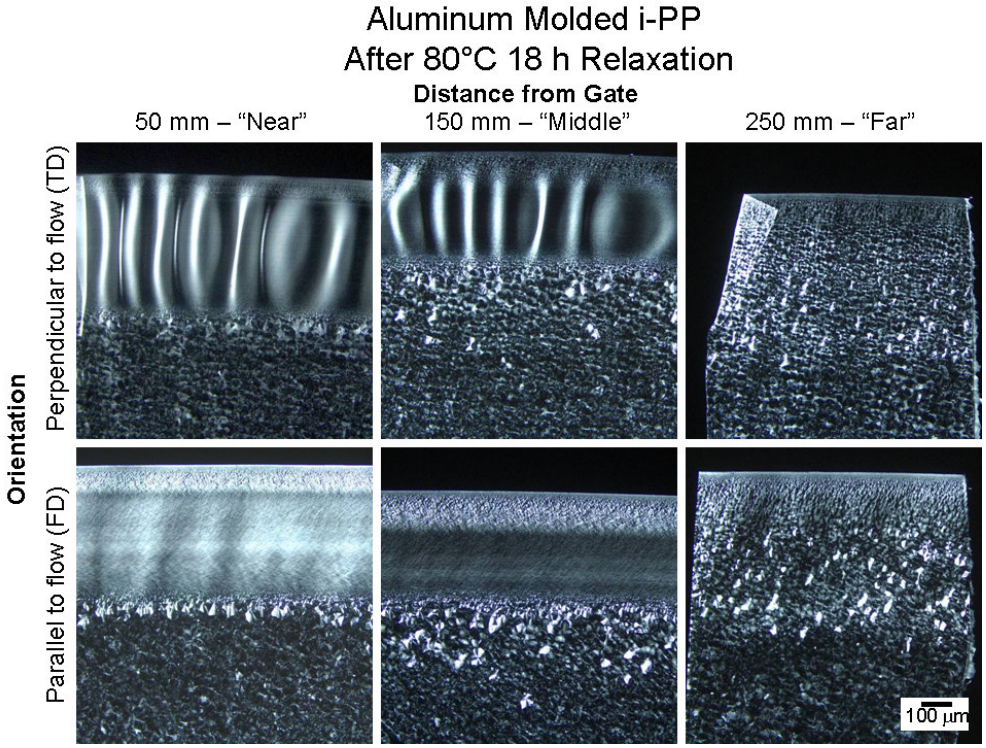

Figure 2-14: Aluminum mold, fast injection speed, after 18 h at 80°C

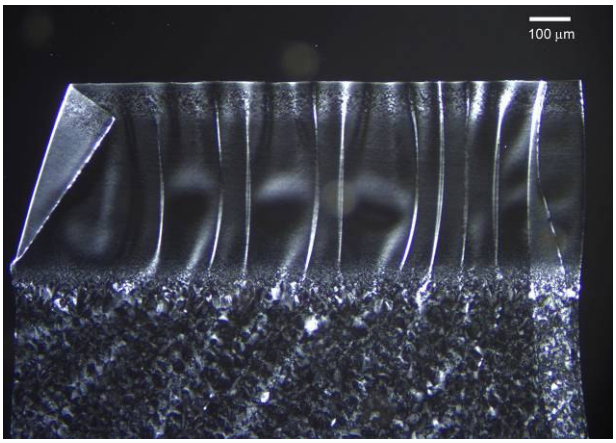

Figure 2-15: Aluminum mold, fast injection speed after 18 h at 110°C

To examine the shape of the blocks off of which the samples had been cryomicrotomed, the Wyko NT3300 optical profilometer was used (Figure 2-16). When the block is sectioned at 5°C, the surface should be completely flat from the microtome knife. However, once the block returned to room temperature, the profilometry shows the block face perpendicular to the flow is no longer flat, but the block face parallel to the flow is. This suggests that the shear zone could have an anisotropic coefficient of thermal expansion, and additional work was done to determine if this was the case.

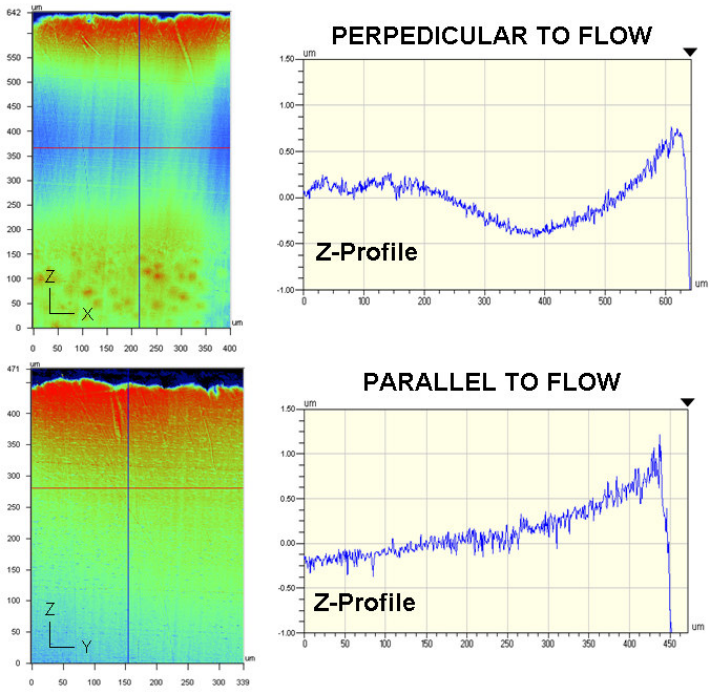

Figure 2-16: Optical profilometry of microtome block face

2.4.B Coefficient of Linear Thermal Expansion (CLTE)

To further investigate the theory that the shear zone had an anisotropic CLTE, samples were taken from plaques in different orientations to flow and at different flow lengths, as shown in Figure 2-17. The effect of orientation was studied by samples taken parallel to the flow (FD, red shading) and perpendicular to the flow (TD, blue shading). The effect of flow length (and therefore size of shear zone) was studied by taking the samples at varying distances from "Near" or starting at ~50 mm from the gate (darker shades) to "Far" or ending at about ~250 mm from the gate (lighter shades). Samples were taken from the two extreme conditions: slow molding in a steel mold and fast molding in an aluminum mold.

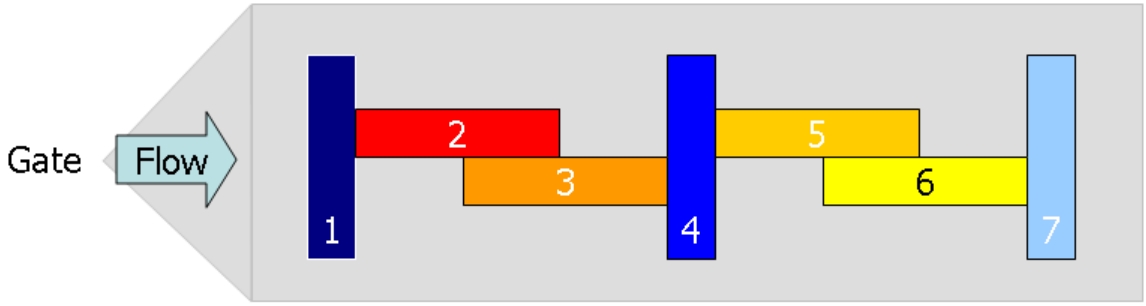

Figure 2-17: Schematic of CLTE sample orientation and location

Dual pushrod dilatometers calculate the expansion of the sample compared to the expansion of a reference material using Equation 2-1 (Touloukian, 1978; Standard Test Method for Linear Thermal Expansion of Solid Materials With a Push-Rod Dilatometer, 2008).

$$\left[\frac{\Delta L}{L_o}\right]_{T_i} = \left[\left(\frac{\Delta L}{L_o}\right)_m + A\right]_{T_i} \qquad \textbf{Equation 2-1}$$

Where:

L_0 = original length of specimen at temperature T_0, mm

ΔL = change in length of specimen between any two temperatures

T_i = temperature at which length is L_i, ℃

m = measured expansion of the reference material

A = numerical calibration constant

The mean coefficient of thermal expansion was calculated using Equation 2-2 over the temperature range 50℃-80℃ and plotted in Figure 2-18.

$$\alpha = \left[\frac{\Delta L}{L_o}\right]_{T_i}\left(\frac{1}{\Delta T}\right) \qquad \textbf{Equation 2-2}$$

Where $\Delta T = T_i - T_o = 80℃ - 50℃ = 30℃$.

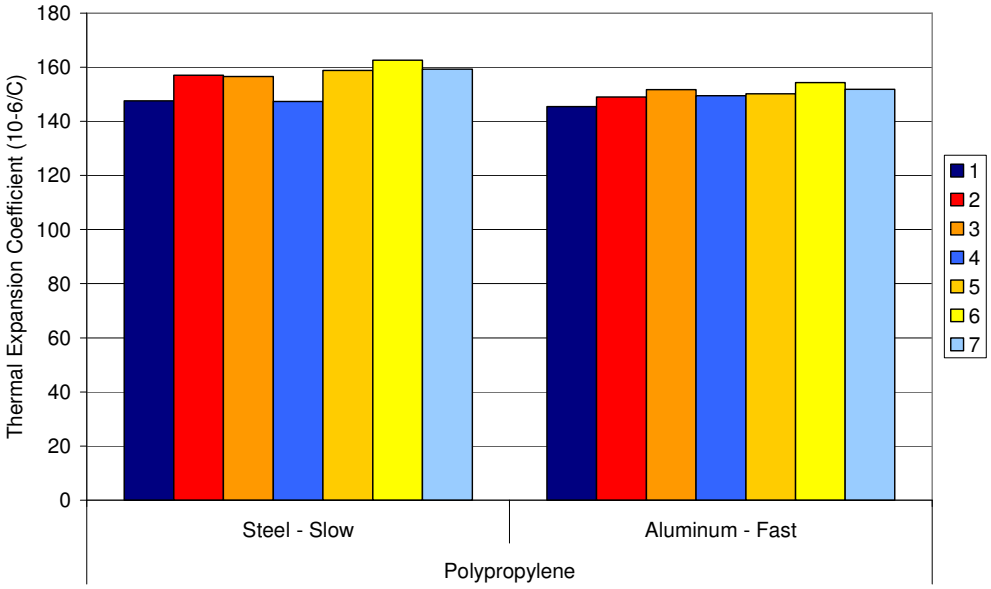

Figure 2-18: Coefficient of thermal expansion as a function of mold material and sample orientation and geometry

No dramatic difference in CLTE was found based on orientation to flow, mold material or distance from the gate. This data does not show evidence of the suspected anisotropy in the shear layer CLTE, but this is possibly due to the fact that this measurement was taken on the entire through-thickness of the sample. This bulk measurement may not be sensitive to differences in the shear layer, which at its thickest only makes up ~20% of the sample.

Since the bulk CLTE measurement did not detect any differences, a new technique was developed to examine the properties of the shear zone as a function of temperature. A programmable INSTEC HCS402 hot stage was used along with the Wyko profilometer to observe the topography of the shear zone as a function of temperature.

Our first attempts created the cross-section by microtoming at room temperature. It was previously assumed the block face would be flat after microtoming at low temperatures, and any resulting curvature at room temperature was due to CLTE differences in the shear zone. If that assumption were true, samples microtomed at room temperature should remain flat. However, as shown in Figure 2-19, the sample still showed curvature in the shear zone. This was the first indication that the wrinkling is due to molded-in stress relieved during microtoming, and not CLTE. This curvature is similar in nature to principles in used in other studies used to investigate molded-in stresses, except instead of layer removal starting at the skin and moving to the core (Treuting, 1951; Coxon, 1980; Siegmann, 1982; Chiu, 1987; Pham, 1993), we are removing layers perpendicularly.

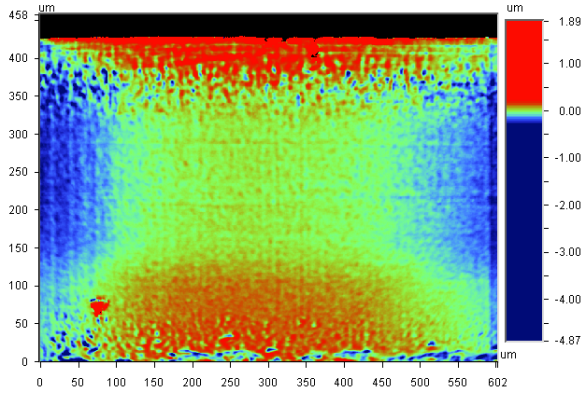

Figure 2-19: Image of aluminum molded, fast injection speed, near the gate, flow into sample microtomed at room temperature

Surface profilometry was examined at room temperature, 50℃, 70℃, 90℃, 110℃, 130℃, and 150℃. All of the following results are for sample molded at the fast, or industrially relevant injection speeds unless otherwise noted. The results for samples molded on both steel and aluminum are compared based on orientation to the flow in Figure 2-20 and Figure 2-21. It should be noted that the movement in the ND-direction may not be due to thermal expansion. The sample, hot stage, and Wyko stage are not fixed, so there could be drift.

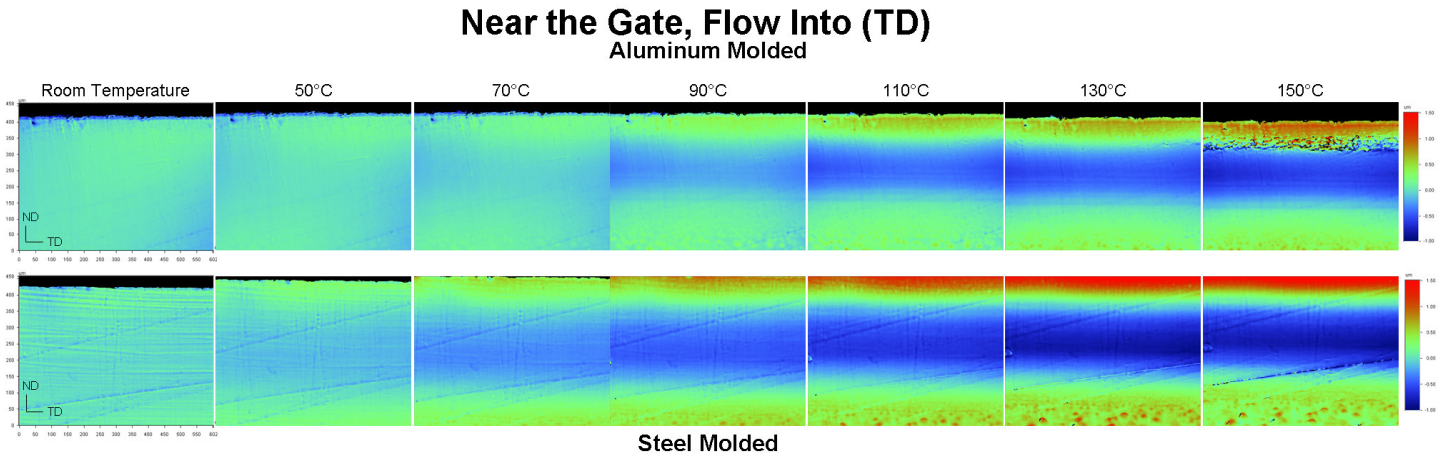

Figure 2-20: Surface profilometry of samples taken near the gate, perpendicular to flow as a function of temperature

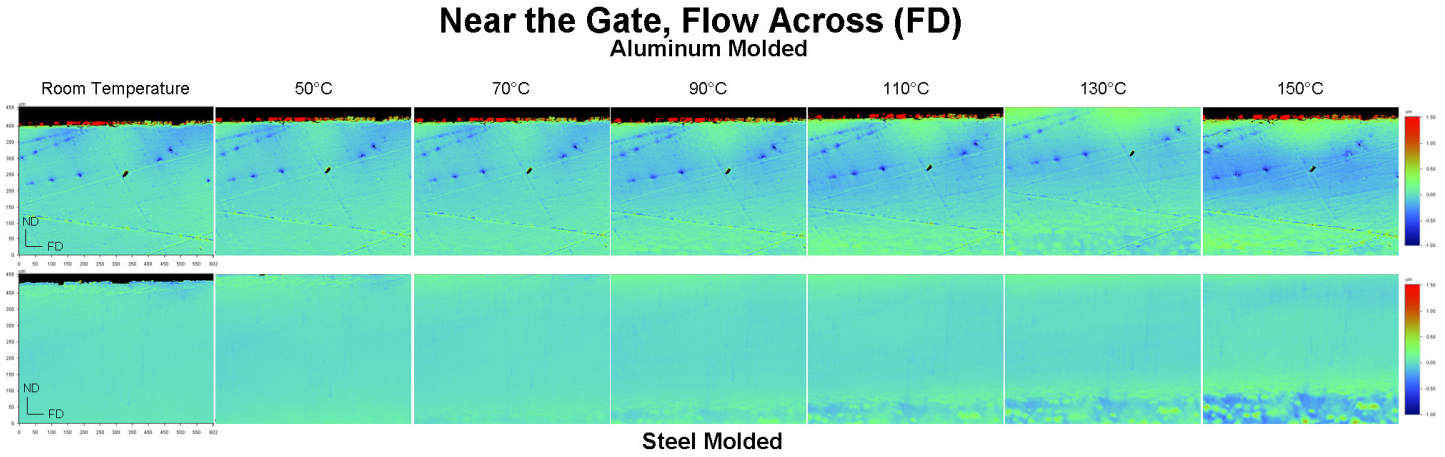

Figure 2-21: Surface profilometry of samples taken near the gate, parallel to flow as a function of temperature

With increased heating, the face of the samples taken perpendicular to the flow (Figure 2-20) shows the shear zone shrinking in the flow direction (FD). This same phenomenon is not seen in samples taken parallel to the flow samples (Figure 2-21). Averaged line profiles in the normal to flow direction (ND) for these samples are shown in Figure 2-22.

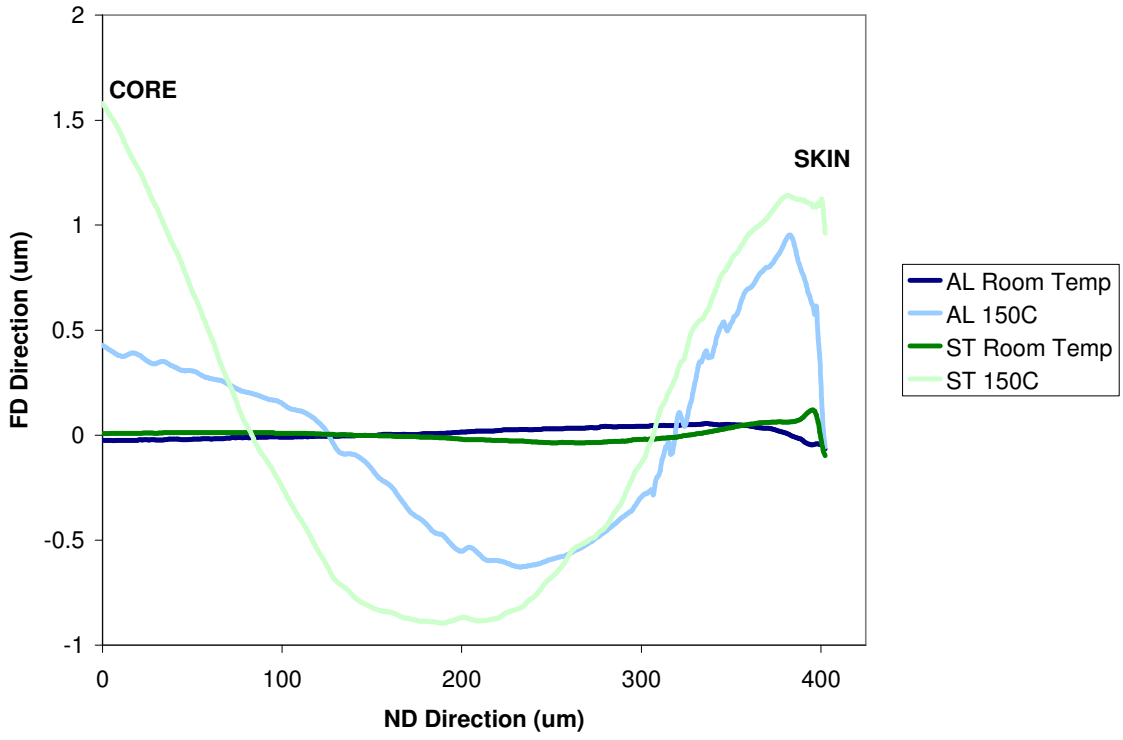

Figure 2-22: Averaged line scans from contour plots of samples taken perpendicular to flow

From the contour plots (Figure 2-20 and Figure 2-21) and the line profiles (Figure 2-22) it is determined that samples made in the steel mold start shrinking in the shear zone at lower temperatures (70℃ vs. 90℃) and also shrink ~0.3 µm more in the FD direction compared to the aluminum molded samples.

The amount of shrinking is indicative of the amount of stress being released in the sample during heating, with larger amounts of molded-in stress indicating a

higher degree of orientation. The steel molded sample shrinks more and is affected over a larger area than the aluminum sample, indicating more molded-in stress. The thermal conductivity of the forged aluminum alloy is more than 4 times that of the P20 steel mold (157 vs. 35 W/m•K), therefore parts in a steel mold are at higher temperatures for a longer periods of time. Also, the quicker cooling rates in the aluminum molded samples could produce higher shear forces resulting in quicker nucleation rates that would lessen shish-kabob orientation (Kumaraswamy, 1999; Kumaraswamy, 2000; Kumaraswamy, 2002).

Figure 2-23 shows results from samples taken far from the gate on the aluminum and steel molded samples perpendicular to the flow. There is no change in the surface profile with heating confirming that the shrinking is localized in the shear zone.

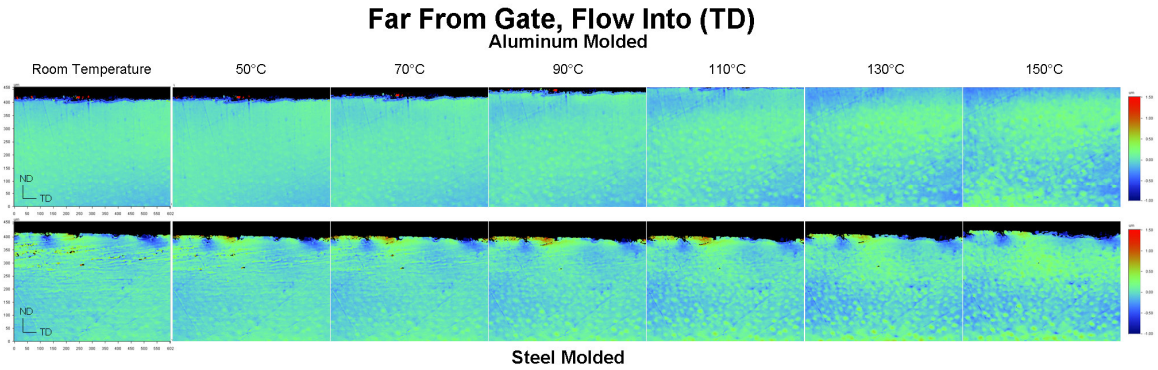

Figure 2-23: Surface profilometry of samples taken far from the gate, perpendicular to flow as a function of temperature

Comparisons of samples from near the gate perpendicular to the flow are compared before, during and after heating in Figure 2-24. This confirms that the change seen in the surface profile is not reversible with heat cycling, and the wrinkling seen in the optical microscopy results is due to molded-in stress, not anisotropic CLTE.

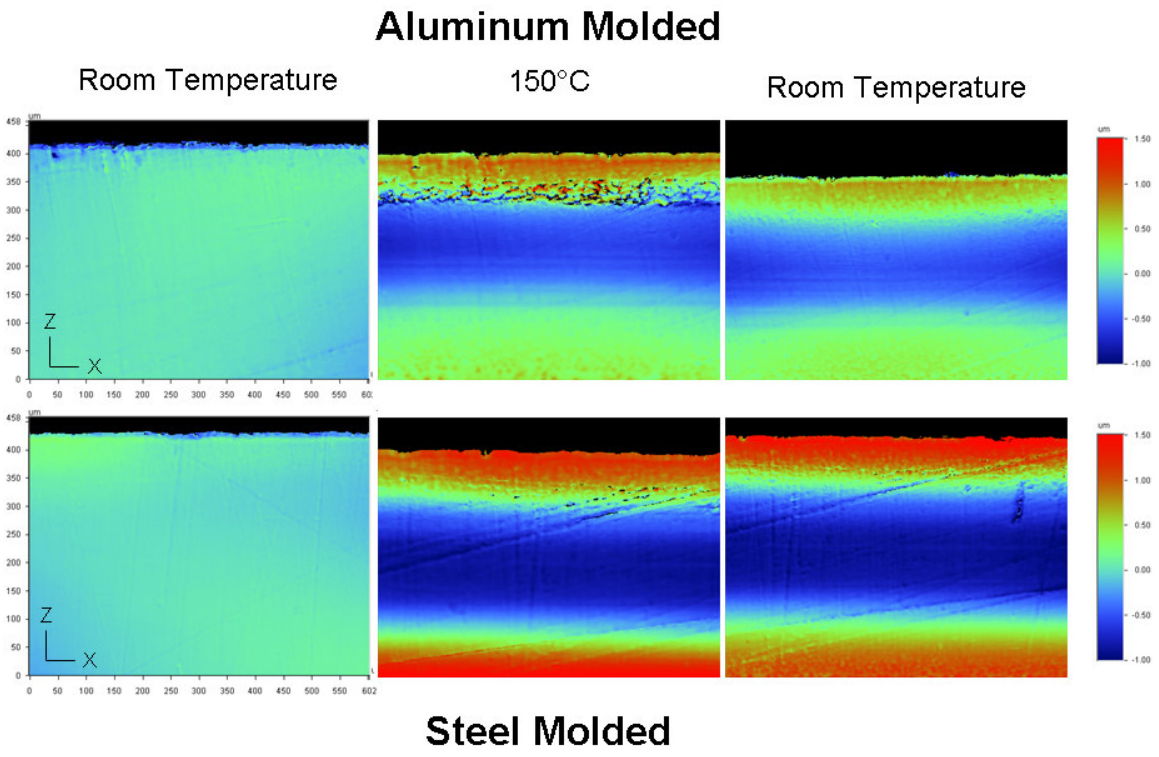

Figure 2-24: Contour plots of samples taken near the gate, perpendicular to flow before, during and after thermal cycling

The effect of injection speed on the shrinking of the shear zone was studied using samples taken near the gate and perpendicular to the flow. The averaged lines scans of the contour plots are shown in Figure 2-25.

Injection speed did not have an effect on the amount of shrinkage in the steel molded parts, and confirms the measurements from the optical microscopy work shown in Figure 2-9 where there was no measureable difference in the size of the shear zone as a function of injection speed. This is likely due to the low thermal conductivity of the steel, and the slower cooling of the part regardless of injection speed.

The injection speed was found to play a role in the amount of shrinkage in the more quickly cooled aluminum molded parts. The faster injection speed resulted in a smaller shear zone with less shrinkage than parts molded with the slower injection speed. The slow injection speed samples have similar shear zone size and shrinkage amounts compared to the steel tool. Faster cooling combined with a faster injection speed could cause faster nucleation rates due to increased shear stress, which could decrease the amount of molded in stress and size of the shear layer (Kumaraswamy, 1999; Kumaraswamy, 2000; Kumaraswamy, 2002).

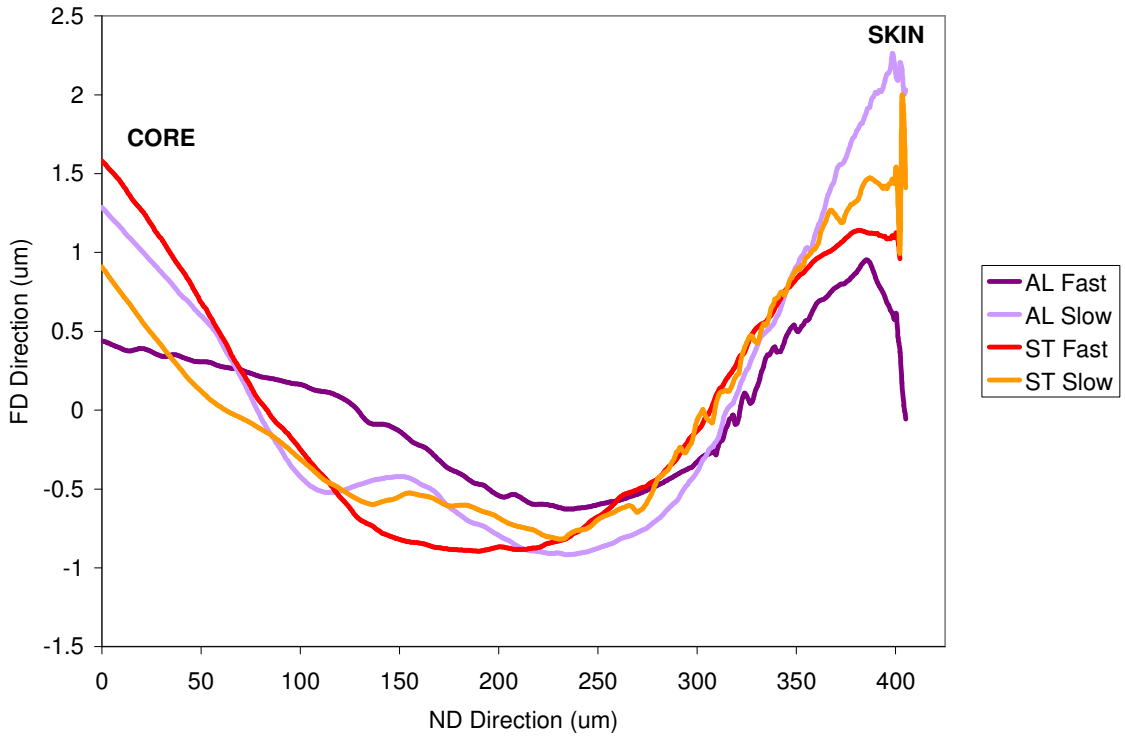

Figure 2-25: Average line scan of contour plot comparing the effect of injection speed for both aluminum and steel molded samples on the stress in the shear zone.

Wrinkling of the shear zone was still present in the optical microscopy results of samples that had been stress relieved at 80℃ and 110℃ for 18h (Figure 2-14 and Figure 2-15), indicating there is still molded-in stress in the shear zone. Wyko profiles of the "relieved" samples are shown in Figure 2-26. The line scans

of relieved samples are compared to as-molded samples at 150℃ in Figure 2-27. These results indicate that much of the molded-in stress was relieved during the 18 hour soak, but without melting the sample, there still will be some residual orientation in the shear zone due to the shish-kabob nature of the structure.

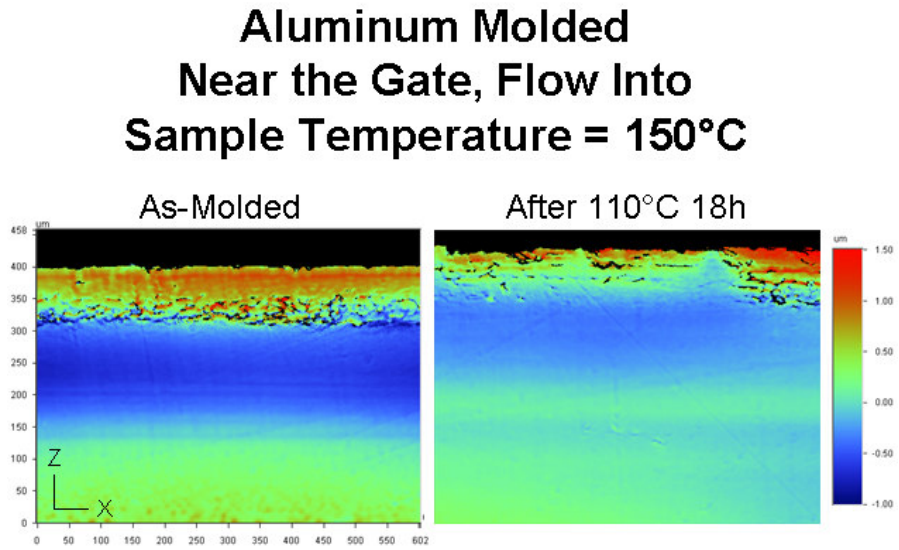

Figure 2-26: Contour plots of as-molded and stress relieved samples taken at 150℃

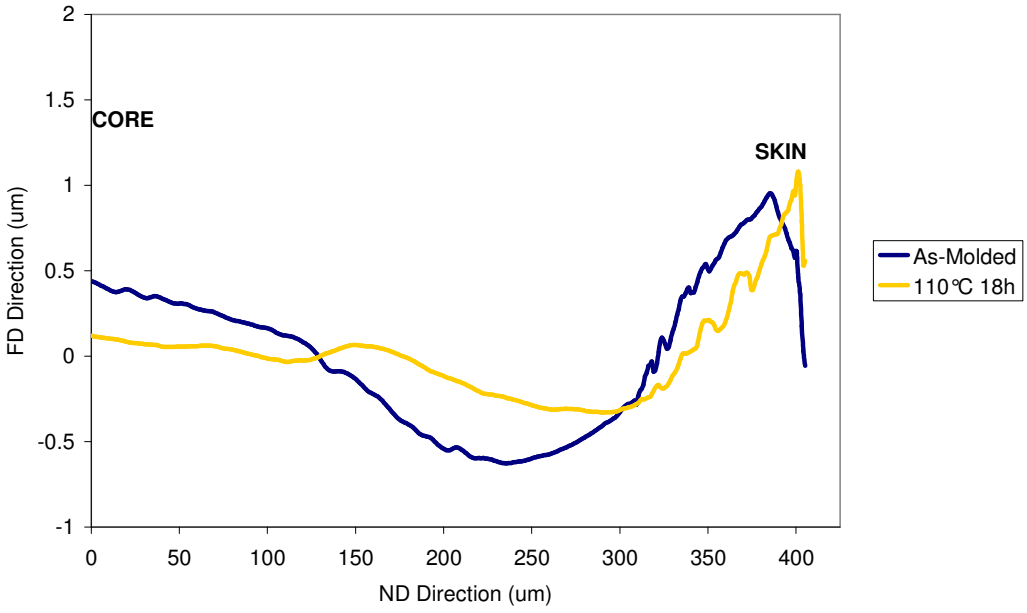

Figure 2-27: Line scans of as-molded and stress relieved aluminum molded parts taken "Near" the gate and flow "Into" sample

The shish-kabob structure in the shear zone formed during injection molding is such that the "shish" or highly elongated chains are oriented in the direction of the flow (Pennings, 1977). When the sections are taken parallel to the flow or the "shish" there is no release of the elongated orientation. In contrast, when sections are taken perpendicular to the flow, sectioning the elongated chains, there is a release of that elongation stress, as shown schematically in Figure 2-28.

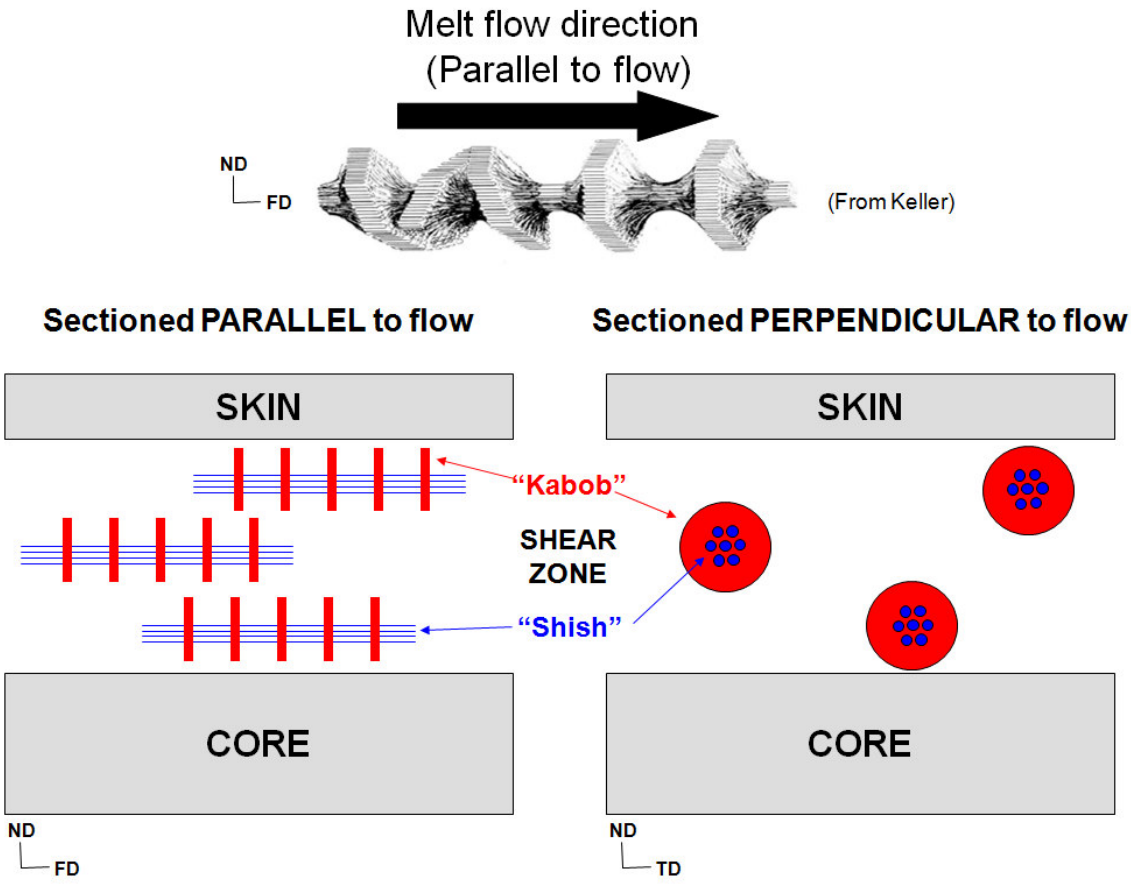

Figure 2-28: Diagram of shish-kabob structure (Pennings, 1977) and the resulting shish-kabob orientation in the thin microtomed sections

As the thin sections perpendicular to flow are being cut by the knife, the stress release caused by sectioning all of the highly elongated "shishes" in the shear zone causes a contraction ($-\sigma_{FD}^{shearzone}$) in the flow direction (FD direction). This contraction, in the shear zone only, in the FD direction must be balanced by an

expansion in the transverse plane. Since the part of the section still attached to the block prevents movement in the normal direction (ND), the expansion is entirely taken up in the transverse direction ($-\sigma_{FD}^{shearzone} = +\sigma_{TD}^{shearzone}$) (Figure 2-29). Due to the fixed length of the core and skin, the expansion of the shear zone in the FD direction is accommodated by wrinkling.

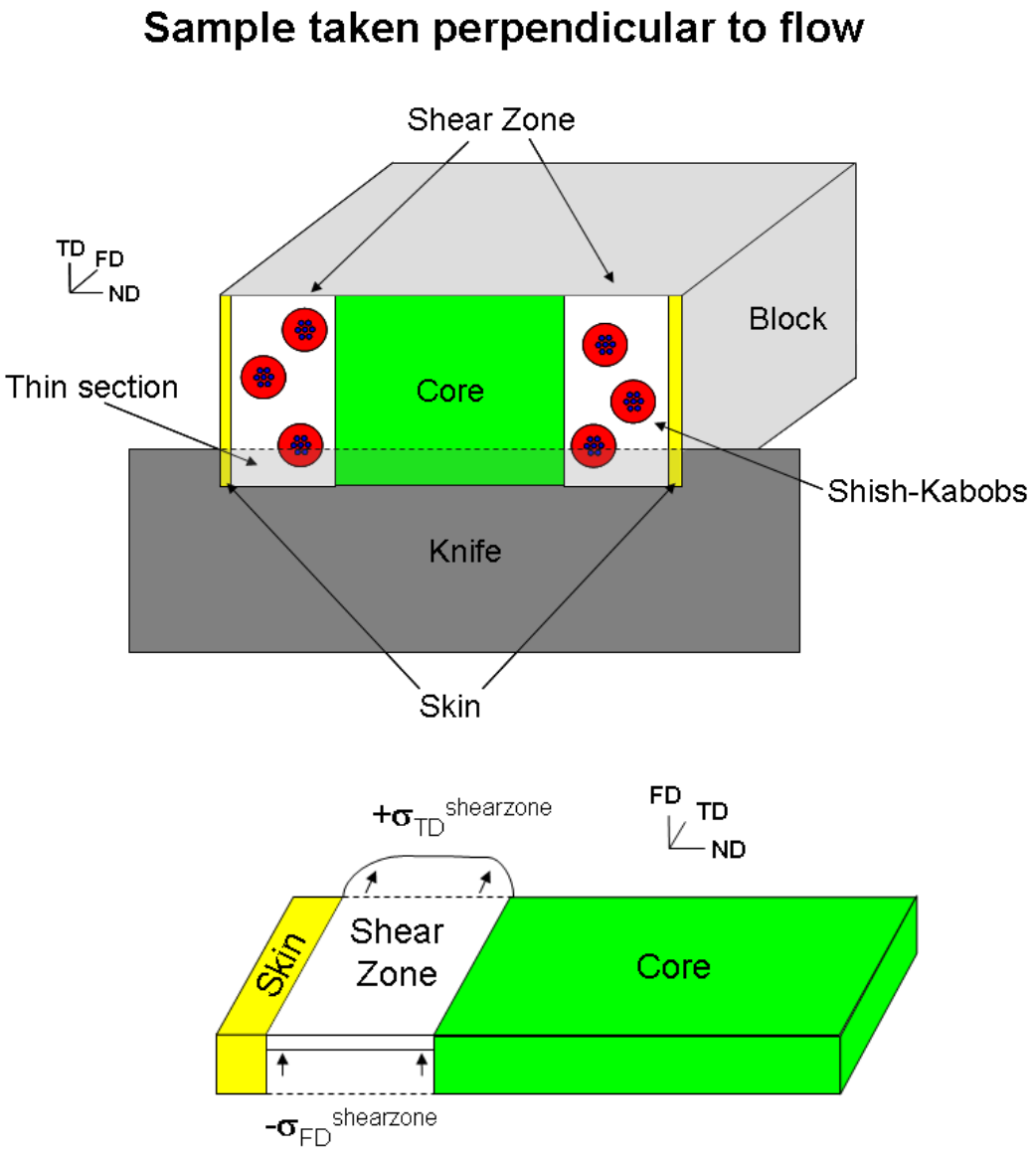

Figure 2-29: Diagram of stresses causing wrinkling of shear zone during thin sectioning

2.4.C Low Temperature Impact Testing

Previous results showed the morphology and amount of stress in the shear layers varied depending on the processing conditions, part geometry and mold material. To determine whether this had an effect on mechanical performance, low temperature impact behavior, which is sensitive to surface conditions, was used to evaluate two extreme conditions: aluminum molded, fast injection speed and steel molded, slow injection speed.

For impact testing, 5 samples of each condition were tested at -40°C with a speed of 2.2 m/s. The (tangential) flexural modulus (*E*) was calculated using elastic beam theory (Equation 2-3) (Standard Test Methods for Flexural Properties of Unreinforced and Reinforced Plastics and Electrical Insulating Materials 2008), where *L* is the span length, *W* is the measured specimen width, *B* is the measured specimen thickness, and *m* is the best fit slope of the linear portion of the load/displacement curve.

$$E = \frac{L^3 m}{4WB^3}$$ **Equation 2-3**

The flexural modulus results are reported in Figure 2-30 and do show an effect of flow direction. The samples taken perpendicular to the material flow have a flexural modulus that is ~25% lower than samples taken parallel to the flow. Neither the flow length, nor whether the sample was molded using steel or aluminum tooling had a significant effect on the flexural modulus. The differences seen are likely due to the orientation with the direction of the flow, which when running along the length of the sample bar would offer greater strengthening than when perpendicular to it.

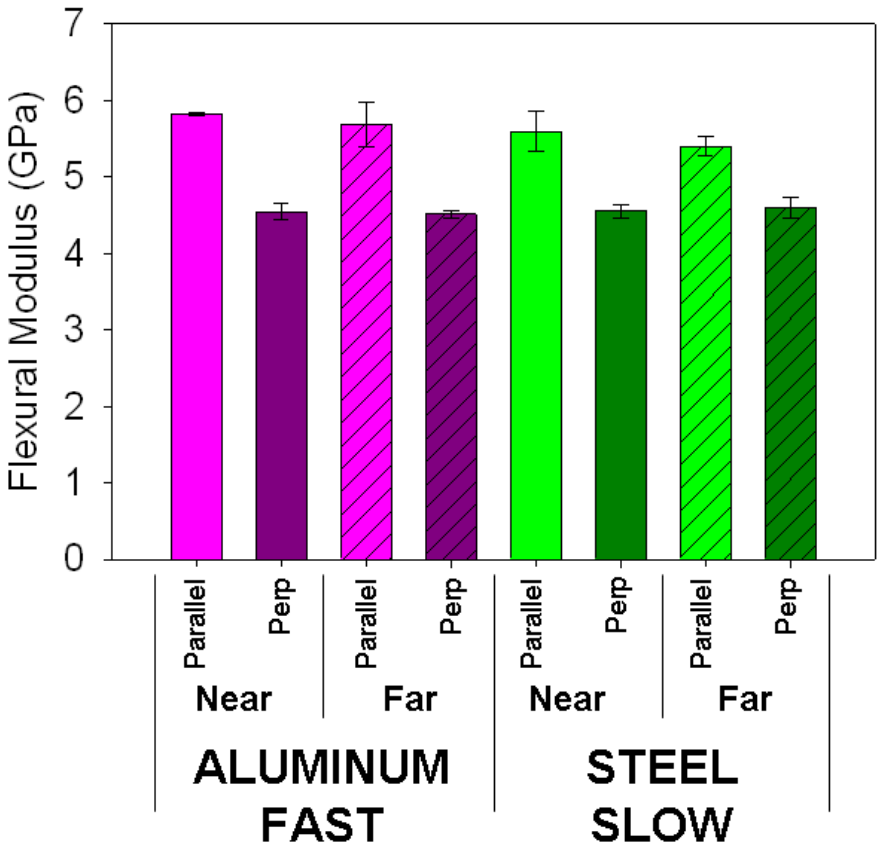

Figure 2-30: Flexural Modulus results of 2.2 m/s impact at 40°C as a function of geometry and mold material

Flexural strength, or maximum flexural stress was calculated with Equation 2-4, where *P* is the maximum load during impact.

$$\sigma = \frac{3PL}{2WB^2} \qquad \textbf{Equation 2-4}$$

The flexural strength results are shown in Figure 2-31, and like the flexural modulus, show a reduction in the samples taken perpendicular to the material flow compared to those taken parallel to the flow. There was a small increase in flexural strength for the aluminum molded samples taken far from the gate, and perpendicular to flow, but everything else was within one standard deviation.

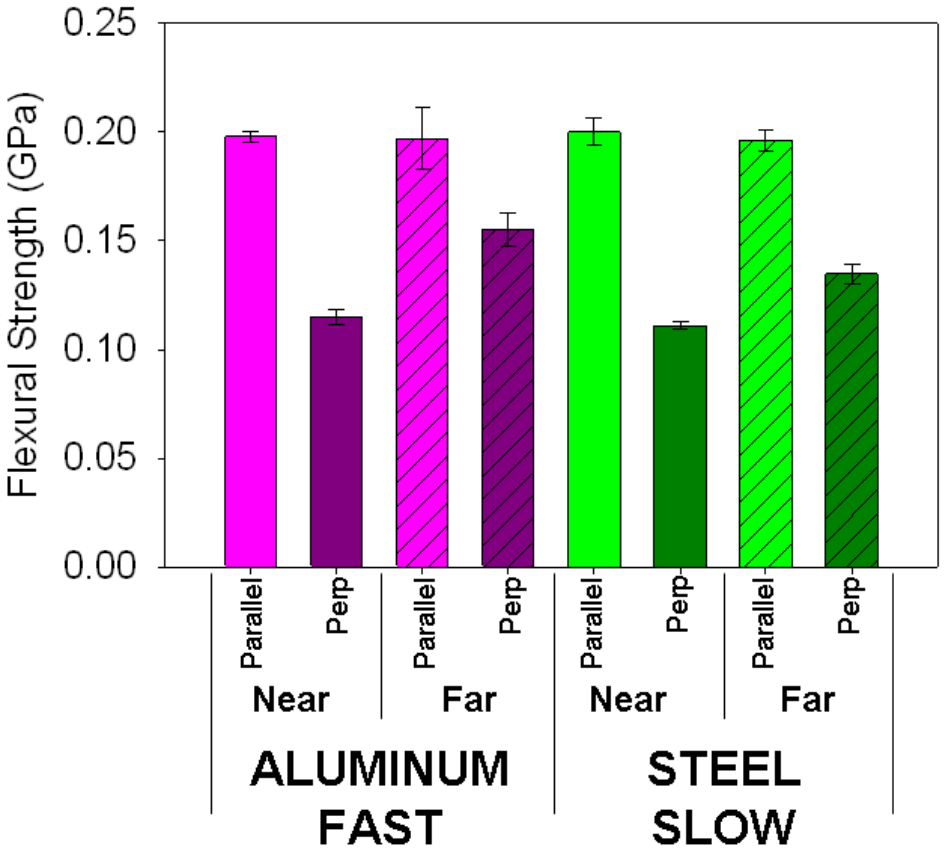

Figure 2-31: Flexural strength results of 2.2 m/s impact at -40°C as a function of geometry and mold material

2.4.D X-Ray Photoelectron Spectroscopy (XPS)

XPS was done to look for any differences in the surface chemistry that could possibly be due to the faster cooling rate of the aluminum mold compared to the steel mold. Survey examples from the surface of an aluminum molded and steel molded polypropylene plaque is shown in Figure 2-14. All of the data was normalized to the carbon (C) 1s peak and shifted to the reference value of 284.6 eV.

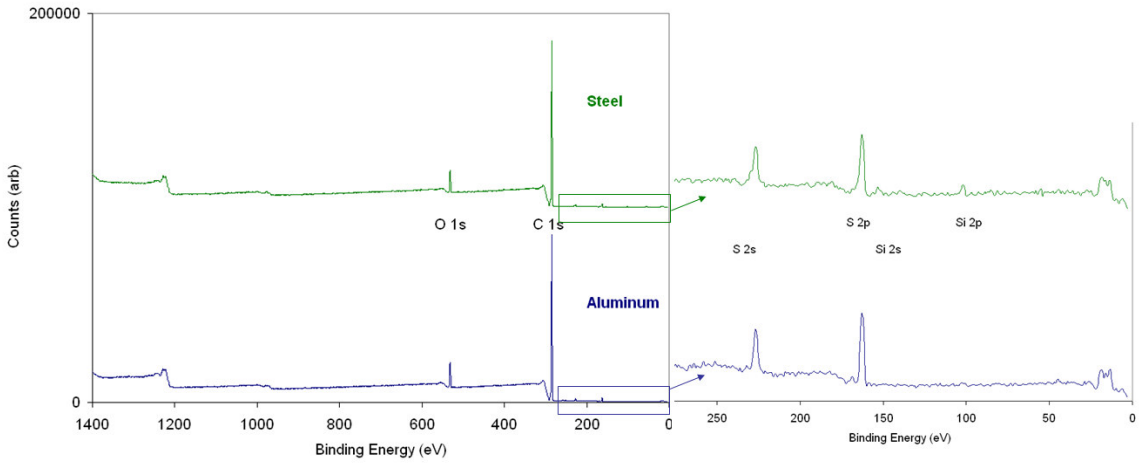

Figure 2-32: XPS of polypropylene surface molded against steel and aluminum

The quantified survey results from an average of two spots per location are shown in Table 2-3. It is assumed that any silicon present on the surface of the samples is likely due to a mold release, and since it was found in equal amounts on all of the surface samples, it was neglected in computing the quantification results.

Table 2-3: Quantification of XPS results (in % at.)

	Aluminum				**Steel**			
	Surface		Bulk		Surface		Bulk	
	Near	Far	Near	Far	Near	Far	Near	Far
C	92.36	94.20	99.00	99.23	92.45	93.89	99.49	98.87
O	6.46	5.20	1.01	0.78	6.41	5.26	0.51	1.13
S	1.19	0.61			1.14	0.86		

No differences are found in the surface of the polypropylene molded against aluminum compared to steel molds. Sulfur was found at the surface of both the aluminum and steel molded samples. This finding correlates with Mielewski's previous results (Mielewski, 1998) and is from the thio-ester used as the heat-stabilizer, typically present in ~0.5 wt% in i-PP. This additive was found to come

preferentially comes to the surface due to immiscibility and fountain flow phenomenon. Our results, which find sulfur on the surface, but not in the bulk, correlate with this finding.

Other than finding sulfur preferentially at the surface of the molded samples, and not in the bulk, the effect of mold material (aluminum and steel) and flow length (near and far from the gate) had no effect on the surface chemistry of i-PP. However, it should also be examined for other industrially relevant TPOs which have many more additives in addition to the added talc and rubber.

2.5 Conclusions

The effect of the geometry as a function of distance from and orientation to the gate was found to have an effect on the morphology of i-PP. Using optical microscopy, the size of the shear zone was found to decrease non-linearly from more than 300 μm thick to zero with increasing distance from the gate. There was no dramatic effect of cooling rate (due to mold material) or injection speed on the size of the shear zone. The distribution of the β-phase was also observed to vary as a function of distance from the gate using optical microscopy. It was found agglomerated at the bottom of the shear zone, where present, but more dispersed throughout the core in the "Far" samples that did not have shear zones. Slightly more β-phase was found in the steel molded samples, as confirmed by WAXS, possibly due to the slower growth rates in the more slowly cooled steel molded samples. Orientation to flow was only observed to affect the shear zone, which wrinkled due to stress relief when sections were taken perpendicular to the flow direction (TD).

The CLTE was measured and no effect of cooling rate (based on mold material), flow length or orientation to flow was found. Since these measurements reflected

a bulk material property, a new measurement technique was developed to measure changes in the near-surface topography as a function of temperature using optical profilometry and a hot stage. Examination of the samples before heating, at elevated temperatures, and after returning to room temperature showed that the change in the surface profile of the shear zone, causing the wrinkling seen in the optical microscopy, was not recoverable, and is therefore due to molded-in stress, not anisotropic CLTE.

Despite having the same sized shear zones, it was discovered that the steel molded samples had more molded-in stress in the shear zone that started to be relieved at a lower temperature compared to the aluminum molded samples. It was confirmed that where there was no shear zone (far from the gate) there was no molded-in stress near the surface. The molded-in stress was found to be dependant on the injection speed for the aluminum molded samples only, with the faster injection speeds having less molded-in stress and a slightly smaller shear zone (which was also observed in the optical microscopy). This is likely due to the faster cooling rate and higher injection speed creating more shear and increasing nucleation rates.

Since wrinkling was still observed in the optical microscopy of the samples that had been stress-relieved at 110°C for 18 hours, profilometry was also performed on those samples. It was found that there was still molded in stress in the shear zone, but it was greatly reduced. What remains is probably due to alignment inherent in the shish-kabob structure which cannot be relieved without fully melting the sample.

It is proposed that the wrinkling seen in the optical microscopy samples taken perpendicular to the flow (TD) is a result of sectioning the elongated "shish",

releasing that elongation stress. Since the only unconstrained direction to relieve that stress is in the transverse direction of the shear zone, the result is wrinkling. When sections are taken parallel to the flow, or along the "shish" direction, there is no release of the elongation stress.

Due to the variations seen in the morphology, impact testing and XPS were conducted to see if these differences had any effect on mechanical properties or surface chemistry for adhesion purposes. High speed impact testing, which is very sensitive to the surface conditions, showed no difference in the flexural modulus and flexural strength as a function of cooling rate (due to mold material) or distance from the gate. There was an ~20-30% reduction in both in samples taken perpendicular to the flow compared to those taken parallel to the flow, likely due to the orientation with the flow being along the length of the bar offering greater strengthening.

XPS results showed no difference in the surface or bulk chemistry of the aluminum and steel molded samples. Small amounts of sulfur were found on both surfaces, due to the preferential segregation of the thioester heat stabilizer used, but there was no effect of flow length or mold material.

This in-depth study of polypropylene homopolymer has provided great insight on the effect of processing conditions, flow orientation and mold geometry on the near-surface morphology. Although no large changes were found in the mechanical or chemical properties, this could change for TPO materials due to their more complex compositions. The foundation build in this chapter using i-PP will help interpret and understand the following work done on more industrially relevant, but harder to study, thermoplastic olefins in Chapter 3.

2.6 References

Brucato, V., S. Piccarolo, et al. (2002). "An experimental methodology to study polymer crystallization under processing conditions. The influence of high cooling rates." Chemical Engineering Science **57**(19): 4129-4143.

Cermak, R., M. Obadal, et al. (2006). "Injection-moulded [alpha]- and [beta]-polypropylenes: II. Tensile properties vs. processing parameters." European Polymer Journal **42**(9): 2185-2191.

Cermak, R., M. Obadal, et al. (2005). "Injection-moulded [alpha]- and [beta]-polypropylenes: I. Structure vs. processing parameters." European Polymer Journal **41**(8): 1838-1845.

Chen, L.-M. and K. Shen (2000). "Biaxial self-reinforcement of isotactic polypropylene prepared in uniaxial oscillating stress field by injection molding. II. Morphology." Journal of Applied Polymer Science **78**(11): 1911-1917.

Chiu, C. P. and M. C. Hsieh (1987). "The Correlation Between the Residual Stresses of ABS Terpolymers and Injection Molding Conditions." J. Eng. Mater. and Technol. **109**(2): 171-175.

Coxon, L. D. and J. R. White (1980). "Residual stresses and aging in injection molded polypropylene." Polymer Engineering & Science **20**(3): 230-236.

Dai, W., P. Lui, et al. (2003). "Self-interference flow of an isotactic polypropylene melt in a cavity during injection molding. II. Morphology and crystallinity." Journal of Applied Polymer Science **88**(12): 2791-2796.

Fitchmun, D. R. and Z. Mencik (1973). "Morphology of Injection-Molded Polypropylene." Journal of Polymer Science: Polymer Physics **11**: 957-971.

Fujiyama, M., H. Awaya, et al. (1977). "Mechanical anisotropy in injection-molded polypropylene." Journal of Applied Polymer Science **21**(12): 3291-3309.

Fujiyama, M. and T. Wakino (1991a). "Distribution of Higher-Order Structures in Injection Moldings of Particulate Filled Polypropylenes." Journal of Applied Polymer Science **43**: 97-128.

Fujiyama, M. and T. Wakino (1991b). "Distribution of higher order structures in injection-molded polypropylene." Journal of Applied Polymer Science **43**: 57-81.

Fujiyama, M., T. Wakino, et al. (1988). "Structure of skin layer in injection-molded polypropylene." Journal of Applied Polymer Science **35**(1): 29-49.

Grein, C., C. J. G. Plummer, et al. (2002). "Influence of [beta] nucleation on the mechanical properties of isotactic polypropylene and rubber modified isotactic polypropylene." Polymer **43**(11): 3279-3293.

Guerrica-Echevarria, G., J. I. Eguiazabal, et al. (1998). "Influence of molding conditions and talc content on the properties of polypropylene composites." European Polymer Journal **34**(8): 1213-1219.

"Impact Test System Model 9250HV."(2002). from http://www.instron.com/impact/9250HV.asp.

Impact Test System Model 9250HV Manual (2002). Instron Corporation.

Janeschitz-Kriegl, H. and E. Ratajski (2005). "Kinetics of polymer crystallization under processing conditions: transformation of dormant nuclei by the action of flow." Polymer **46**(11): 3856-3870.

Jang, B. Z., D. R. Uhlmann, et al. (1984). "Crystalline morphology of polypropylene and rubber-modified polypropylene." Journal of Applied Polymer Science **29**(12): 4377-4393.

Kadota, M., M. Cakmaka, et al. (1999). "Structural hierarchy developed in co-injection molded polystyrene/polypropylene parts." Polymer **40**(11): 3119-3145.

Kalay, G. and M. J. Bevis (1997). "Processing and physical property relationships in injection-molded isotactic polypropylene. 2. morphology and crystallinity." Journal of Polymer Science Part B: Polymer Physics **35**(2): 265-291.

Kantz, M. R., H. D. N. Jr., et al. (1972). "The skin-core morphology and structure-property relationships in injection-molded polypropylene." Journal of Applied Polymer Science **16**: 1279-1260.

Karger-Kocsis, J. and K. Friedrich (1989). "Effect of skin-core morphology on fatigue crack propagation in injection moulded polypropylene homopolymer." International Journal of Fatigue **11**(3): 161-168.

Katti, S. S. and M. Schultz (1982). "The microstructure of injection-molded semicrystalline polymers: A review." Polymer Engineering & Science **22**(16): 1001-1017.

Keith, H. D., J. F. J. Padden, et al. (1959). "Evidence for a Second Crystal Form of Polypropylene." Journal of Applied Physics **30**(10): 1485-1488.

Kennedy, P. (2008). The Effect of Colorants on Material Properties - is Virgin Material Data Good Enough? iMUG Conference, Dearborn, MI.

Kumaraswamy, G., A. M. Issaian, et al. (1999). "Shear-Enhanced Crystallization in Isotactic Polypropylene. 1. Correspondence between in Situ Rheo-

Optics and ex Situ Structure Determination." Macromolecules **32**(22): 7537-7547.

Kumaraswamy, G., J. A. Kornfield, et al. (2002). "Shear-Enhanced Crystallization in Isotactic Polypropylene. 3. Evidence for a Kinetic Pathway to Nucleation." Macromolecules **35**(5): 1762-1769.

Kumaraswamy, G., R. K. Verma, et al. (2000). "Shear-enhanced crystallization in isotactic polypropylenePart 2. Analysis of the formation of the oriented “skin&rdquo." Polymer **41**(25): 8931-8940.

Liu, G. and G. Edward (2001). "Correlation between morpology distribution of injection molded polypropylene and processing history identified by numerical simulation." Journal of Injection Molding Technology **5**(3): 133-140.

Mencik, Z. and D. R. Fitchmun (1973). "Texture of Injection-Molded Polypropylene." Journal of Polymer Science: Polymer Physics **11**: 973-989.

Miel, R. (2009a) "Honda hits gold with aluminum molds " Plastics News, from http://plasticsnews.com/toolbox/printer.html?id=1240847756

Miel, R. (2009b) "Metal's Monetary Magnetism " Plastics News, from http://plasticsnews.com/toolbox/printer.html?id=1240847951

Mielewski, D. (1998). Weld Line Morphology of Injection Molded Polypropylene. Department of Chemical Engineering. Ann Arbor, University of Michigan. **Ph.D.:** 137.

Padden, J. F. J. and H. D. Keith (1959). "Spherulitic Crystallization in Polypropylene." Journal of Applied Physics **30**(10): 1479-1484.

Park, J., K. Eom, et al. (2002). "Chemical Etching Technique for the Investigation of Melt-crystallized Isotactic Polypropylene Spherulite and Lamellar Morphology by Scanning Electron Microscopy." Microscopy and Microanalysis **7**(03): 276-286.

Pennings, A. J. (1977). "Bundle-like nucleation and longitudinal growth of fibrillar polymer crystals from flowing solutions." Journal of Polymer Science: Polymer Symposia **59**(1): 55-86.

Pham, H. T., C. P. Bosnyak, et al. (1993). "Residual stresses in injection molded polycarbonate rectangular bars." Polymer Engineering & Science **33**(24): 1634-1643.

Phillips, R., G. Herbert, et al. (1994). "High modulus polypropylene: Effect of polymer and processing variables on morphology and properties." Polymer Engineering & Science **34**(23): 1731-1743.

Polypropylene Handbook (2005). Munich, Hanser.

Schrauwen, B., L. Breemen, et al. (2004). "Structure, Deformation, and Failure of Flow-Oriented Semicrystalline Polymers." Macromolecules **37**(23): 8618-8633.

Siegmann, A., A. Buchman, et al. (1982). "Residual stresses in polymers III: The influence of injection-molding process conditions." Polymer Engineering & Science **22**(9): 560-568.

Standard Test Method for Linear Thermal Expansion of Solid Materials With a Push-Rod Dilatometer (2008). ASTM Standard E 228, ASTM. **E 228**.

Standard Test Methods for Flexural Properties of Unreinforced and Reinforced Plastics and Electrical Insulating Materials (2008). ASTM. **D790:** 11.

Tanem, B. S., T. Kamfjord, et al. (2003). "Sample preparation and AFM analysis of heterophase polypropylene systems." Polymer **44**(15): 4283-4291.

Touloukian, Y. S., R. K. Kiry, et al., Eds. (1978). Thermophysical Properties of Matter, Plenum Publishing Corporation.

Treuting, R. G. and W. T. Read, Jr. (1951). "A Mechanical Determination of Biaxial Residual Stress in Sheet Materials." Journal of Applied Physics **22**(2): 130-134.

Trotignon, J.-P. and J. Verdu (1987). "Skin-core structure-fatigue behavior relationships for injection-molded parts of polypropylene. I. Influence of molecular weight and injection conditions on the morphology." Journal of Applied Polymer Science **34**: 1-18.

Trotignon, J. P., J. L. Labrun, et al. (1982). "Crystalline polymorphism and orientation in injection-moulded polypropylene." Plastics and Rubber Processing and Applications **2**(3): 247-251.

"Tup 3B-SRL."(2000). from http://impact-response.com.

Turner-Jones, A., J. M. Aizlewood, et al. (1964). "Crystalline Forms of Isotactic Polypropylene." Makromolekulare Chemie **75**: 134-158.

Wenig, W. and F. Herzog (1993). "Injection molding of polypropylene: X-ray investigation of the skin-core morphology." Journal of Applied Polymer Science **50**(12): 2163-2171.

Wright, D. G. M., R. Dunk, et al. (1988). "The effect of crystallinity on the properties of injection moulded polypropylene and polyacetal." Polymer **29**: 793-796.

Zipper, P., A. Janosi, et al. (1996). "Comparative X-ray scattering, microscopical, and mechanical studies on rectangular plates injection molded from

different types of isotactic polypropylene." Polymer Engineering & Science **36**(4): 467-482.

Chapter 3

Effect of Cooling Rate and Surface Treatment on Rubber Morphology and Paint Adhesion of Compounded and Reactor Grade TPO

3.1 Introduction

In automotive applications, polypropylene is typically modified with fillers such as rubber, talc, additives, heat stabilizers and other materials that improve properties, lower cost, and improve molding capability and paintability (Kiland, 2001; Ryntz, 2005; Deng, 2009). Ethylene-propylene rubber (EPR) and Ethylene-Propylene-Diene (EPDM) are the most common types of rubber used, and they can be reactor-polymerized or compounded (Maier, 1998). The amount of rubber used depends on the application and the required balance between strength and toughness, with the ultimate tensile strength and modulus decreasing and impact strength increasing with increasing rubber content up to 30-40% (Karger-Kocsis, 1987; Bedia, 2000). The rubber is the dispersed phase in the iPP matrix at concentrations up to approximately 70% before there is a phase inversion (Ho, 1981; Ghijsels, 1982; D'Orazio, 2001), and is the configuration referred to hereafter unless otherwise stated.

In amorphous polymers like polystyrene and poly(methyl methacrylate), rubber additions do not significantly affect the matrix. But for semi-crystalline polymers, like polypropylene, the rubber domains do affect the nucleation and crystallization kinetics (Coppola, 1987). The resulting spherulitic and macro morphology is strongly dependent on processing conditions (Pasquini, 2005;

Zhong, 2005) and the properties of the rubber, matrix, and any other components (such as talc) (D'Orazio, 2001; Strebel, 2004).

Using the knowledge gained from studies on neat isotactic polypropylene (iPP), the effects of processing on the morphology and properties of both compounded and reactor grade TPOs is investigated in this chapter. Again, this will be the first in-depth investigation of the effects of molding parameters, flow length and orientation on TPO, factors which were all found to have an effect on the near surface morphology and properties of polypropylene in Chapter 2. There is less literature pertaining to TPO in the public domain, partially due to the wide variety of possible formulations and the challenges in examining the microstructure. Like the i-PP research in Chapter 2, there are only a few papers that investigate the morphology as a function of molding parameters or orientation on injection molded TPO morphology (Ono, 2005; Zhou, 2005), and those are on small (<150 mm) samples and did not investigate the effect of flow length. Since TPO materials are used in large parts in the automotive industry (fascias can be up to 1.5 m long), this work examining larger plaques (300 mm) and the effect of flow length on morphology. This information will be used to improve the molding and performance of these large parts used in the automotive industry, saving time and money in production.

This study is also the first investigation of the effect of considerable changes in the heat transfer rate from the melt to the mold, through the use of aluminum tooling, on the resulting morphology and properties of TPO. The effect of the dramatic change in cooling rate on the surface microstructure is more important to understand on the industrially relevant TPO materials, since there is likely to be more variation due to wide formulation ranges. Also, a significant portion of automotive TPO components are painted, and adhesion mechanism is strongly dependent on the surface morphology and chemistry. A better understanding of

the effect of processing and material composition will help to predict behavior in the field and make improvements in both future and existing parts.

This chapter builds on the results from Chapter 2, using the techniques developed to look at residual stress in the shear zone, and develops new techniques to look at details in the microstructure that are no longer visible using optical microscopy as a function of molding conditions and geometry. Due to the ever-changing formulations for the matrix, talc, rubber and other additives, it is difficult to directly compare the different TPO formulations to each other or to neat polypropylene. This chapter opens with a literature review of work done on TPO morphology to date. The experimental work begins with an optical microscopy inspection, which proves to be not nearly as informative as with neat polypropylene due to the smaller-scale microstructure. Since the morphology could not be observed in any detail with optical microscopy, higher resolution techniques including Atomic Force Microscopy (AFM) and Transmission Electron Microscopy (TEM) were utilized for improved resolution to help understand the effect of processing conditions and geometry. X-ray Photoelectron Spectroscopy (XPS) was also utilized to compare the effect of cooling rate and material composition on the surface chemistry. Comparisons of the coefficient of thermal expansion (CLTE) and optical profilometry of cross-sections as a function of part temperature to the polypropylene results were used to understand the effect of the rubber, talc and other additives on the bulk morphology. The effect of the geometry, material and processing factors, as well as various surface treatments, were correlated with adhesion performance.

3.2 Literature Review

3.2.A Spherulitic Morphology

Most authors have found the rubber inclusions act as a nucleator, resulting in smaller, more irregular PP spherulites in the matrix and a decrease in the non-crystalline fraction (Karger - Kocsis, 1979; Coppola, 1987; Karger-Kocsis, 1987; Zhang, 2002) compared to neat i-PP. As little as 5% EPR added reduced the spherulite size by more than 50% (Karger - Kocsis, 1979). The α-spherulites in the TPOs tended to have more positive birefringence (Type I) (Yokoyama, 1997) and the amount of β-phase decreased with increasing rubber content (Karger - Kocsis, 1979; Ho, 1981; Cakmak, 2000).

Depending on the properties of the added rubber and the crystallization conditions, the rubber has been found in both inter- and intraspherulitic positions (Coppola, 1987; Karger-Kocsis, 1987; Yokoyama, 1997). During isothermal crystallization, the rubber particles were found predominately in interspherulitic positions during slow cooling, resulting in some coalescence of the rubber particles. During faster cooling, the rubber gets trapped by the fast PP spherulite growth, resulting in a more homogenous rubber distribution (Coppola, 1987).

The rubber particle microstructure can affect the crystallization process and the inner structure of the spherulites including crystalline lamellar thickness and amorphous interlayer thickness (D'Orazio, 1999). The rubber particle microstructure can be affected by the type of material used, such as EPR vs. EPDM and the composition and stereospecificity of the given rubber. The ethylene content of EPR was found to change the morphology of the rubber inclusions, moving from a single semi-crystalline polyethylene core in an amorphous rubbery ethylene-propylene shell at low ethylene concentrations, to a rubbery shell with multiple semi-crystalline polyethylene cores (Kim, 1998). The

stereospecificity of the EPR (dictated by the catalyst used) was found to affect the formation of the rubber in the blend. Rubber generated from a titanium based catalyst (higher stereospecificity compared to the traditional vanadium catalyst) had a much finer dispersion in the matrix, but for rubbers from both catalysts the dispersion coarseness increased with an increasing viscosity ratio (D'Orazio, 1999).

3.2.B Macro Morphology

Typically, the morphology of TPO is considered to consist of a skin and core structure much like neat iPP (Figure 3-1) (Karger-Kocsis, 1987). The skin layer, has in some instances been shown to be an essentially pure iPP layer that is 5-10 μm thick at the very surface (Karger-Kocsis, 1987; Nysten, 1999). Below that is a shear layer where the rubber is highly elongated and has been measured as anywhere from 350 μm (Ho, 1981) to 600 μm (Cakmak, 2000) to as thick as 1200 μm (D'Orazio, 1999) depending on the composition and properties of the materials used. The shear layer thickness was found to decreasing with increasing melt flow rate ratios of the rubber and matrix (Strebel, 2004), and also varied depending on processing conditions and measurement techniques. The elongation of the rubber in the shear layer is due to the high shear rates and steep thermal gradients present there(Ho, 1981). The core layer is comprised of nearly spherical rubber particles, either due to the reduced shear stress in the middle of the part or the slower crystallization time, which allows for relaxation into a spherical shape (Ho, 1981; Nysten, 1999; Zhong, 2005). The concentration of rubber increases moving in from the skin to the core (Karger-Kocsis, 1987).

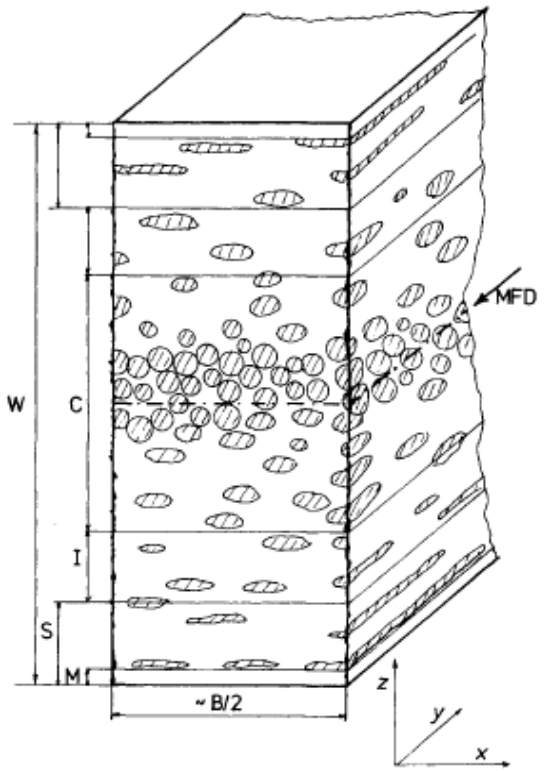

Figure 3-1: Schematic of the layered structure of TPO. C is the core with spherical rubber particles, I and S are the transcrystalline or shear zone with ellipsoidal or fibrillar rubber particles, M is the surface layer which is pure PP. MFD indicates the melt flow direction. (Karger-Kocsis, 1987)

3.2.C Morphology Evaluation

The advantages of optical microscopy are: 1) the sample preparation is relatively easy compared to other techniques because only a thin sample (1-15 μm) is needed and 2) good resolution (~0.5 μm) can be achieved over large areas (millimeters). Visualization of the skin-core morphology and the spherulites with polarized light microscopy works very well with neat i-PP as demonstrated in Chapter 2. However, additions of nucleating agents, such as talc and rubber results in a much finer, irregular spherulitic microstructure in TPO (Karger-Kocsis, 1987), making the spherulites indistinguishable at magnifications used in optical microscopy as demonstrated in Figure 3-2.

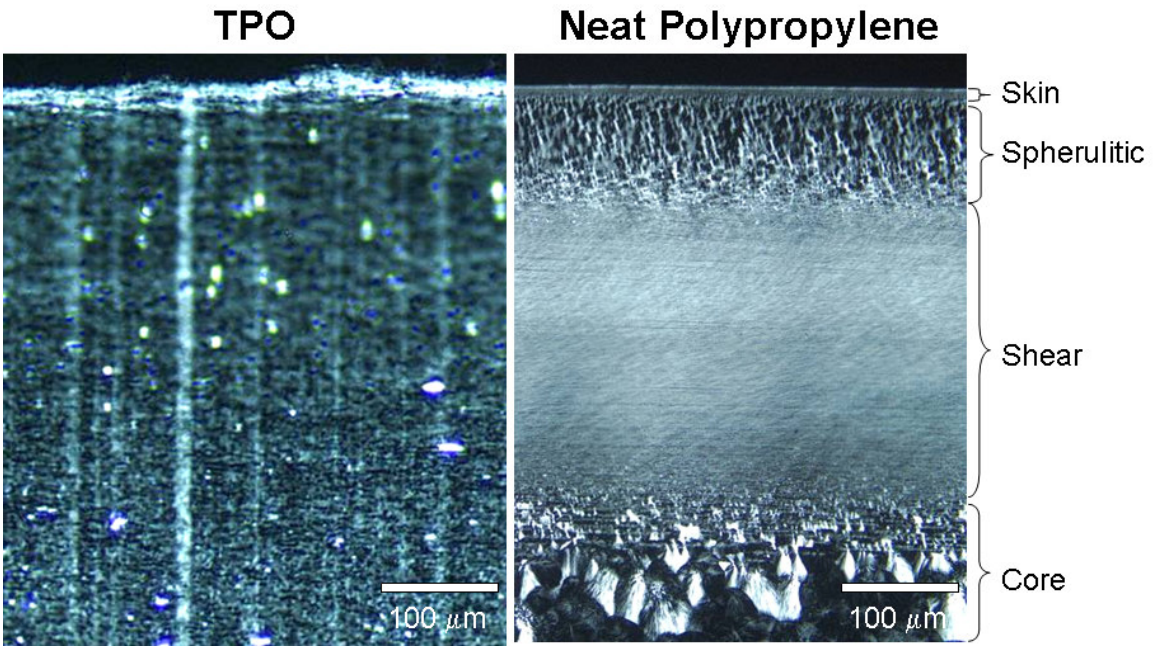

Figure 3-2: Optical microscopy of TPO compared to neat polypropylene

Electron microscopy (scanning or transmission) has been used to obtain higher resolution images of the morphology of TPO. However, contrast in electron microscopy is due to topography (SEM only) or composition (SEM and TEM), so additional sample preparation is needed to use this technique. To visualize the spherulitic or rubber morphology, etching or staining is needed. Etching removes the amorphous and lower crystallinity rubber in TPO creating topography. Staining attaches heavy metals to unsaturated bonds and low crystallinity regions (the rubber phase in TPO), providing contrast due to the difference in atomic number. In addition to these techniques, samples are typically coated with carbon, gold or another conductive metal to reduce charging. A review of these techniques can be found in Sano (Sano, 1986). Disadvantages to using these sample preparation methods include: they can be sensitive to time and temperature of beam exposure, there is no one common sample preparation method, the chemicals involved can be dangerous or toxic, and the behavior of the material(s) to the chemical is not always known.

Atomic Force Microscopy (AFM) (Nysten, 1995; Magonov, 1996; Tomasetti, 1998; Ivanov, 1999; Nie, 1999; Nysten, 1999; Tomasetti, 1999; Wu, 1999; Swaminathan, 2000; Tomasetti, 2000; Nguyen, 2001; Chang, 2002; Tanem, 2003; Choi, 2004; Lee, 2005; Pantani, 2005; Ryntz, 2005; Van Assche, 2005; Lee, 2006) can also be used to evaluate polymer morphology and material properties. There are several different operating modes for the AFM, with the two most common being Contact Mode and Tapping Mode. In Contact Mode, the tip of the probe is in constant contact with the surface and the instrument uses a feedback loop to maintain a constant deflection of the probe on the surface. The topography of the surface, as well as the lateral force on the cantilever (friction) can be measured with this technique. In Tapping Mode, the probe is oscillated slightly below its resonance frequency and contacts the sample at the bottom of the swing using a feedback loop to maintain the amplitude of the oscillation. The topography can be measured using this mode as well, and is more appropriate for use with delicate samples. Phase imaging in Tapping Mode can be used to detect areas of different viscoelastic properties within the sample due to the change in phase of the tip oscillation from contact with regions with a lower (blue) or higher (green) tan δ (Figure 3-3). In our work, the phase imaging will be used to image the softer, more viscoelastic rubber phase, which will be darker than the surrounding harder matrix.

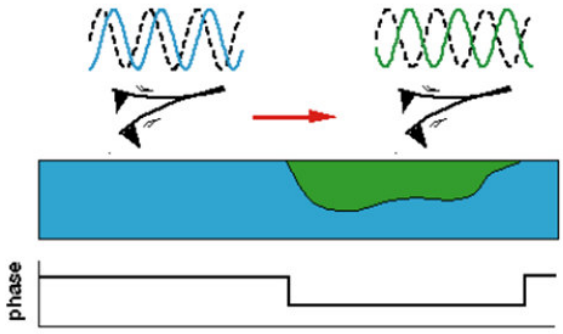

Figure 3-3: Illustration of principle of AFM phase imaging technique

Authors have used Contact Mode to detect changes in topography due to spherulite growth (Ivanov, 1999) or exposure to UV (Nie, 1999), and Tapping Mode to detect the other phases in TPOs and copolymers (rubber, talc, etc.) (Wu, 1999; Swaminathan, 2000; Nguyen, 2001; Chang, 2002; Tanem, 2003; Choi, 2004; Lee, 2005; Pantani, 2005; Lee, 2006). Force curves taken during AFM can provide information on modulus (Tomasetti, 1998; Tomasetti, 1999; Tomasetti, 2000) and adhesion forces at the surface (El Ghzaoui, 1999; Gu, 2004). Advantages to AFM are high resolution (1 - 10 nm, depending on tip and sample geometry, AFM hardware), imaging over relatively large areas (100 μm x 100 μm) with no alteration of the chemistry of the sample (etching or staining) and no issues with degradation from an electron beam.

3.2.D Effect of Morphology on Properties

Theories on how the rubber inclusions improve the ductility of polypropylene include: changing the stress state in matrix around particles by inducing crazing, shear yielding, cavitation and particle stretching, tearing and debonding (Karger-Kocsis, 1987; Kim, 1996; Petrovic, 1996; Kim, 1998; Tang, 2003); decreasing the noncrystalline component and the spherulite dimensions due to nucleation effect of the rubber, which results in a higher degree of interconnection via tie molecules and a lubricating effect acting on the matrix during the transformation from a spherulitic structure to a fibrillar one during mechanical deformation (Coppola, 1987). Therefore, the properties of the starting materials (matrix and inclusions) as well as their morphology are expected to have a strong role in determining impact behavior.

Tensile yield stress and modulus in TPOs were found to decrease with increasing rubber content, but the elongation at break and impact strength improved (Coppola, 1987; Karger-Kocsis, 1987; Choudhary, 1991; Petrovic, 1996; D'Orazio, 1999; Bedia, 2000; Pasquini, 2005). The impact strength of the

blends depended on average rubber particle size and distribution, average spherulite size but not phase (Grein, 2002), and crystallinity. Crazing and shear yielding can both occur without interference in systems with an average particle size of less than ~0.6 μm, which improves the impact strength (Karger-Kocsis, 1987). However, in systems with larger particles, the shear bands stop craze propagation, leading to only moderate impact strengths (Karger-Kocsis, 1987). Higher levels of polypropylene in the EPR results in better compatibilization with the PP matrix, and higher elongation to break when compared with blends of equal amount of rubber containing less polypropylene (Nomura, 1995). Additions of PE to the EPR rubber induced a core-shell morphology which improved the impact strength and elongation to break, but had no other effect on mechanical properties (Petrovic, 1996). Talc additions with the rubber always decreased the modulus, but low levels (<5%) can increase the elongation at break (Long, 1996). At higher volumes, the talc decreased the elongation at break due to increased cavitation (Long, 1996; Guerrica-Echevarria, 1998). PP and talc blends without rubber showed an increase in modulus with a constant yield stress when talc was varied between 10-40% (Guerrica-Echevarria, 1998).

Paint adhesion is another important material property, especially in the automotive industry where most of the TPO is painted. Polypropylene has a low surface energy (~ 30 mJ/m^2) (Ryntz, 2005), which leads to poor wettability. It also lacks polar functionality, and has good resistance to solvents. These properties make paint adhesion to polypropylene difficult to acheive (Ryntz, 2005). Addition of amorphous elastomer rubber improves adhesion slightly, but typically surface modifications such as plasma treatment, ultraviolet irradiation (Nie, 1999), or chlorinated polyolefin (CPO) adhesion promoter primers are still needed (Morris, 1998).

The effect of rubber morphology at the surface has been studied by several authors. Some authors have found a thin (≤ 5 μm) layer of essentially pure polypropylene at the surface (Ryntz, 1996; Morris, 1998; Tomasetti, 1998; Tomasetti, 1999; Tang, 2002; Tang, 2003; Ryntz, 2005), while others have found rubber nodules at the surface (Mirabella, 2000; Tomasetti, 2000). One author found very thin (nm) layers of heat stabilizer materials (thio-esters) covering the surface of an injection molded industrial polypropylene (Mielewski, 1998). This was determined using XPS and was theorized to have occurred due to fountain flow of incompatible droplets in the polypropylene matrix. These layers, as well as other possible additives that could be on the surface could have an impact on surface mechanical behavior and adhesion.

The morphology of the rubber and the degree of crystallinity at the surface was found to have a large impact on adhesion performance, especially if a CPO adhesion promoter is used (Ryntz, 1996; Mirabella, 2000). Having a higher viscosity ratio between the rubber and the polypropylene promotes thinner, sheet-like rubber closer to the surface as opposed to the almost spherical rubber formed in low viscosity ratio samples and lower crystallinity at the surface promotes adhesion (Nysten, 1999), but this must be balanced with cohesive failures (Tang, 2002).

Most paint adhesion testing is qualitative in nature, such as scribe and tape pull testing (ASTM D3359). Because of the variability in this test, and to better understand durability performance, other qualitative tests are also used to determine the adhesion performance including: immersion testing (ASTM D870), thermal shock (ASTM 6944), scratch, mar and abrasion resistance (ASTM D4060, D5178), and impact testing at various temperatures (ASTM 2794). Recently, a more quantitative adhesion test was developed where an aluminum stub is glued to the surface of the coating and the tensile force needed to remove

the coating is measured (ASTM 5179). While this method is indeed more quantitative, it involves specialized lab equipment, flat surfaces and the correct adhesive so that the failure occurs between the paint and the substrate, not between the stub and the paint.

Professor Martin's group has demonstrated a quantitative adhesion test that does not necessarily involve special equipment and eliminates the possibility of the failure between the stub and the paint interface (Tang, 2001). Tensile forces are generated by either placing the painted surface in tension using either an Instron or a mandrel bend (elastica). This tensile stress produces a shear stress between the coating and substrate due to the difference in elastic moduli between the paint and polymer.

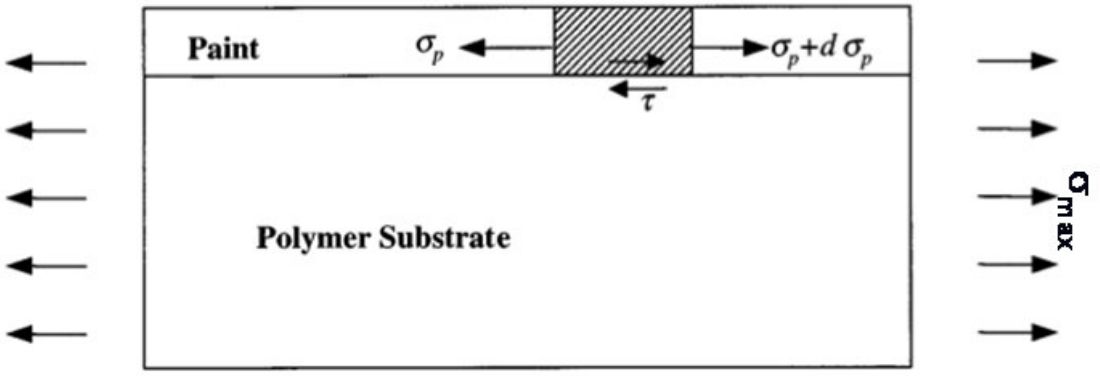

Figure 3-4: Using tension to create a shear stress at the paint/polymer interface for quantitative adhesion testing(Tang, 2001)

The shear strength of the interface (τ) can be calculated from the tensile strength of the paint (σ_{max}), the film thickness (h_p) and the crack spacing at saturation ($\bar{l}$) using Equation 3.1:

$$\tau = 1.337\, h_p \frac{\sigma_{\max}}{\bar{l}}$$

Equation 3.1

3.3 Experimental

Plaques (100mm x 300mm x 3.5 mm) with a 100mm fan end gate were molded out of Hifax TYC 773P compounded TPO with ~ 12% talc, and Hifax CA 387 reactor grade TPO which contains no talc (LyondellBasell, USA) on a 350 ton Van Dorn press. Various combinations of processing conditions were used and are shown in Table 3-1. The nozzle temperature was 216°C, and both halves of the mold were set at 21°C. Actual mold temperatures after start-up ranged from 54-63°C depending on mold material and injection speed (aluminum tool and slower injection speeds were cooler). The injection pressure was 500 bars. The injection molding machine used to make the plaques did not have a quantitative measure of injection speed, but two different speeds were examined with the "Fast" injection speed being representative of typical industrial processing speeds (~90 mm/s) and approximately 5 times faster than the "Slow" injection speed (~10 mm/s). End gated plaques were chosen because they offered the greatest understanding of the direction of material flow to study the effect of sample orientation.

Table 3-1: DOE of Process Variables for Injection Molding of TPO Samples

Resin	Mold Material	Flow Rate*
773 Compounded	Steel	Slow
		Fast
	Aluminum	Slow
		Fast
387 Reactor Grade	Steel	Fast
	Aluminum	Fast

*Flow rate was measured qualitatively on the injection molding machine where Fast ≈ 5 Slow

For all of the experiments except for the CLTE measurements, painted plaques were used. Plaques in each molding condition were painted using either a traditional adhesion promoter (Ad-Pro) or a flame surface treatment to examine the effect of each on surface morphology. Before their respective surface treatments, the plaques were power-washed. After surface treatments, the set of samples with PPG MPP4100 Adhesion Promoter was flashed for 5 minutes prior to basecoat application. Both the samples with the Ad-Pro and the flame treated samples were then painted at the same time with an Oxford White PPG CBC8554 1K basecoat, flashed for 5 minutes, and then a PPG TKU2000C 2K clearcoat was applied. After the clearcoat, plaques were flashed for 10 minutes and then baked for 30 minutes at 121°C. The layer thicknesses are shown in (Table 3-2).

Table 3-2: Layer thicknesses of painted TPO plaques

Layer	Layer Thickness (μm)	
	Set 1	Set 2
PPG Adhesion Promoter	N/A*	8
PPG 1K White Base Coat	33	33
PPG 2K Clearcoat	40	40

*flame treated

3.3.A Optical Microscopy

Thin sections (5 μm) were cryomicrotomed using a glass knife at 5°C. This temperature was chosen to make the block sufficiently hard to cut smoothly without stretching the sample, but not become brittle (below T_g). Samples were microtomed perpendicular to thickness to prevent compression. The thin slices were sandwiched between a glass slide and coverslip using immersion oil (Cargille Type A), and the "Class A" surface was examined under crossed polars in an optical transmission light microscope.

3.3.B Surface Profilometry

A sample cross-section was first polished to a 0.3 μm finish using alumina suspensions. The surface profile of the cross-sections was measured using a Wyko NT3300 optical profilometer (Veeco Instruments, USA). A programmable INSTEC HCS402 hot stage was used along with the Wyko to raise the temperature of the sample. Samples were equilibrated at a given temperature for at least 10 minutes (until the image had stabilized) before the measurements were taken. All of the scans were filtered using Wyko software to remove any sample tilt, and the background (room temperature) scans were subtracted from the elevated temperature measurements and results were averaged across the sample for the line scan data.

3.3.C Coefficient of Linear Thermal Expansion (CLTE)

The coefficient of linear thermal expansion (CLTE) was measured using a dual pushrod Dilatronic dilatometer (Theta Industries, Inc., USA) with 50 mm. X 8 mm. full thickness samples with the edges polished to 400 grit. The samples were run from 30°C to 100°C at a rate of 0.5°C per minute and compared to a NIST fused silica reference (SRM 739).

To investigate the possibility of an anisotropic CLTE, samples were taken from plaques in different orientations and at different distances from the gate, as shown in Figure 2-17. The effect of orientation was studied by samples taken perpendicular to the flow (red shading) and parallel to the flow (blue shading). The effect of distance from the gate (amount of anisotropic shear zone) was studied by taking the samples at varying distances from "Near" or starting at ~50 mm from the gate (darker shades) to "Far" or ending at about 250 mm from the gate (lighter shades).

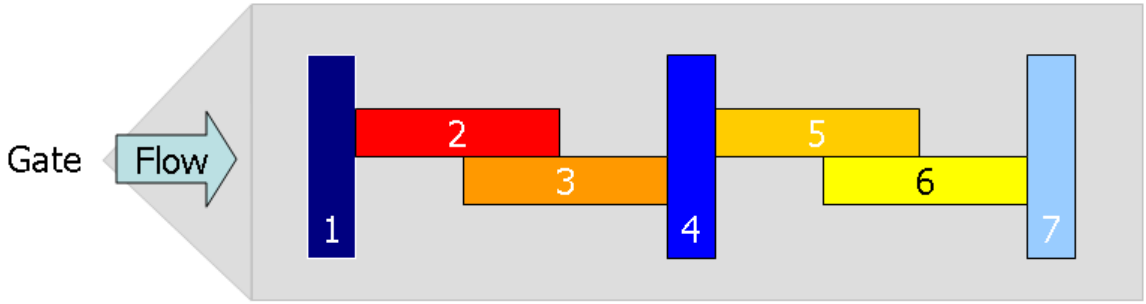

Figure 3-5: Schematic of CLTE sample orientation and location

3.3.D Atomic Force Microscopy

Sample preparation for adequate imaging of cross sections near the as-molded surface proved to be a difficult task. Several attempts to embed un-painted samples in various media (epoxy, wax, etc.) were unsuccessful due to the lack of adhesion with the low surface energy polymers, especially with the force needed to clamp the sample in the microtome chuck for sectioning without chatter. The surface does not microtome flat (possibly due to the difference in CLTE between the polymer and the epoxy), and the gap between the epoxy and the polymer make it difficult to image using AFM because the tip falls off the sample, into the gap, causing artifacts in the image (Figure 3-6).

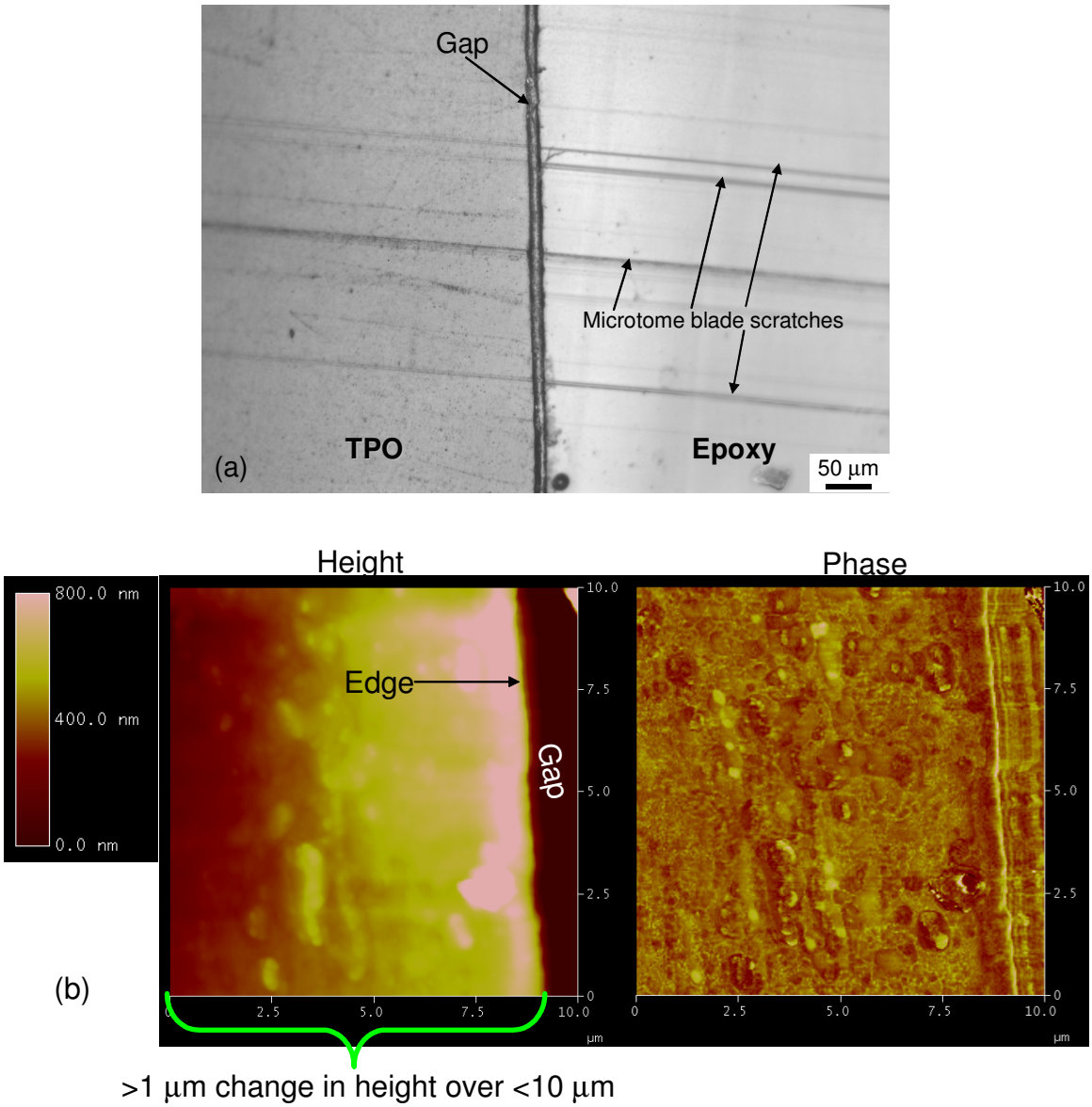

Figure 3-6: (a) optical and (b) AFM images of embedded, uncoated TPO

Because understanding the near-surface morphology is very important for our study of coating adhesion, painted plaques were used to study the effect of processing conditions and geometry. Microtoming painted plaques allowed for flatter cross-sections and better AFM imaging of the near-surface morphology, but the possible effects of the painting process must be considered.

Samples were removed from the plaques in two locations to assess the effect of flow length. "Near" samples were taken approximately 50 mm from the gate while "Far" samples were taken approximately 250 mm from the gate. Orientation parallel and perpendicular to the flow was assessed at both sites and found to be the same for the length-scale examined for all combinations of variables, therefore only samples taken parallel to flow are shown for simplicity. Both height and phase data was collected with a Veeco Nanoscope V controller and Multimode AFM in tapping mode with TESP silicon nitride tips.

3.3.E Transmission Electron Microscopy

Samples were prepared and examined by Jihua Chen in Professor Martin's group at the University of Michigan. Samples of 773 compounded TPO molded with aluminum and steel tooling were stained with RuO_4 for 1 hour (Tang, 2003). The stained blocks were sectioned to a ~70 nm thickness using an oscillating Diatome Diamond Ultramicrotome knife for examination in the Phillips CM12 TEM equipped with X-ray Energy Dispersive Spectroscopy (XEDS) at 120keV.

3.3.F X-Ray Photoelectron Spectroscopy (XPS)

X-ray Photoelectron Spectroscopy (XPS) was done on a Kratos AXIS 165 Electron Spectrometer (Kratos Analytical, England) using a monochromatic Al Kα (1486.6 eV) source operated at 12 kV and 20 mA. Data was collected using hybrid mode magnification. A 20 eV pass energy was used for high resolution spectra, and an 80 eV pass energy was used for surveys. Data analysis was completed using manufacturer provided software. Binding energies were referenced to the aliphatic carbon 1s line at 284.6 eV.

3.3.G Adhesion Testing

Plaques of 773 compounded TPO were painted with a PPG MPP4100 Adhesion Promoter, PPG CBC8554 1K white basecoat, and PPG TKU2000C 2K clearcoat paint system as described in the beginning of the Experimental section. Sets of samples were also produced with a second and third pass of the basecoat/clearcoat in order to understand the effect of changing σ_{max} and h_p with increasing layers of paint. The adhesion samples were prepared and analyzed by Brenda Vyletel of Professor Martin's group at University of Michigan. For both the Instron tensile and elastica tests the samples were cut into 10 cm x 1 cm bars and the edges were polished to a 9 μm finish to minimize edge effects. The tensile samples were pulled at a rate of 1 mm/min, though there was found to be no effect of strain rate on results up to rates as high as 4 mm/min. The elastica samples were bent around a 16mm diameter tube.

3.4 Results and Discussion

3.4.A Optical microscopy

While shear regions were not able to be resolved in the optical microscopy of TPO, wrinkling, similar to that found in the neat polypropylene shear zones, was found in the 387 reactor grade samples. Figure 3-7 shows samples from the steel molded compounded and reactor grade TPOs and the neat polypropylene taken near the gate with the flow going into the sample (TD). The layers on the top of the TPO samples are paint. Some wrinkling (though not to the same degree) was found in the reactor grade TPO sample in the region where the shear zone was found in the neat polypropylene. No wrinkling was seen in the 773 compounded TPO.

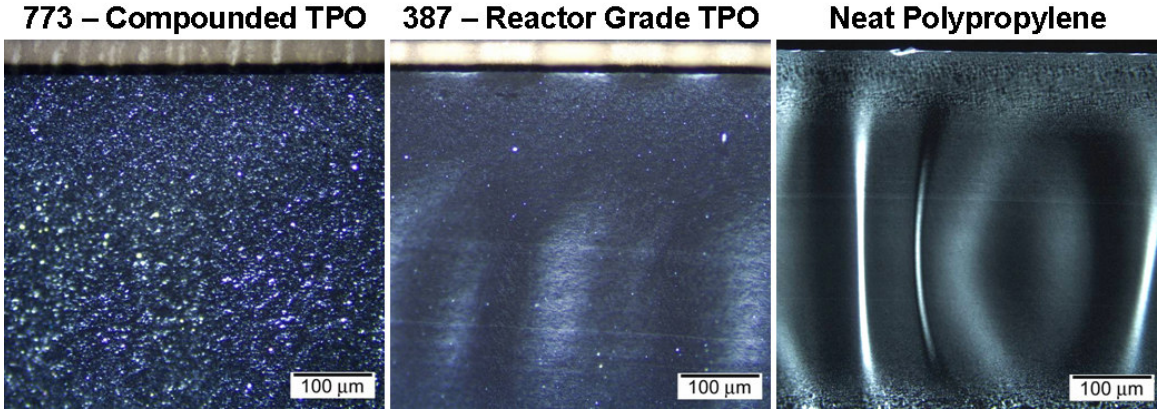

Figure 3-7: Optical microscopy comparison of steel molded TPO and neat polypropylene taken near the gate, flow into the sample

In Chapter 2, the wrinkling was found to be related to the high amount of molded-in stress of the shear layer due to the orientation of shish-kabob microstructure. The presence of wrinkling in the reactor grade sample, which has no talc, but not in the compounded sample with talc, suggests that accelerated nucleation due to the talc is affecting the size, microstructure, and/or degree of alignment of the shear zone (Fujiyama, 1991; Velasco, 1996).

3.4.B Surface Profilometry

This behavior was investigated further using the hot stage and optical profilometry technique developed and described in Chapter 2. There was no difference found in the size or amount of shrink in the shear zone between the steel molded and aluminum molded part for either material (Figure 3-8). There was a difference based on material composition, where the 387 reactor grade TPO shrunk more (~0.2 µm) compared to 773 TPO (~0.1 µm) over a larger shear zone (~300 µm for 387 TPO vs. ~200 µm for 773 TPO). The size of the shear zone of 387 reactor grade TPO is about the same size as the i-PP examined in Chapter 2, but the amount of shrinkage was much less (~0.2 µm vs. ~1.5-2.5 µm). These findings confirm that faster nucleation (773 TPO > 387 TPO > i-PP)

results in smaller shear zones with less stress at the surface and explains why there is less wrinkling in the thin sections taken for optical microscopy for the TPO materials.

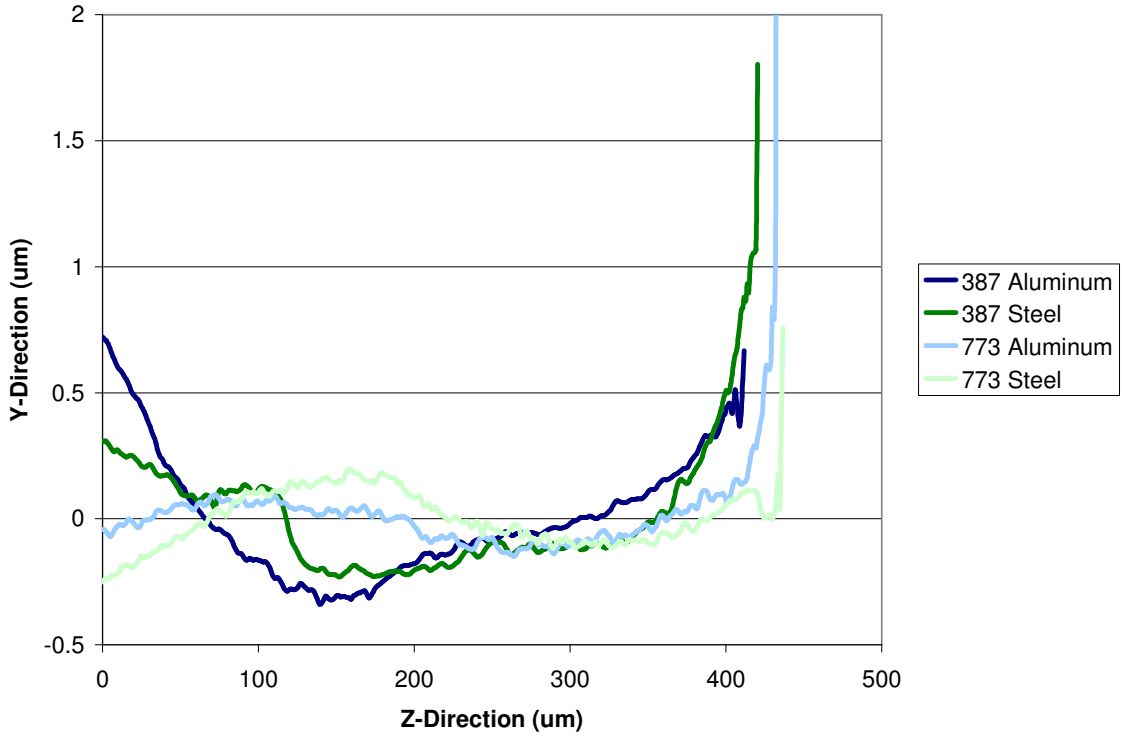

Figure 3-8: Averaged line scans of Wyko profilometry of 386 reactor grade and 773 compounded TPO at 150°C near the gate and perpendicular to flow

3.4.C Coefficient of Linear Thermal Expansion (CLTE)

The mean coefficient of thermal expansion was calculated using Equation 3-1, which is the slope of the temperature vs. expansion chart.

$$\alpha = \left[\frac{\Delta L}{L_o}\right]_{T_i}\left(\frac{1}{\Delta T}\right) \qquad \textbf{Equation 3-1}$$

Where:

L_0 = original length of specimen at temperature T_0, mm

ΔL = change in length of specimen between any two temperatures

T_i = temperature at which length is L_i, ℃

$\Delta T = T_i - T_o = 90℃ - 40℃ = 50℃$.

The coefficient of linear thermal expansion (CLTE) was studied for both mold materials for the two TPO materials (Figure 3-9). In Chapter 2, it was found that orientation to flow did not affect the CLTE of the neat polypropylene, but that is not the case with these TPO materials. A large difference was found between samples taken parallel to the flow, which were about 20-30% higher than samples taken perpendicular to the flow. This shows that the morphology of the rubber additions strongly affects the CLTE.

The CLTE of the 387 reactor grade TPO is about the same as the CLTE of the neat polypropylene measured in Chapter 2 (~$150x10^{-6}$/℃) perpendicular to the flow, but lower in directions parallel to the flow. This was not expected because typically the addition of rubber, which is a high CLTE material, increases CLTE. However, this was an industrially available resin, and not simply rubber added to an i-PP matrix, so other compositional differences could be affecting the CLTE. While the 773 compounded TPO also has rubber in it, the average CLTE is lower than both the compounded material without talc and the i-PP studied in Chapter 2, because of the addition of talc, a low CLTE material (Wu, 2004).

Like the neat polypropylene measured in Chapter 2, for the fast injection conditions there does not seem to be a significant difference in the CLTE for either material whether molded using steel or aluminum.

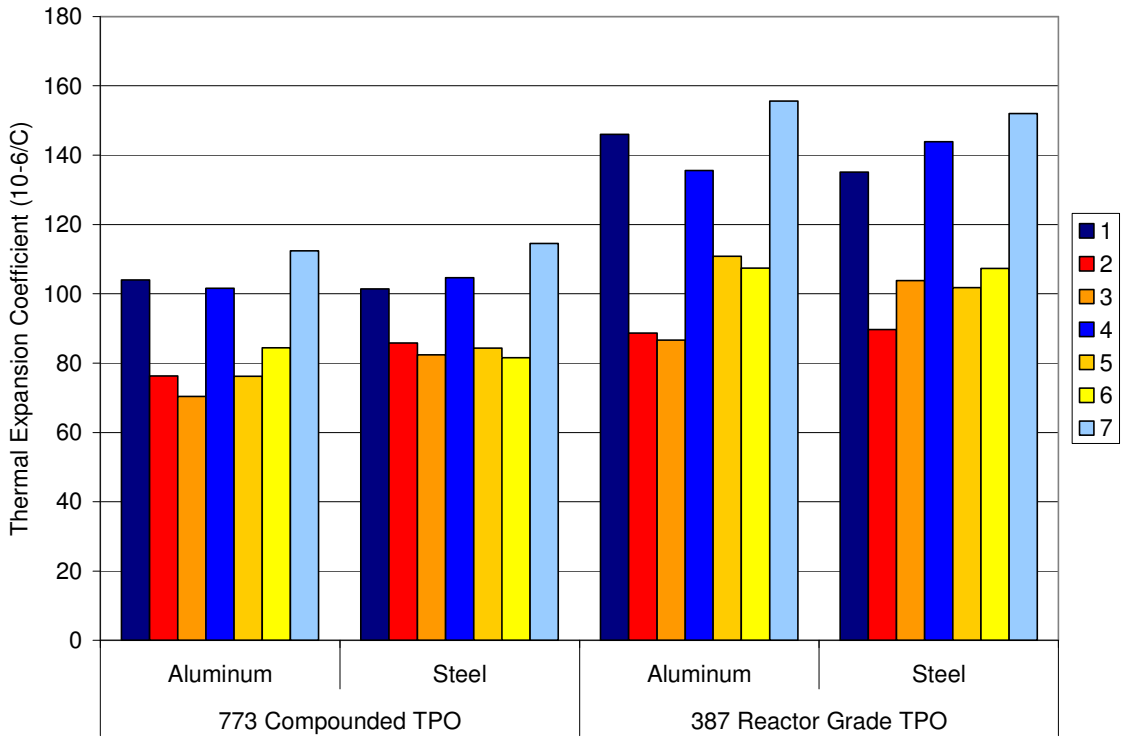

Figure 3-9: Comparison of α for aluminum and steel molded 773 compounded and 387 reactor grade TPOs molded at fast injection speeds.

Comparing the effect of injection speed on the 773 TPO for both aluminum and steel shows that for the steel molded samples, there does not seem to be an effect of injection speed, but there are some differences for the aluminum molded samples (Figure 3-10). Ono and Wu have both reported that the CLTE of TPO blends are heavily dependent on the morphology of the rubber (Wu, 2004; Ono, 2005; Ono, 2006), which is in turn dependent on the processing conditions and the material composition. Ono observed the changes in rubber morphology and CLTE values due to varying the viscosity of the i-PP matrix for 30:70 blends of

poly(ethylene-*co*-octene) rubber (EOR): i-PP. It was found that as η_{EOR}:$\eta_{i\text{-}pp}$ increased, the rubber phase progressively changed shape from "slab" or "sheet-like" to "cylindrical" to "spherical" shaped in the near skin region and the anisotropy of the CLTE decreased (Ono, 2005). While the anisotropy of the CLTE decreased, the CLTE values in the parallel and perpendicular to flow directions increased with increasing viscosity ratios, which was also observed by Wu (Wu, 2004). This suggests that the decreased CLTE of the slowly injected aluminum molded sample may be a result of more sheet-like rubber compared to the more quickly molded sample. It is also possible that there is some effect of molded-in stress, which would be decreased for the slowly molded sample.

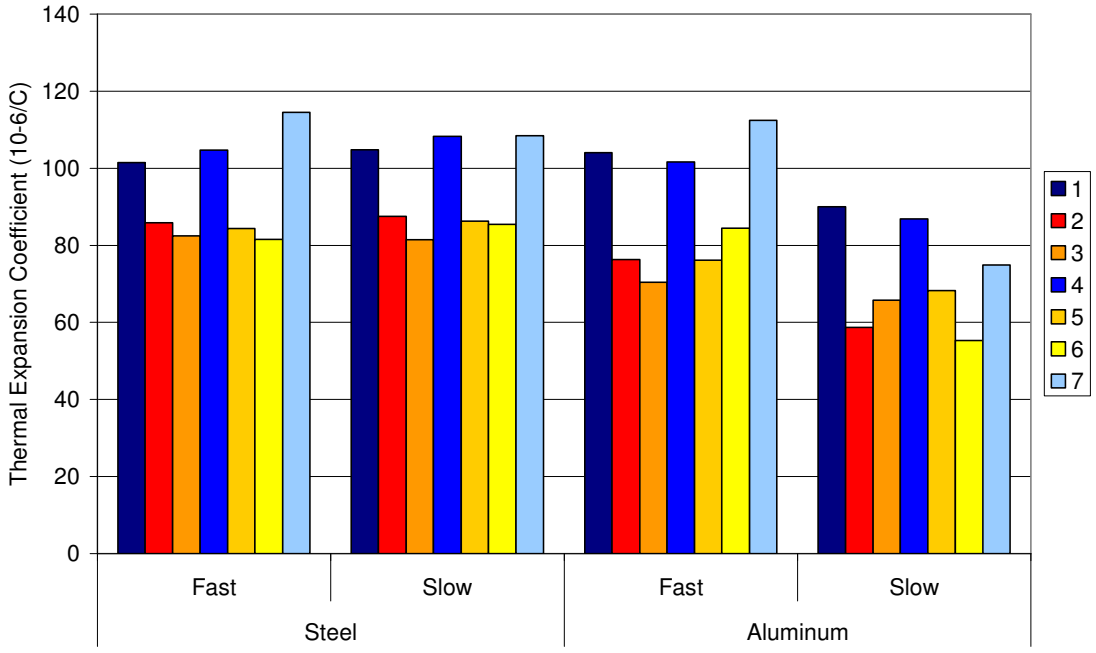

Figure 3-10: Comparison of α for aluminum and steel molded 773 compounded TPO for both fast and slow injection speeds.

3.4.D Atomic Force Microscopy (AFM)

Painted plaques exposed to two different surface treatments were investigated. Chlorinated PolyOlefin (CPO) adhesion promoters (Ad-Pro) are the most

common surface treatments used in the U.S. for painting TPO for automotive applications. Many studies have been done to understand the mechanism by which the adhesion promoter works (Aoki, 1968; Clemens, 1994; Ryntz, 1994; Ryntz, 1995; Ryntz, 1995; Ryntz, 1996; Ryntz, 1996; Ryntz, 1997; Morris, 1998; Mirabella, 2000; Ryntz, 2001; Lawniczak, 2005; Ryntz, 2005; Yin, 2005; Yin, 2007), but it is still not fully understood. Flame or plasma pre-treatments are more common in European automotive production. This solvent-free method works by attaching oxygen functionality to the surface of the TPO, raising the polar contribution and increasing the surface energy for paint adhesion (Clemens, 1994; Nihlstrand, 1997, 1997; Nie, 1999; Jung, 2006).

The interaction between CPO and TPO has been investigated with several different techniques by various authors. Morris et. al. used fluorescent tagging of the CPO solvent to show that the migration of the solvent can be as great as deep as 200μm during baking, but Raman microscopy showed that the CPO itself only penetrated 20 μm on unbaked and 27 μm on baked samples (Morris, 1998). Ryntz et. al. found the penetration of the CPO to be only 3-10 μm deep using both Laser Scanning Confocal Microscopy and ToF-SIMS techniques (Ryntz, 2005). Examination of the surface using STXM or TEM with EDS showed CPO penetration to be much less, 340 nm and 20-50 nm deep respectively (Mirabella, 2000; Yin, 2007). The wide variation in the values of CPO penetration in TPO is likely due to the variety of materials used, variations in injection molding parameters, and the different measurement techniques. It could also be due to the differences found in surface composition, resulting from different material compositions and processing conditions. Several authors report finding an i-PP rich surface layer ranging from several hundred nanometers to several microns (Tomasetti, 1999; Tomasetti, 2000; Tang, 2002), while others find rubber at the surface (Mirabella, 2000). One thing that is agreed upon and proven is the adhesion of CPO to TPO is much greater than to i-PP and the shape and distribution of the rubber near the surface, which is a

function of the processing conditions and material, plays an important role in CPO adhesion (Tomasetti, 1998; Deng, 2009).

Flame treatments improve adhesion by oxidizing the surface, producing polar sites and lower surface energy. While flame treatments, if done correctly, do raise the part temperature about 10-38℃, it is for a very short time. Therefore, it is expected that plaques that are flame treated would have a surface morphology that is much closer to the as-molded surface morphology compared to an Ad-Pro treated plaque, which hypothetically relies on swelling the rubber phase for its increased adhesion properties (Ryntz, 2005).

AFM tapping mode phase images of compounded 773 TPO samples molded at the fast (industrially relevant) speed on both aluminum and steel molds show no large scale effect of the CPO Ad-Pro on the rubber morphology as compared to the flame treated samples (Figure 3-11). Closer examination (Figure 3-12) shows a possible effect of the Ad Pro on the rubber in the first 3-5 μm, characterized by swelling of the rubber in the phase image. This would be within the reported ranges in the literature.

For the 773 TPO samples molded at a fast injection speed, there was no large-scale effect of the cooling rate effect of the mold material (aluminum vs. steel) found on the surface morphology (Figure 3-11). AFM evaluation of the compounded 773 TPO microstructure was found to be more difficult than that of the reactor grade 387 TPO due to the presence of the brittle talc phase that does not microtome smoothly, resulting in a rougher surface.

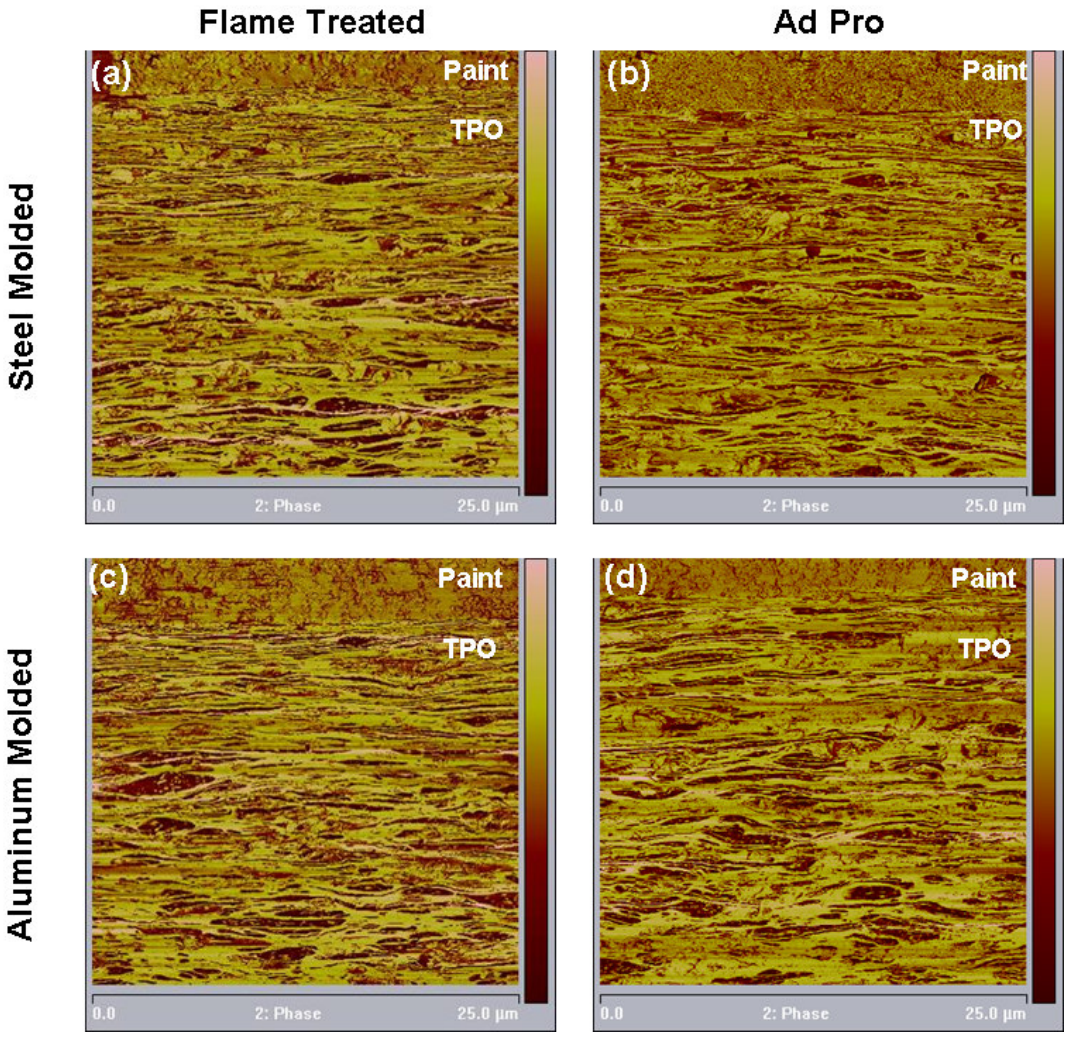

Figure 3-11: AFM phase images of 773 compounded TPO fast injection speed samples taken near the gate (25 µm X 25 µm)

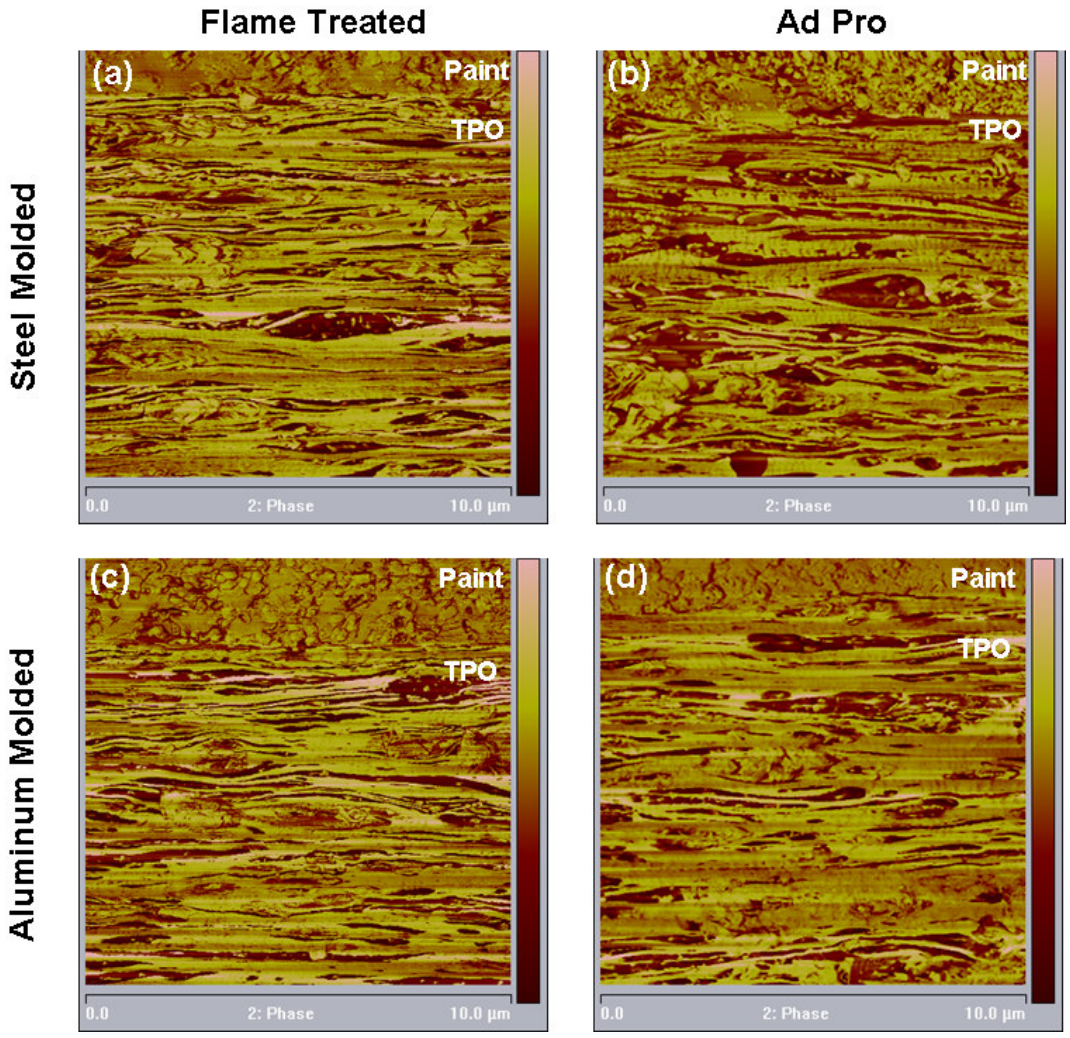

Figure 3-12: AFM phase images of 773 compounded TPO fast injection speed samples taken near the gate (10 µm X 10 µm)

The reactor grade 387 TPO material does not have any talc in it, making the microtomed cross-section smoother and therefore AFM imaging easier. However, the results cannot be directly correlated to the compounded 773 TPO material because of the different material compositions. The reactor grade 387 TPO does show a larger effect of the Ad Pro on the surface morphology, for both aluminum and steel molded samples, compared to the compounded 773 TPO. The rubber phase in the reactor grade 387 TPO appears swollen/more prevalent in the first 10 µm of samples that have been treated with Ad-Pro compared to the flame treated samples (Figure 3-13).

The effect of cooling rate on morphology also had more of an impact on the reactor grade 387 samples compared to the compounded 773 TPO. The steel molded samples have much larger, lower aspect ratio rubber particles compared to the aluminum molded samples, with the average particle size being ~ 4 x 0.7 μm compared to ~ 2 x 0.4 μm, respectively. This is possibly due to the fast cooling at the surface for the aluminum molded samples, so the rubber that is elongated during fountain flow does not have as much time to relax as it does in the steel tools (Tadmor, 1974). This difference in rubber morphology of the aluminum molded reactor grade 387 TPO did not result in lower CLTE values of the aluminum molded samples compared to the steel molded samples. This suggests that the difference is likely only at the near-surface, and the bulk morphology (which dominates the CLTE measurement) is similar.

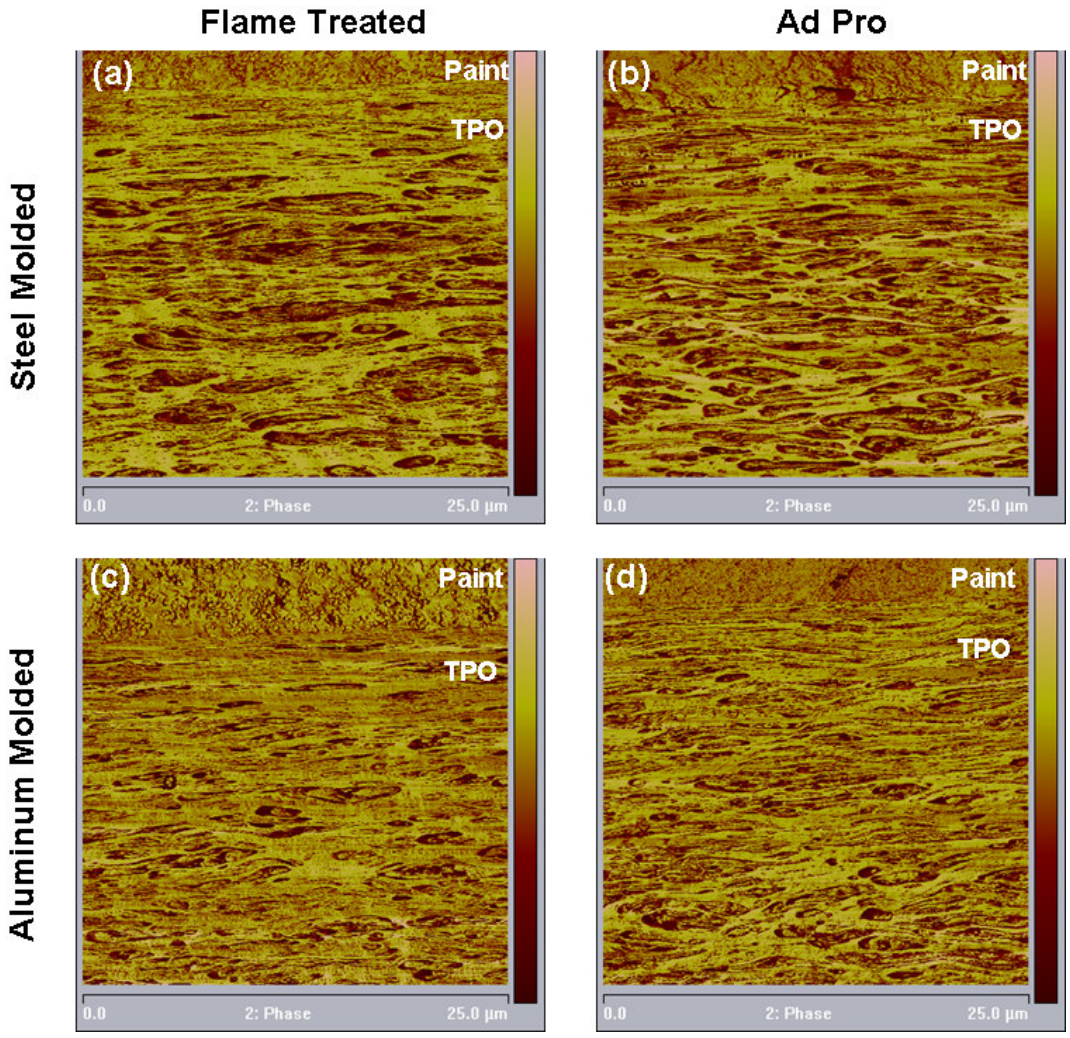

Figure 3-13: AFM phase images of 387 reactor grade TPO fast injection speed samples taken near the gate (25 µm X 25 µm)

The effect of injection speed on the morphology of the rubber near the surface was examined for the compounded 773 TPO material. It was found that samples molded with traditional steel tooling did show an effect of injection speed on rubber morphology with the slower molded samples having larger, less elongated rubber at the surface for the compounded 773 TPO both near (Figure 3-14, a-b) and far from the gate. Any effect found was independent of surface treatment, so only the flame treated samples are shown for simplicity. This less elongated rubber found in the slowly injected sample is likely due to a smaller velocity profile, resulting in lower shear and elongational forces near the surface on the

slower molded samples. There was no difference seen in the CLTE values however, again suggesting this difference is only at the surface and the bulk is similar.

The inverse is true for the aluminum molded samples, where the rubber morphology appears smaller in the slowly molded samples (Figure 3-14, c-d). Since the CLTE of the slowly molded aluminum molded 773 TPO samples did decrease slightly compared to the fast molded samples, this suggests it is possible that the smaller rubber phase decreases the CLTE, or that there is an effect of lower molded-in stress or orientation due to lower injection speeds that is frozen in with the quicker cooling of the aluminum tool.

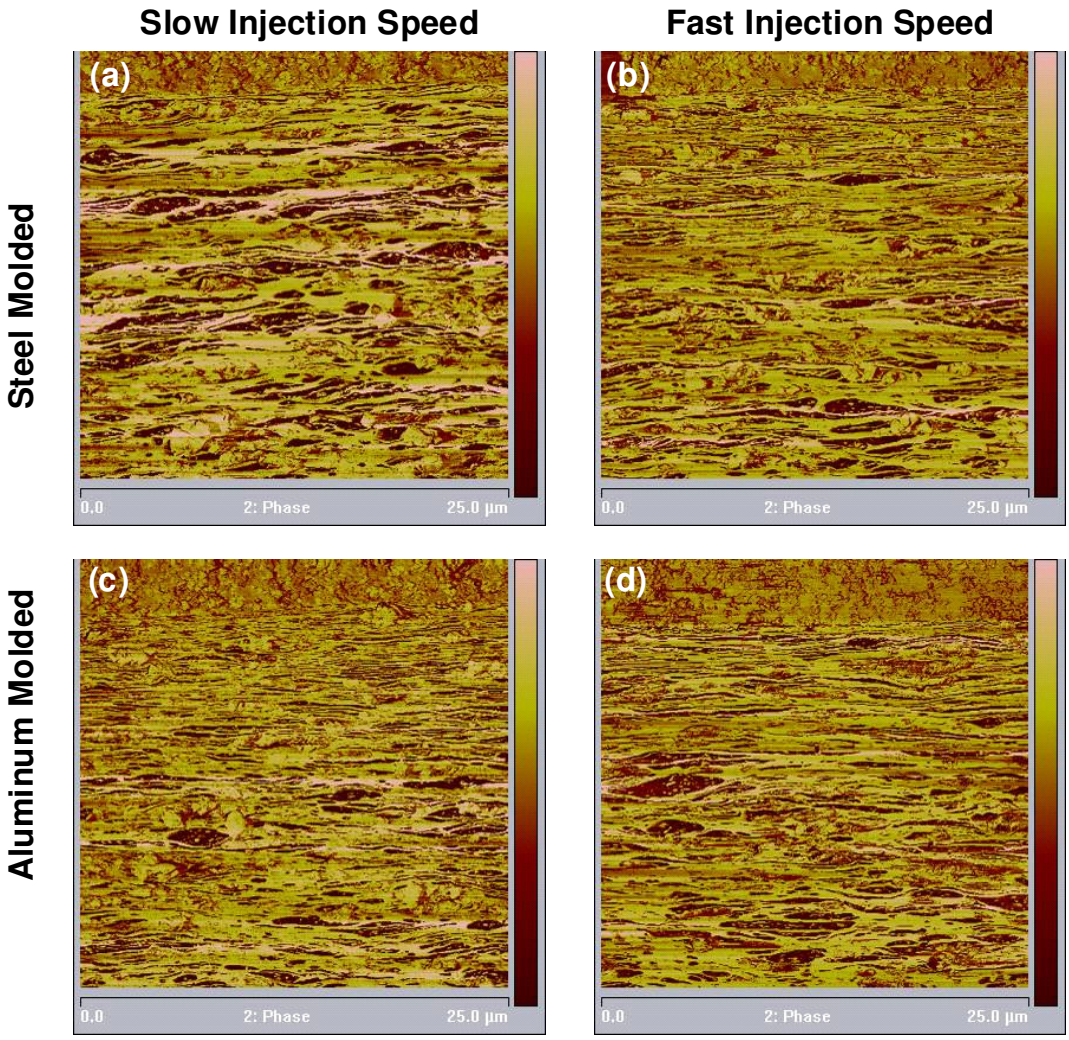

Figure 3-14: AFM Phase images of Steel (a, b) and Aluminum (c, d) molded 773 TPO samples taken near the gate and painted after flame treatment (25 µm x 25 µm)

The effect of distance from the gate was studied for both reactor grade and compounded material, and there was no large-scale effect found for either material under any conditions. It is possible that any effect of the gate on the near-surface morphology may disappear in the first 50 mm before the closest sample is examined. It is more likely that, like the i-PP in Chapter 2, the differences due to flow length are found further into the bulk compared to what is being investigated with AFM.

As-molded samples were examined in cross-section, but despite numerous attempts, there was no adequate way found to prepare the sample to examine the surface edge without artifacts at the surface (Figure 3-15). No large-scale effect of either surface treatment was found, so only the steel molded samples are shown for simplicity. To verify the AFM findings and for closer examination of the surface morphology, TEM was also employed.

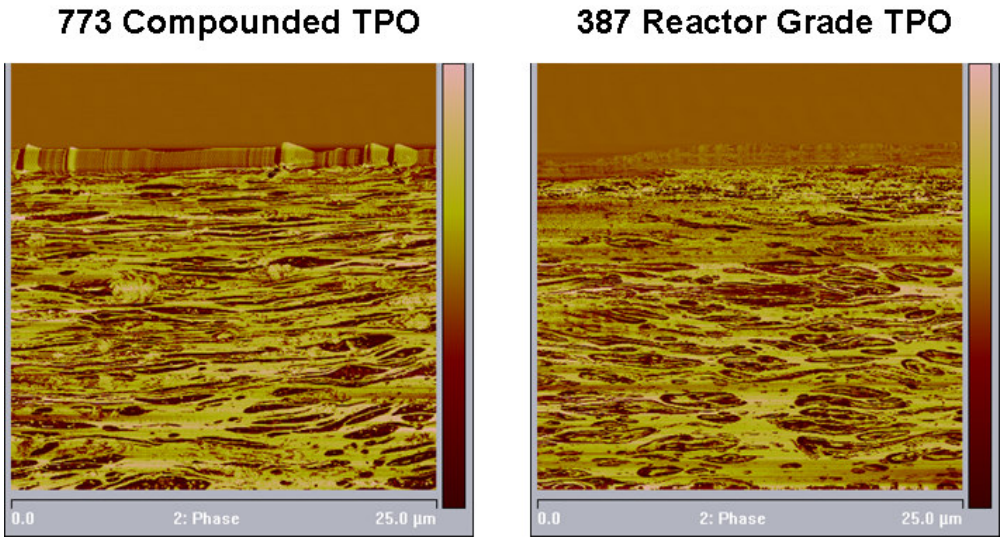

Figure 3-15: As-molded on steel (a) 773 compounded and (b) 387 reactor grade TPO

3.4.E Transmission Electron Microscopy

Transmission Electron Microscopy (TEM) was done on aluminum and steel molded compounded 773 TPO to compare to the findings of the AFM work discussed above. The TEM images confirmed the AFM findings that there was no large-scale difference in rubber morphology near the surface for the fast-injection speed samples. However, it was noted that the thin sections taken from aluminum molded samples had better adhesion with the Ad-Pro layer compared to the steel molded samples for the compounded 773 TPO material (Figure 3-16).

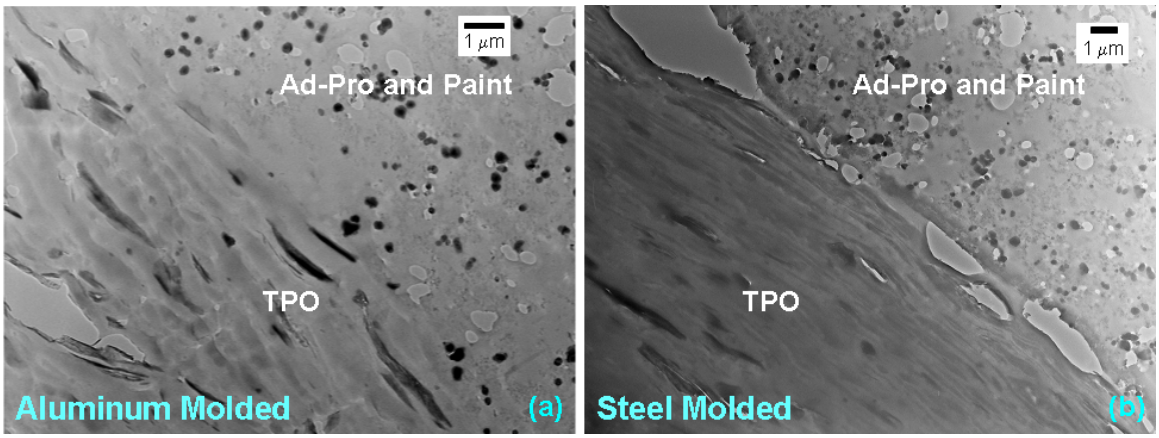

Figure 3-16: TEM images of (a) aluminum molded and (b) steel molded painted 773 TPO

When EDS was performed on the stained sections, it was found that there was a thin layer (~0.7 μm) at the top of the aluminum molded TPO that was stained more heavily with ruthenium, indicating a layer with less crystallinity. This lower crystallinity layer could be a result of the faster cooling rate of the aluminum tooling compared to traditional steel tooling, and may have an effect on adhesion, so it was investigated further with X-ray Photoelectron Spectroscopy.

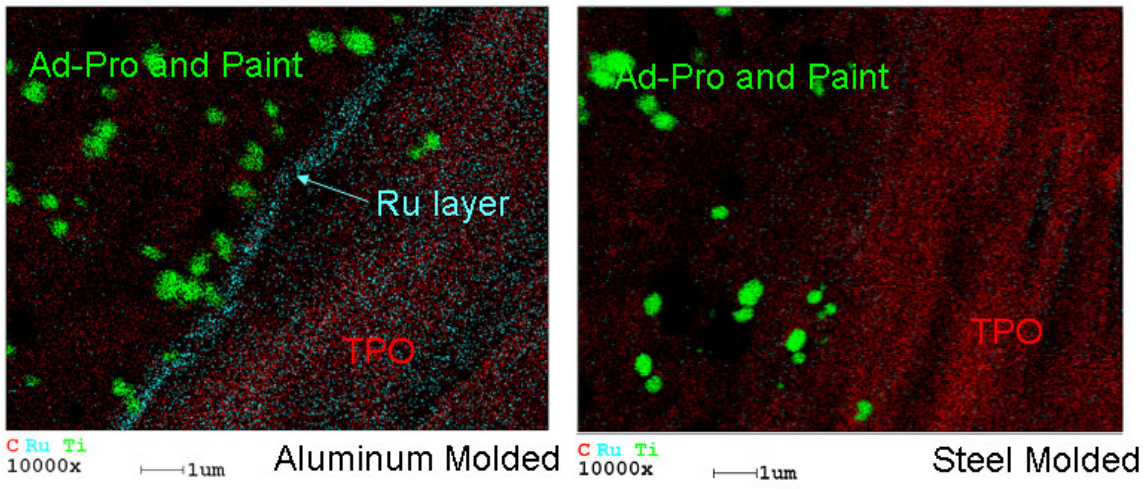

Figure 3-17: EDS of TEM foils showing a thin, more heavily stained surface on the aluminum molded polymer surface

3.4.F X-Ray Photoelectron Spectroscopy (XPS)

XPS was performed on the surface of samples molded against steel and aluminum for both the reactor grade and compounded TPO. The reactor grade 387 TPO showed no effect of mold material on surface chemistry, with the quantified survey data showing only carbon and oxygen, with some very small traces of Si and Na that are most likely from handling. High-resolution analysis of the carbon 1s peak also showed no differences between the aluminum and steel molded reactor grade 387 TPO (Figure 3-18).

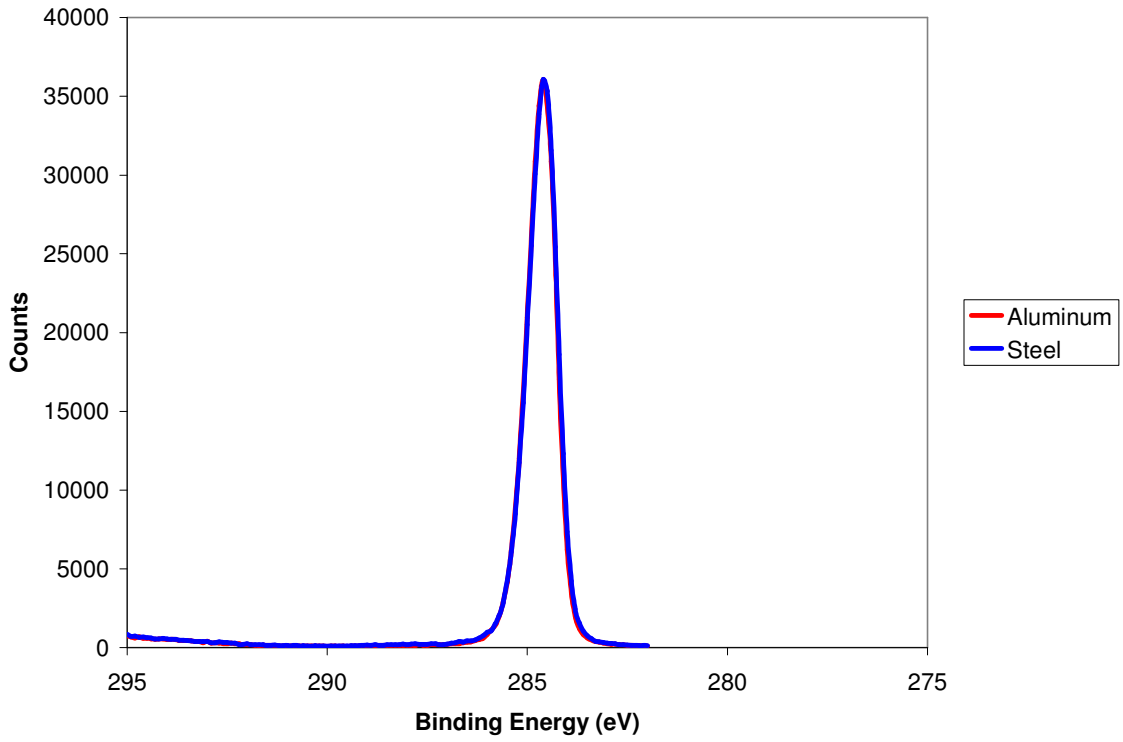

Figure 3-18: High Resolution C 1s scan of aluminum and steel molded 387 reactor grade TPO

Analysis of the compounded 773 TPO did show a difference between the surface aluminum and steel molded samples (Figure 3-19). The survey data showed that nitrogen was found in a significant amount (~2.5 at%) on the surface of the aluminum molded samples, but was not present on the surface of the steel molded compounded 773 TPO samples or the bulk of either sample. This was true regardless of the distance from the gate as shown in the quantified survey

data shown in Table 3-3. The Si, Na and S found could be from additives in the material or could be contamination from handling despite efforts to minimize it. The Mg and Ca found in the bulk of the sample, but not on the surface, are due to the talc in the compounded formulation.

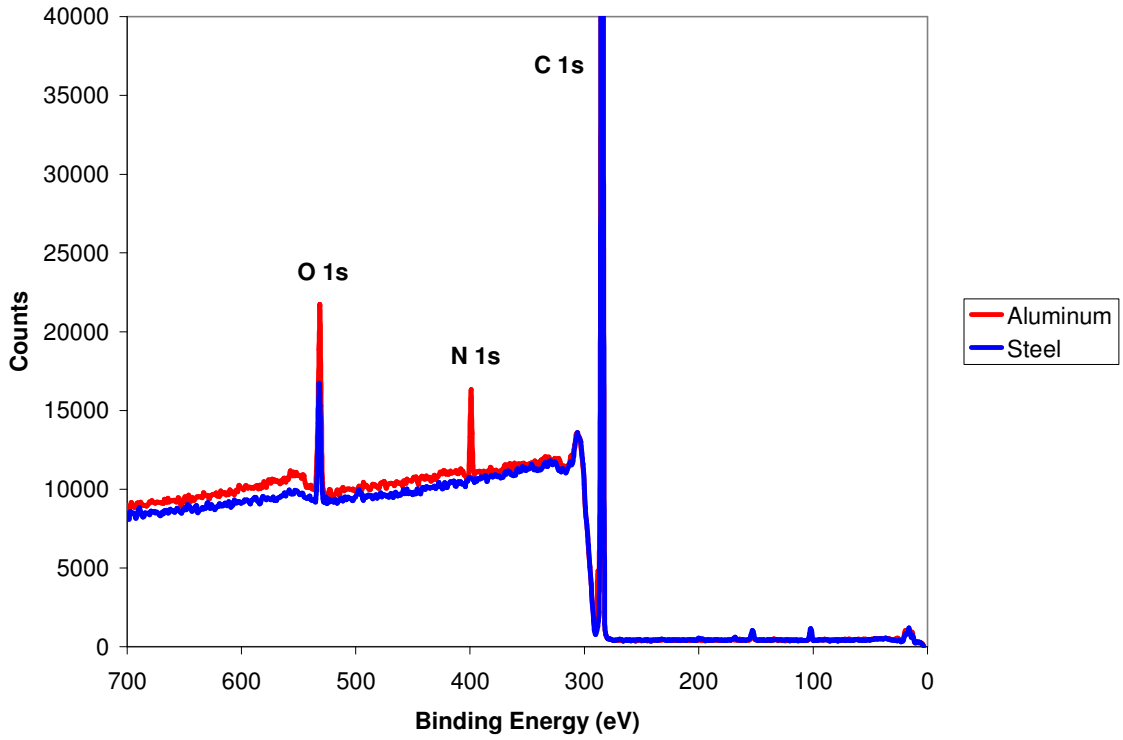

Figure 3-19: Survey scan of surface of aluminum and steel molded 773 TPO

Table 3-3: Quantified XPS Survey data for 773 Compounded TPO

Mold Material		Al	St	Al	St	Al	St
Distance From Gate		Near	Near	Far	Far		
Surface/Bulk		Surface	Surface	Surface	Surface	Bulk	Bulk
at.%	C	92.17	95.87	91.13	94.79	89.03	90.25
	O	4.84	3.20	5.74	4.11	7.88	6.57
	N	2.65		2.23			
	Si	0.34	0.72	0.89	0.97	1.82	1.90
	Na		0.10		0.12	0.43	
	S		0.11				
	Mg					0.57	0.70
	Ca					0.27	0.59

Unlike the reactor grade 386 TPO material, there were also differences seen in the high resolution carbon 1s scans of the surface of the aluminum and steel molded compounded 773 TPO samples (Figure 3-20). The main peak of the aluminum molded sample is slightly wider than that of the steel molded sample and also has second peak around 288 eV binding energy, likely related to the nitrogen at the surface, that was not present in the steel molded sample.

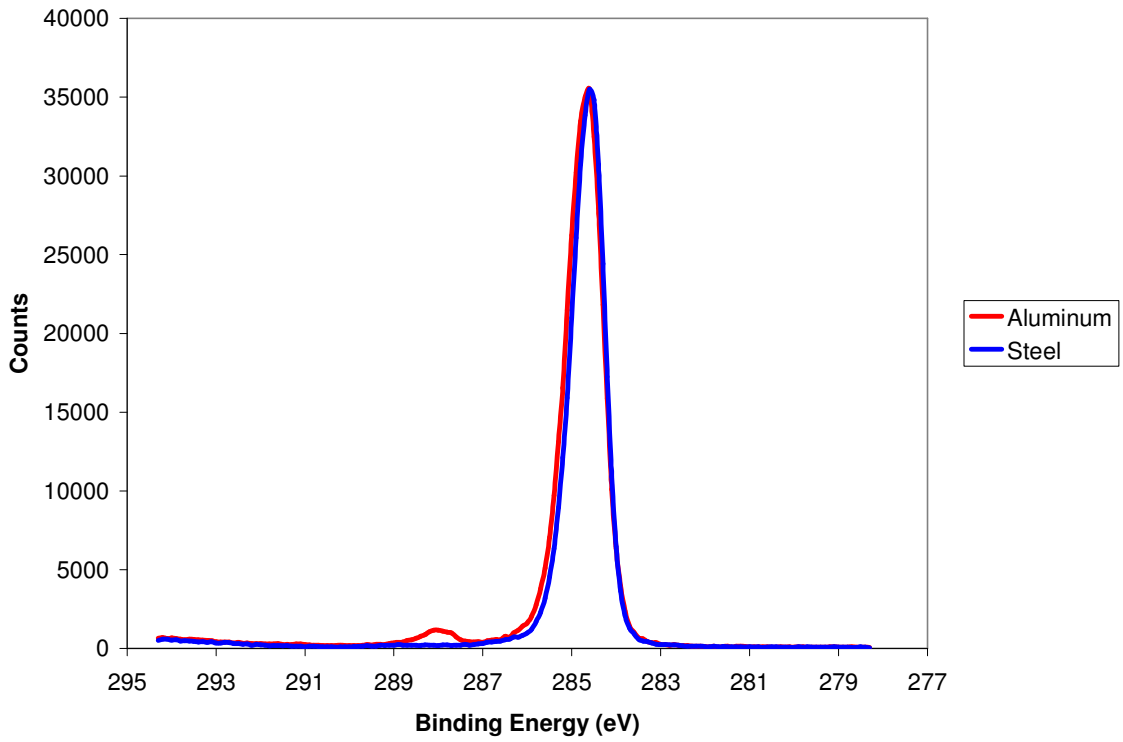

Figure 3-20: High resolution C 1s scan of surface of aluminum and steel molded 773 compounded TPO

Since nitrogen was not found in the bulk of the aluminum molded sample or anywhere on the steel molded samples, it is concluded that a thin, nitrogen containing surface layer is formed on the aluminum molded samples. This could possibly be a nitrogen-containing additive that is being trapped at the surface due to the fountain flow effect (Tadmor, 1974; Mielewski, 1998) and faster cooling rates of the aluminum molded samples. Since this is a commercially available TPO, we do not have detailed information about the material composition or additive packages, but it is known that this material does contain a UV inhibitor which typically contains amines. This nitrogen-rich layer on the aluminum molded samples is likely the same lower crystallinity layer that we are seeing with the heavier ruthenium staining in the TEM micrographs (Figure 3-17).

This finding demonstrates that aluminum tooling could be possibly be used to preferentially bring or trap certain additives to the surface. This should be further explored to determine the exact mechanism and if it can be exploited to preferentially coat TPO with higher surface energy components that would improve adhesion.

Given the findings from TEM and XPS, adhesion testing was done to determine if this thin layer on the aluminum molded samples had any effect on the paint adhesion compared to the steel molded samples, especially since the appearance of the TEM thin slices indicated possibly improved paint adhesion on the aluminum molded samples.

3.4.G Adhesion Testing

Compounded 773 TPO plaques were molded at a fast injection speed against both aluminum and steel tooling and painted with Ad-Pro, basecoat and clearcoat. Prepared samples were tested using both tensile testing (Figure 3-21) or elastica bending and the crack spacing was measured at saturation to calculate the interfacial shear strength as previously described in Equation 3.1. The samples were also analyzed in cross-section after testing and it was verified that 1) the three paint layers (adhesion promoter, basecoat and clearcoat) cracked and behaved as one layer, and 2) that the adhesion loss was between the Ad-Pro and the TPO interface (Figure 3-22).

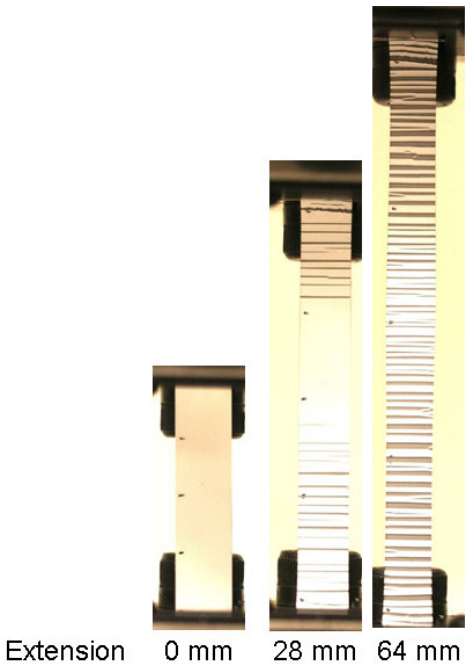

Figure 3-21: Example of tensile adhesion test results

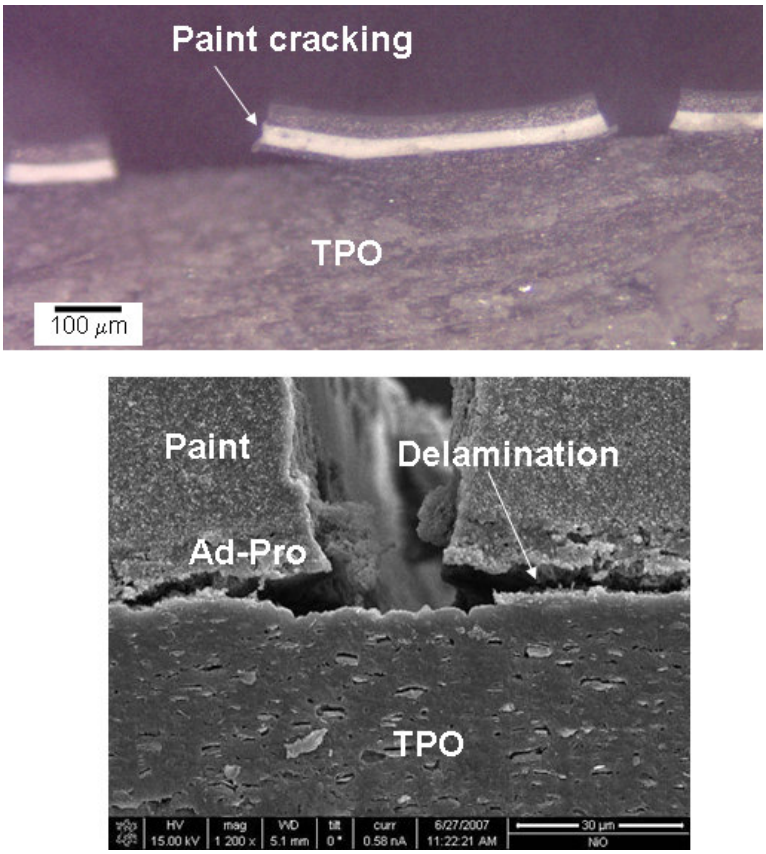

Figure 3-22: Examination of cross section using (a) optical microscopy and (b) SEM

The shear strength of the TPO/Ad-Pro interface was calculated for both aluminum and steel molded compounded 773 TPO using the tensile and elastica test methods and the results are shown in Figure 3-23. No significant difference in adhesion strength was found between the aluminum or steel molded samples, which was the same result as the qualitative cross-hatch adhesion testing that was performed at Ford Motor Company, where all of the aluminum and steel molded plaques of both TPO formulations passed testing with 0% removed. The data in Figure 3-23 also shows that the tensile and elastica tests produce equivalent results and that the data correlates well with increasing film thickness/strength.

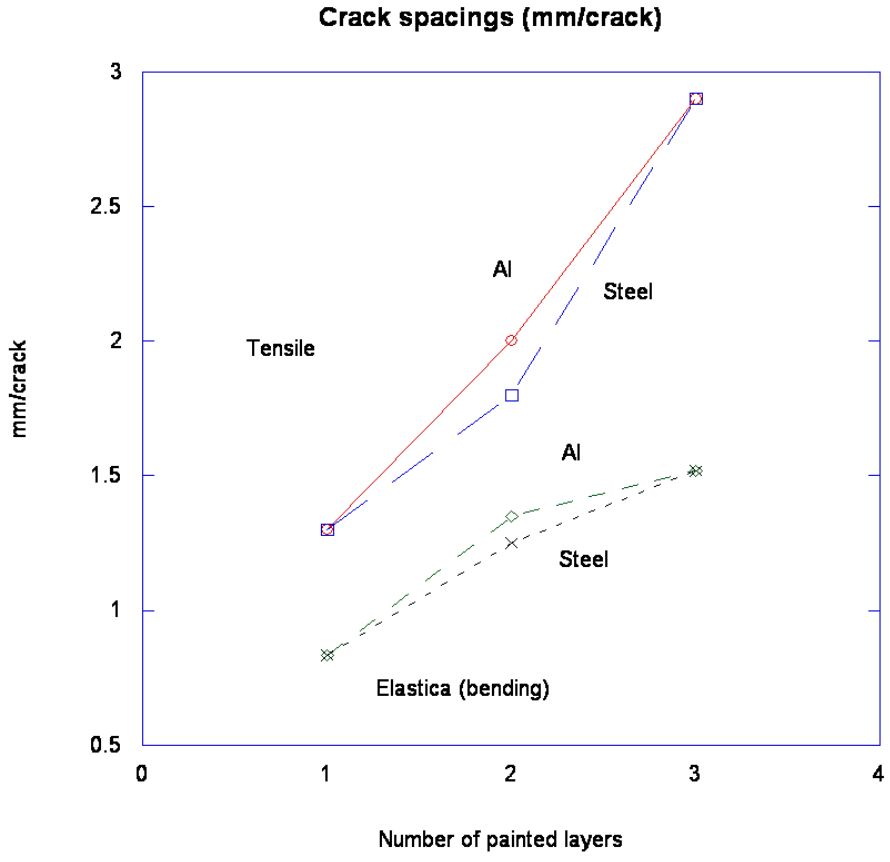

Figure 3-23: Calculated interfacial shear stress of aluminum and steel molded 773 TPO painted samples using elastica and tensile testing methods

While the nitrogen enriched surface of the aluminum molded sample was not found to either improve or degrade adhesion, it would be worth further investigating the possibility of utilizing the rapid cooling rate of the aluminum tooling to "trap" a thin additive film at the surface that could help improve adhesion without further surface treatments of the use of adhesion promoters.

3.5 Conclusions

The work in Chapter 2 on neat polypropylene was used as a starting point for the work done in this Chapter on TPO, but there were several differences found due to the additions of rubber, talc and other additives to the polypropylene despite using the same tools and the same molding conditions. Due to the faster nucleation rate of the TPO materials, the morphology was too small to be accurately observed with optical microscopy. The increased nucleation rate also led to lesser degrees of wrinkling in the shear zone of samples taken near the gate, perpendicular to the flow. Optical profilometry taken at elevated temperatures confirmed that the size and amount of stress in the shear zone decreased with the increasing nucleation rates of the TPO formulations. The amount of stress in the shear zone, which goes as i-PP >> reactor grade 387 TPO (rubber only) > compounded 773 TPO (rubber +talc) was affected significantly by addition of rubber, with a smaller improvement with the further addition of talc. The size of the shear zone which goes as i-PP = reactor grade 387 TPO (rubber only) > compounded 773 TPO (rubber +talc) was found to only be affected by the addition of talc. Note that these are only general observations, since the rubber and overall formulations are different between the two TPO materials used.

Both TPO materials showed a strong anisotropy in the measured CLTE values due to the morphology of the rubber as a function of orientation to the flow, which was not the case for the isotropic i-PP in Chapter 2. The rubber additions did not

increase the CLTE as expected, which is likely due to the fact that the TPO materials were industrially available resin formulations, which is not simply additions of rubber to an i-PP matrix. The addition of low CLTE talc did decrease the CLTE of the compounded 773 TPO, as expected. Like i-PP, at industrially relevant injection molding speeds, there was no difference between the CLTE of either TPO formulation based on being molded against aluminum or steel.

Because the smaller morphology of the TPO could not be resolved with optical microscopy, tapping mode AFM phase imaging was used to identify the rubber domains due to their lower elastic modulus compared to the surrounding polypropylene matrix. Unfortunately, due to the low surface energy, it was impossible to adequately embed as-molded TPO samples for cross-sectioning and AFM examination without artifacts due to the loss of contact of the tip at the surface edge. Therefore, samples were painted using two different surface treatment methods, CPO adhesion promoter and flame treatment, and their effects on the near-surface morphology was also studied.

It was found when molded at the industrially relevant (fast) injection speeds, there was no significant effect of the mold material on the near surface rubber morphology for the compounded 773 TPO, but there was on the reactor grade 387 TPO. The rubber phase in the steel molded (more slowly cooled) 387 TPO samples showed larger rubber particles with a lower aspect ratio compared to the aluminum molded samples, the average particle size being ~ 4 x 0.7 μm compared to ~ 2 x 0.4 μm, respectively. It is suspected that the faster cooled aluminum molded samples froze the rubber that had been elongated during fountain flow, whereas the more slowly cooled steel molded samples had some time for the rubber to relax. These different cooling rates likely didn't have as big of an effect on the compounded 773 TPO due to its faster nucleation rate from the presence of talc. Because there was no difference in the CLTE for the

reactor grade 387 TPO molded against steel vs. aluminum, these differences in morphology due to the cooling rate are probably only at the surface, not throughout the bulk. This difference in surface morphology could still affect adhesion.

To compliment the AFM work, TEM studies were done on compounded 773 TPO that had be molded with aluminum and steel and painted. The near-surface rubber morphology again showed no difference based on mold material, but there was a difference observed in the appearance of the thin sections. The thin sections that were cut from the aluminum molded compounded 773 TPO retained more adhesion to the Ad-Pro layer compared to those molded against steel. EDS of the TEM samples indicated that there was a thin layer (~0.7 μm) at the surface of the aluminum molded sample that was more heavily stained with ruthenium that was not present on the steel molded sample. This indicates that there is a less crystalline layer on the aluminum molded sample, probably due to the rapid cooling rate.

XPS was conducted to further investigate the differences at the surface that were seen on the aluminum molded sample. For the reactor grade 387 TPO, both the general survey scans and the high resolution carbon 1s scan showed no difference between the samples molded on aluminum or steel. There was, however, a difference in surface chemistry between the aluminum and steel molded compounded 773 TPO. The thin layer of less-crystallinity observed in the TEM/EDS work on the aluminum molded sample was found to contain ~2.5 at% nitrogen, which was not found at the surface of the steel molded samples or in the bulk of either sample. This was found to be true regardless of distance from the gate. The high resolution carbon 1s peak also showed differences between the aluminum and steel molded samples. The aluminum molded sample had a slightly wider main C 1s peak, as well as an additional peak at

~288 eV binding energy, which is likely related to the nitrogen. It is suspected that a low molecular weight, nitrogen containing additive is being driven to the surface during fountain flow and trapped there with the rapid "quenching" of the surface from the high thermal conductivity of the aluminum mold. Because this is a commercially supplied resin, the formulation is not known, so it cannot be exactly determined what is at the surface; however the resin does have a UV stabilizer package, which traditionally contains amines.

This finding is the first reported instance of the rapid cooling of aluminum tooling possibly affecting the surface chemistry. Combined with the findings in Chapter 2, which showed that an immiscible thio-ester heat stabilizer was found preferentially at the surface due to fountain flow phenomena, indicates that it may be possible and beneficial if we could "design" TPO to bring a high surface energy additive to the surface to improve adhesion without the use of traditional Ad-Pro or flame surface treatments.

Because we did see differences in the surface due to the tooling material, adhesion testing was done to determine what effect this might have on properties. Using a quantitative adhesion test, the interfacial shear stress of the paint/polymer interface was determined by measuring the crack spacing of the paint at saturation when the surface is placed in tension. There was no significant difference in adhesion found between the aluminum and steel molded compounded 773 TPO that showed different surface chemistry in the XPS study. This does not indicate that there is not opportunity here, just that the layer that was at the surface either did not affect adhesion or that its effect was masked by the use of the Ad-Pro prior to painting the samples. These findings correlated with the traditional qualitative scribe testing done at Ford Motor Company which showed no difference between either of the TPO materials whether they were molded on aluminum or steel.

While there were some similarities to the findings in Chapter 2 on neat polypropylene, there were also many differences found – not only between TPO and neat i-PP, but also between the two different TPO formulations. These findings confirm why it is so difficult to get accurate modeling results from software such as MoldFlow - because the surface morphology and performance can be affected by not only material formulation changes (which occur frequently in industrially relevant resins), but also based on processing. It is hoped that some of these findings can help refine those models, and can also provide possible future opportunities to design TPO formulations to possibly exploit differences in surface chemistry on rapidly cooled aluminum molded parts.

3.6 References

Aoki, Y. (1968). "The role of crystallinity of polymer in the adhesion between chlorinated isotactic polypropylene and isotactic polypropylene." Journal of Polymer Science Part C: Polymer Symposia **23**(2): 855-864.

Bedia, E. L., N. Astrini, et al. (2000). "Characterization of polypropylene and ethylene-propylene copolymer blends for industrial applications." Journal of Applied Polymer Science **78**(6): 1200-1208.

Cakmak, M. and S. W. Cronin (2000). "The effect of composition and processing conditions on the structure development in injection molded dynamically vulcanized PP/EPDM blends." Rubber Chem. and Tech. **73**(4): 753-778.

Chang, A. C., L. Tau, et al. (2002). "Structure of blown film from blends of polyethylene and high melt strength polypropylene." Polymer **43**(18): 4923-4933.

Choi, W. J. and S. C. Kim (2004). "Effects of talc orientation and non-isothermal crystallization rate on crystal orientation of polypropylene in injection-molded polypropylene/ethylene-propylene rubber/talc blends." Polymer **45**(7): 2393-2401.

Choudhary, V., H. S. Varma, et al. (1991). "Polyolefin blends: effect of EPDM rubber on crystallization, morphology and mechanical properties of polypropylene/EPDM blends. 1." Polymer **32**(14): 2534-2540.

Clemens, R. J., G. N. Batts, et al. (1994). "How do chlorinated poly(olefins) promote adhesion of coatings to poly(propylene)?" Progress in Organic Coatings **24**(1-4): 43-54.

Coppola, F., R. Greco, et al. (1987). "Mechanical properties and morphology of isotactic polypropylene/ethylene-propylene copolymer blends." Polymer **28**(1): 47-56.

D'Orazio, L. and G. Cecchin (2001). "Isotactic polypropylene/ethylene-co-propylene blends: effects of composition on rheology, morphology and properties of injection moulded samples." Polymer **42**(6): 2675-2684.

D'Orazio, L., C. Mancarella, et al. (1999). "Isotactic polypropylene/ethylene-co-propylene blends: effects of the copolymer microstructure and content on rheology, morphology and properties of injection moulded samples." Polymer **40**(10): 2745-2757.

Deng, K., N. Felorzabihi, et al. (2009). "Influence of position and composition on adhesion to injection-molded TPO plaques as model automotive parts." Polymer **50**(21): 5084-5093.

El Ghzaoui, A. (1999). "Determination of surface energy of polymers by force microscopy." Journal of Applied Physics **85**(2): 1231-1233.

Fujiyama, M. and T. Wakino (1991). "Crystal orientation in injection molding of talc-filled polypropylene." Journal of Applied Polymer Science **42**(1): 9-20.

Ghijsels, A., N. Groesbeek, et al. (1982). "Multiple crystallization behaviour of polypropylene/thermoplastic rubber blends and its use in assessing blend morphology." Polymer **23**(13): 1913-1916.

Grein, C., C. J. G. Plummer, et al. (2002). "Influence of [beta] nucleation on the mechanical properties of isotactic polypropylene and rubber modified isotactic polypropylene." Polymer **43**(11): 3279-3293.

Gu, X., Y. C. Jean, et al. (2004). "Advanced Techniques for Nanocharacterization Of Polymeric Coating Surfaces." JCT Research **1**(3): 191-200.

Guerrica-Echevarria, G., J. I. Eguiazabal, et al. (1998). "Influence of molding conditions and talc content on the properties of polypropylene composites." European Polymer Journal **34**(8): 1213-1219.

Ho, W.-J. and R. Salovey (1981). "Processing of polyolefin blends." Polymer Engineering & Science **21**(13): 839-843.

Ivanov, D. A., B. Nysten, et al. (1999). "Atomic force microscopy imaging of single polymer spherulites during crystallization: application to a semi-crystalline blend." Polymer **40**(21): 5899-5905.

Jung, C. K., I. S. Bae, et al. (2006). "Development of painting technology using plasma surface technology for automobile parts." Thin Solid Films **506-507**: 316-322.

Karger-Kocsis, J. and I. Csikai (1987). "Skin-Core morphology and failure of injection-molded specimens of impact-modified polypropylene blends." Polymer Engineering & Science **27**(4): 241-253.

Karger-Kocsis, J., A. Kallo, et al. (1979). "Morphological study on the effect of elastomeric impact modifiers in polypropylene systems." Polymer **20**(1): 37-43.

Kiland, B. R., M. W. Urban, et al. (2001). "Surface depth-profiling of polymer compounds using step-scan photoacoustic spectroscopy (S2 PAS)." Polymer **42**(1): 337-344.

Kim, G.-M., G. H. Michler, et al. (1996). "Relationship between morphology and micromechanical toughening mechanisms in modified polypropylenes." Journal of Applied Polymer Science **60**(9): 1391-1403.

Kim, G. M. and G. H. Michler (1998). "Micromechanical deformation processes in toughened and particle-filled semicrystalline polymers: Part 1.

Characterization of deformation processes in dependence on phase morphology." Polymer **39**(23): 5689-5697.

Lawniczak, J. E., K. A. Williams, et al. (2005). "Characterization of Adhesion Performance of Topcoats and Adhesion Promoters on TPO Substrates." JCT CoatingsTech **2**(5): 399-405.

Lee, H.-s., P. D. Fasulo, et al. (2005). "TPO based nanocomposites. Part 1. Morphology and mechanical properties." Polymer **46**(25): 11673-11689.

Lee, H.-s., P. D. Fasulo, et al. (2006). "TPO based nanocomposites. Part 2. Thermal expansion behavior." Polymer **47**(10): 3528-3539.

Long, Y. and R. A. Shanks (1996). "PP-elastomer-filler hybrids. I. Processing, microstructure, and mechanical properties." Journal of Applied Polymer Science **61**(11): 1877-1885.

Magonov, S. N. and M.-H. Whangbo (1996). Surface Analysis with STM and AFM. New York, VCH.

Maier, C. and T. Calafut (1998). Polypropylene - The Definitive User's Guide and Databook., William Andrew Publishing/Plastics Design Library.

Mielewski, D. (1998). Weld Line Morphology of Injection Molded Polypropylene. Department of Chemical Engineering. Ann Arbor, University of Michigan. **Ph.D.:** 137.

Mirabella, F. M., N. Dioh, et al. (2000). "Theoretical analysis and experimental characterization of the TPO/adhesion promoter/paint interface of painted thermoplastic polyolefins (TPO)." Polymer Engineering & Science **40**(9): 2000-2006.

Morris, H. R., B. Munroe, et al. (1998). "Fluorescence and Raman Chemical Imaging of Thermoplastic Olefin (TPO) Adhesion Promotion." Langmuir **14**(9): 2426-2434.

Nguyen, T., X. Gu, et al. (2001). Characterization of Coating System Interphases With Phase Imaging AFM. Adhesion Society Annual Meeting, Williamsburg, VA, Adhesion Society.

Nie, H. Y., M. J. Walzak, et al. (1999). "Atomic force microscopy study of polypropylene surfaces treated by UV and ozone exposure: modification of morphology and adhesion force." Applied Surface Science **144-145**: 627-632.

Nihlstrand, A., T. Hjertberg, et al. (1997a). "Adhesion properties of oxygen plasma-treated polypropylene-based copolymers." Polymer **38**(7): 1557-1563.

Nihlstrand, A., T. Hjertberg, et al. (1997b). "Plasma treatment of polyolefins: Influence of material composition: 2. Lacquer adhesion and locus of failure." Polymer **38**(14): 3591-3599.

Nomura, T., T. Nishio, et al. (1995). "Compatibility and tensile behavior of polypropylene/ethylene-propylene rubber blends." Polymer Engineering & Science **35**(16): 1261-1271.

Nysten, B., A. Ghanem, et al. (1999). "Influence of EP/PP viscosity ratio on the surface morphology and elasticity of injection moulded PP/EP." Polymer International **48**(4): 334-338.

Nysten, B., R. Legras, et al. (1995). "Atomic force microscopy imaging of viscoelastic properties in toughened polypropylene resins." Journal of Applied Physics **78**(10): 5953-5958.

Ono, M., H. Nishioka, et al. (2006). "Study on Three-dimensional Structures in Injection-molded iPP/Poly(ethylene-co-octene) by Transmission Electron Microtomography." e-Journal of Soft Materials **2**: 56-61.

Ono, M., J. Washiyama, et al. (2005). "Anisotropic thermal expansion in polypropylene/poly(ethylene-co-octene) binary blends: influence of arrays of elastomer domains." Polymer **46**(13): 4899-4908.

Pantani, R., I. Coccorullo, et al. (2005). "Modeling of morphology evolution in the injection molding process of thermoplastic polymers." Progress in Polymer Science **30**(12): 1185-1222.

Petrovic, Z. S., J. Budinski-Simendic, et al. (1996). "Effect of addition of polyethylene on properties of polypropylene/ethylene-propylene rubber blends." Journal of Applied Polymer Science **59**(2): 301-310.

Polypropylene Handbook (2005). Munich, Hanser.

Ryntz, R. A. (1994). "Coating adhesion to low surface free energy substrates." Progress in Organic Coatings **25**(1): 73-83.

Ryntz, R. A. (1996a). "The effects of thermoplastic poly(olefin) (TPO) morphology on subsequent paintability and thermal shock performance." Progress in Organic Coatings **27**(1-4): 241-254.

Ryntz, R. A. (2005a). "Attaining Durable Painted Plastic Components." JCT Research **2**(5): 351-360.

Ryntz, R. A. (2005b). Real World Performance of Painted Plastic Components, Federation of Societies for Coatings Technology, 492 Norristown Rd , Blue Bell, PA, 19422-2350, USA,.

Ryntz, R. A., D. Britz, et al. (2001). Measuring adhesion to poly(olefins): the role of adhesion promoter and substrate, Federation of Societies for Coatings Technology, 492 Norristown Rd , Blue Bell, PA, 19422, USA.

Ryntz, R. A. and B. Buzdon (1997). "The relationship between clearcoat permeability and adhesion promoter penetration to the gasoline resistance of painted TPO substrates." Progress in Organic Coatings **32**(1-4): 167-172.

Ryntz, R. A., A. McNeight, et al. (1996b). How molding conditions affect adhesion of coatings to TPOs, Society of Plastics Engineers, 14 Fairfield Dr , Brookfield Center, CT, 06804-0403, USA, [URL:http://www.4spe.org/].

Ryntz, R. A., A. C. Ramamurthy, et al. (1995a). Stone impact damage to painted plastic substrates, Federation of Societies for Coatings Technology, 492 Norristown Rd , Blue Bell, PA, 19422, USA.

Ryntz, R. A., Q. Xie, et al. (1995b). Effects of coating solvents on the morphology of thermoplastic polyolefins (TPO), Federation of Societies for Coatings Technology, 492 Norristown Rd , Blue Bell, PA, 19422, USA.

Sano, H., T. Usami, et al. (1986). "Lamellar morphologies of melt-crystallized polyethylene, isotactic polypropylene and ethylene-propylene copolymers by the RuO4 staining technique." Polymer **27**(10): 1497-1504.

Strebel, J. J., F. Mirabella, et al. (2004). "Injection molded automotive TPO - a multilayer composite structure of varied orientations." Polymer Engineering and Science **44**(8): 1588-1593.

Swaminathan, K. and D. W. M. Marr (2000). "Morphology characterization of high-impact resistant polypropylene using AFM and SALS." Journal of Applied Polymer Science **78**(2): 452-457.

Tadmor, Z. (1974). "Molecular orientation in injection molding." Journal of Applied Polymer Science **18**(6): 1753-1772.

Tanem, B. S., T. Kamfjord, et al. (2003). "Sample preparation and AFM analysis of heterophase polypropylene systems." Polymer **44**(15): 4283-4291.

Tang, H., B. Foran, et al. (2001). "Quantitative measurement of adhesion between polypropylene blends and paints by tensile mechanical testing." Polymer Engineering & Science **41**(3): 440-448.

Tang, H. and D. C. Martin (2002). "Microstructural studies of interfacial deformation in painted thermoplastic polyolefins (TPOs)." Journal of Materials Science **37**(22): 4783-4791.

Tang, H. and D. C. Martin (2003). "Near-surface deformation under scratches in polypropylene blends Part I Microscopic characterization of deformation." Journal of Materials Science **38**(4): 803-815.

Tomasetti, E., R. Legras, et al. (2000). "Plastic deformation in polypropylene/(ethylene-propylene) copolymer blend during paint debonding." Polymer **41**(17): 6597-6602.

Tomasetti, E., R. Legras, et al. (1998). "Quantitative approach towards the measurement of polypropylene/(ethylene-propylene) copolymer blends surface elastic properties by AFM." Nanotechnology **9**: 305-315.

Tomasetti, E., B. Nysten, et al. (1999). "Surface characterization of polypropylene/(ethylene-propylene) copolymer blends (PP/EP): application to injection-moulded systems." Surface and Interface Analysis **27**(8): 735-742.

Van Assche, G., A. Ghanem, et al. (2005). "Through-thickness analysis of the skin layer thickness of multi-layered biaxially-oriented polypropylene films by micro-thermal analysis." Polymer **46**(18): 7132-7139.

Velasco, J. I., J. A. D. Saja, et al. (1996). "Crystallization behavior of polypropylene filled with surface-modified talc." Journal of Applied Polymer Science **61**(1): 125-132.

Wu, C.-M., M. Chen, et al. (1999). "The role of metastability in the micromorphologic features of sheared isotactic polypropylene melts." Polymer **40**(15): 4195-4203.

Wu, G., K. Nishida, et al. (2004). "Rubber as additives to lower thermal expansion coefficient of plastics: 1. Morphology and properties." Polymer **45**(9): 3085-3090.

Yin, Z., Y. Ma, et al. (2005). "Adhesion of CPO onto high modulus TPO: Lap-shear tests in conjunction with microscopy studies of the fracture surface structure." Polymer **46**(25): 11610-11623.

Yin, Z., J. Yang, et al. (2007). "Quantitative probing the interfacial structure of TPO/CPO blends by transmission electron microscopy via EDX." Polymer **48**(5): 1297-1305.

Yokoyama, Y. and T. Ricco (1997). "Crystallization and morphology of reactor-made blends of isotactic polypropylene and ethylene-propylene rubber." Journal of Applied Polymer Science **66**(6): 1007-1014.

Zhang, M., Y. Liu, et al. (2002). "The effect of elastomeric nano[hyphen]particles on the mechanical properties and crystallization behavior of polypropylene." Polymer **43**(19): 5133-5138.

Zhong, G.-J. and Z.-M. Li (2005). "Injection molding-induced morphology of thermoplastic polymer blends." Polymer Engineering & Science **45**(12): 1655-1665.to

Zhou, Y. and P. K. Mallick (2005). "Effects of melt temperature and hold pressure on the tensile and fatigue properties of an injection molded talc-filled polypropylene." Polymer Engineering & Science **45**(6): 755-763.

Chapter 4

Performance of Electroplated ABS and PC/ABS as a function of Injection Molding Processing Conditions

4.1 Introduction

Electroplating plastic components has been a technique used for many years in a variety of industries, including automotive applications such as grilles and foglamp surrounds, kitchen and bath products such as faucets and handles, decorative functions such as caps and buttons, RFI/EMI-shielding and other electronic applications, and toys (Nielsen, 1985; Anis, 1994; Teixeira, 2005). The most commonly used polymers for these applications are ABS, which consists of a matrix of styrene and acrylonitrile copolymer (SAN) with grafted particulate phase of butadiene elastomer, and PC/ABS, which blends various amounts of polycarbonate (PC) with ABS (Concise Encyclopedia of Plastics, 2000; Polymer Blends Handbook, Volumes 1-2, 2002).

Producing large, high quality electroplated parts, such as automotive grilles, presents bigger challenges than smaller pieces. As the size of the electroplated parts increases, the mismatch between the mechanical and thermal properties of the plastic and metal are exacerbated. Larger parts with complicated geometries are more likely to have increased amounts of molded-in stress and be harder to plate with even metal thicknesses.

The electroplating process and adhesion mechanism is relatively well understood and covered in the literature, and will be summarized in the literature review. The effect of material selection and processing parameters on the electroplating and resulting performance are not as well understood or reported and is investigated in this chapter. This work is also the first to focus on large parts (automotive grilles) and the challenges they pose. The literature review covers the plating process, ABS and PC/ABS materials, and methods used to evaluate the performance of plated plastic components. An L8 Design of Experiments (DOE) was used to investigate the effect of processing conditions on the bulk, or molded-in, stress and the surface stress of automotive grilles. The bulk stress was evaluated using a stress-relief thermal cycle with strain gauged parts. The surface stress was evaluated with both glacial acetic acid testing and Scanning Electron Microscopy (SEM) evaluation of the resulting etched microstructure.

The effect of material and processing condition variables was evaluated with a variety of adhesion testing including cross-hatch adhesion testing and tensile/mandrel bend tests. The conclusions compare the findings of this chapter to the previous findings on the effect of processing on painted TPO materials.

While electroplated PC/ABS materials employ a completely different type of polymer and a different coating mechanism compared to the painted TPO materials discussed in the earlier chapters, the performance of these parts is related to rubber morphology, which has a similar dependence on material, geometry, and processing as TPO. For example, faster injection speeds were found to result in more elongated rubber near the surface of the semi-crystalline 773 compounded TPO in Chapter 3. A similar effect of injection speed was found on the rubber phase in the amorphous ABS materials examined in this chapter, with the elongated rubber resulting in poorer adhesion performance. There was also an effect of material choice on the rubber morphology found in

Chapter 3, where the rubber in the compounded TPO had a higher aspect ratio and was more elongated compared to the rubber in the reactor grade TPO. Material differences were also found to play a role in the rubber morphology, and therefore adhesion performance, in the ABS materials in this chapter. By building on the knowledge gained from semi-crystalline materials in previous chapters, a more in-depth understanding of the effect of the molding process and geometry on rubber morphology, surface chemistry, molded-in stress and adhesion was gained for electroplated amorphous materials. This knowledge will help develop a set of guidelines for future designs and mitigate quality issues.

4.2 Literature Review

4.2.A Electroplating Process

Plating polymer pieces with thin metal layers is not an easy task due to the large differences in thermal expansion coefficients, and other inherent property differences between the polymer and metal, as well as the complicated fields generated by complex geometries in the electroplating baths. Because of all of these differences, the process of electroplating plastics is a complicated one with many steps, which are described below (Electroplating Fundamentals, 2008).

4.2.A.i Surface Preparation

1. Solvent etch – This step is not always performed, but is used for PC/ABS blends containing > 55% PC. Higher concentrations of PC result in less rubber being available from the ABS blend, so solvent is used to swell what rubber is present making it more available during the next etching step
2. Etching – A bath of chromic and sulfuric acid is used to oxidize and remove the butadiene rubber phase, creating a porous surface that becomes more hydrophilic. The bath is typically around 67-77°C and

parts are typically etched for 6-8 minutes in the case of ABS and 8-12 minutes in the case of PC/ABS. The bath should be monitored for trivalent chromium concentrations to evaluate bath chemistry control.

3. Neutralization – Reduces the hexavalent chromium from the etch bath to its trivalent state.
4. Activation – An aqueous palladium-tin colloid (Pd particles surrounded by a $SnCl_2$) shell is deposited in the microscopic holes created by etching. This step provides catalytic sites for the growth of the electroless layer (Yen, 1995).
5. Accelerator – This step removes the tin chloride shell of the activator colloid, leaving 1-2 nm Pd particles in the etch sites as the catalyst for the next step. This step must be done soon after activation to prevent the $SnCl_2$ shell from oxidizing (Yen, 1995). This step also helps removes any residual hexavalent chromium left from the etching step.
6. Electroless Nickel or Copper - Deposits a thin, adherent metallic film on the surface of the part by chemical reduction. This layer makes the surface conductive for future electroplating operations. Electroless copper is preferred for larger parts because of its ductility, but the bath chemistry is harder to control than electroless nickel.

4.2.A.ii Electroless Plating

1. Copper Strike – Creates a fuse between the part and rack and builds up the electroless layer creating a more conductive layer and preventing burn off.
2. Acid Copper – The main copper layer that provides leveling and brightness as well as ductility for improved thermal cycling performance and higher impact resistance.
3. Copper Activator – Prepares acid copper layer for further plating
4. Semi-bright Nickel - Typically accounts for 2/3 of the duplex nickel structure. It is the columnar, more ductile, of the nickel layers and is also less active, providing more corrosion control.

5. Bright Nickel – Is the other 1/3 of the duplex nickel structure, which is laminar and provides most of the shine and brightness seen in the final product. It is harder and less ductile than the other layers, and is more chemically active than the semi-bright nickel.
6. Microporous Nickel – Is less active than the bright nickel layer and typically has ~10,000 pores/cm^2. This helps spread the corrosion current over many small cells and directs any corrosion in the bright nickel layers into thin vertical columns, instead of large, lateral patches which can cause cloudiness.
7. Chromium – This layer is very thin compared to the others (usually less than 0.5 μm). It is the source of the "blue" color of metalized plastics, and also provides scratch protection and prevents oxidation of the nickel layers.

Some of these different metal layers can be resolved optically after a polished cross-section is etched with a 1:4 solution of nitric and glacial acetic acid as shown in Figure 4-1. The thickness of the different layers is dependent on the processing and geometry of these parts, and has an effect on the performance.

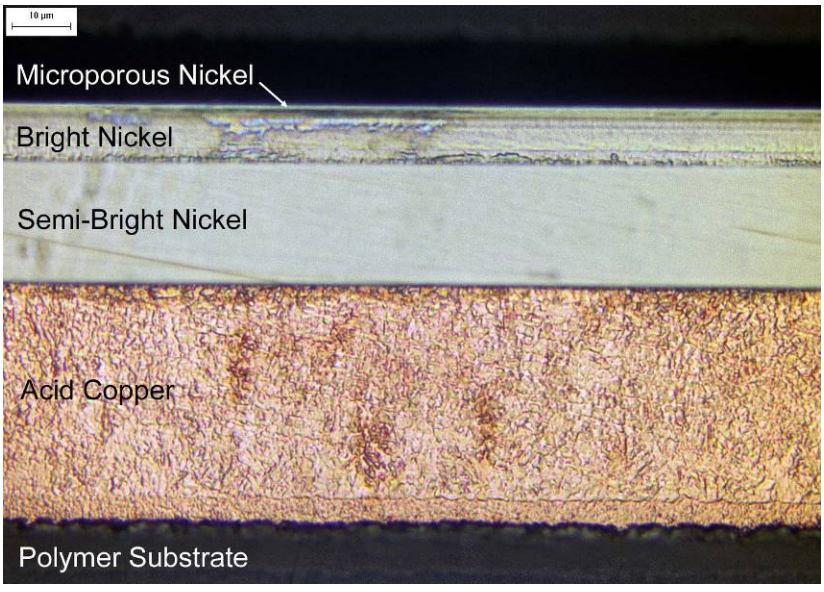

Figure 4-1: Optical micrograph of etched cross-section showing different metal layers

4.2.B Polymer Morphology and Metal Adhesion

The source of the adhesion strength in metal plated ABS and PC/ABS is the subject of some debate in the literature, but the general consensus is that the majority of the adhesion is due to a mechanical bond, as opposed to a chemical one (Beacom, 1970). In ABS and PC/ABS, the butadiene exists as a discrete rubber phase which is removed during the etching phase providing the sites for the mechanical bonding. The shape, amount, and distribution of the butadiene sites are determined by the polymer formulation, processing and mold geometry (Takahashi, 1997; Utracki, 1998; Choi, 2000). Blending PC with ABS improves the impact strength and heat resistance of the part, but makes plating more difficult due to fewer rubber particles being available at the surface (Yang, 1999). The surface and bulk morphology both affect the adhesion performance of the chromed part and will both be examined.

4.2.C Surface Morphology

For the best adhesion, the butadiene rubber at the surface should be round and well distributed, which, when removed, provides "lock and key" sites for the best mechanical bond with the electroless copper layer (Kato, 1968, 1968). This principle is demonstrated for an ABS based material in the schematic in Figure 4-2a. Elongated butadiene at the surface does not provide as good of a mechanical interlock (Figure 4-2b).

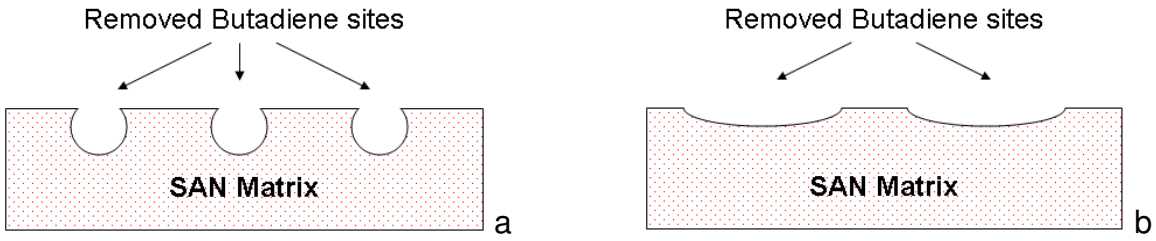

Figure 4-2: Comparison of butadiene morphology. (a) round, well distributed particles forming good mechanical "lock and key" adhesion. (b) elongated butadiene particles which are poor mechanical sites for chrome adhesion

The shape, size and distribution of the butadiene at the surface is a function of the amount of PC (if any), the molecular weight distribution and degree of cross-linking (determining the viscosity) of the butadiene, any compatibilizers used, the resin mixing history, part processing conditions and part geometry (Li, 1990; Takahashi, 1997; Yang, 1999; Tan, 2006). Due to the "fountain flow" effect in injection molded polymers (Rose, 1961; Tadmor, 1974), the surface of the part is experiencing predominantly elongational flow, not the shear effects found toward the middle of the part due the injection molding process. This phenomenon was schematically described by Tadmor (Figure 4-3) and is responsible for the skin-core structure of injection molded polymers, as discussed for polypropylene and TPO in Chapters 2 and 3 (Tadmor, 1974). Elongational flows have been shown to be the most effective in changing the morphology of polymer blends, such as ABS and PC/ABS, resulting in a very different morphology at the surface compared to the core (Utracki, 2002).

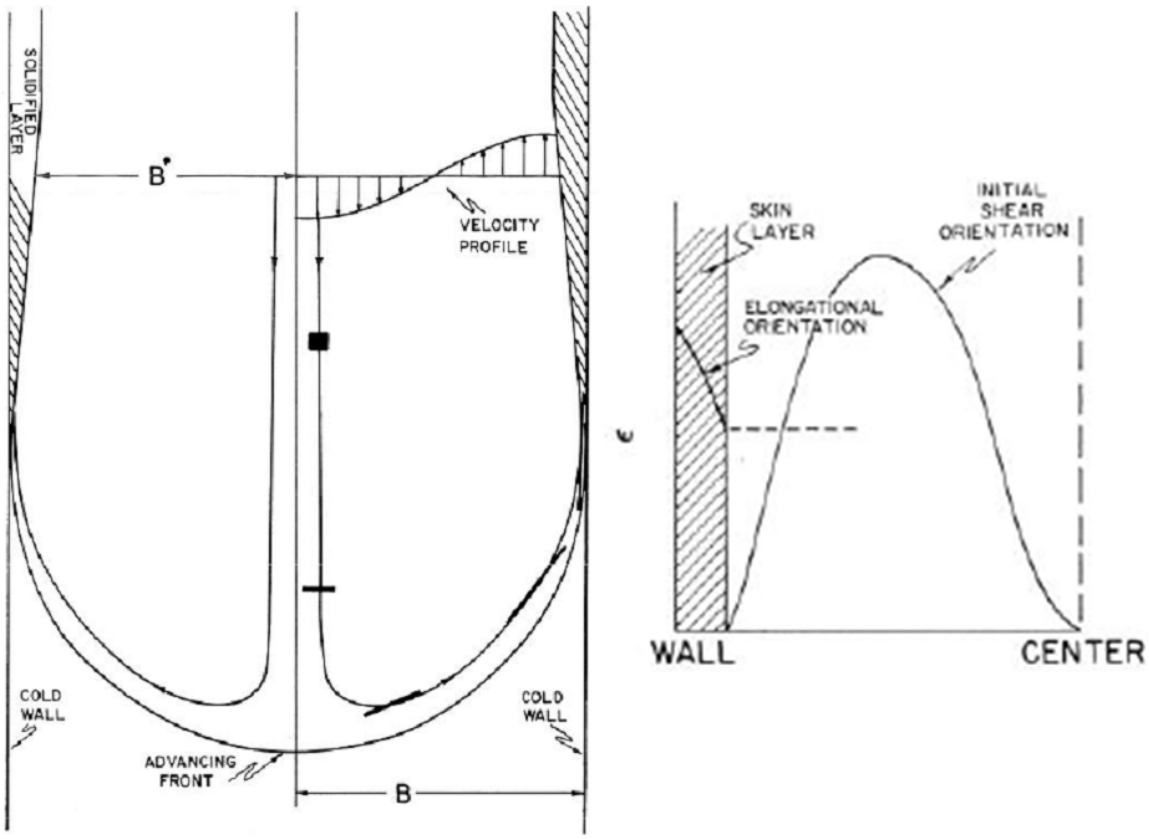

Figure 4-3: "Fountain flow" in injection molded polymers (Tadmor, 1974)

In ABS, an increased amount of rubber sharply increases the viscosity of the material. Casale et. al. found that adding 40% graft rubber to an SAN matrix with an average molecular weight of 68,000 had the same effect as doubling the molecular weight to 140,000 (Casale, 1975). Typically, resin manufacturers reduce the molecular weight of the matrix to adjust the overall resin viscosity to produce a material that is easier to injection mold, however this must be balanced with a loss of mechanical properties (Bucknall, 1977). The overall viscosity of the melt determines how much stress is seen during injection molding, and affects the surface morphology. The viscosity ratio between the rubber and the matrix also has an effect on the surface morphology, with a larger ratio allowing the rubber to maintain a more spherical shape, which is better for adhesion (Yang, 1999).

The size of the rubber, either inherent to the rubber itself or due to the thickness or molecular weight of the graft layer, has also been found to affect surface morphology (Chang, 1996). Studies have found the smaller rubber particle sizes (0.08 μm) can lead to agglomeration independent of graft type or amount. The amount of agglomeration for larger rubber particles (>0.19 μm) was dependent on graph amount, molecular weight, and mismatch with the matrix (Chang, 1996). Rubber agglomeration increased with large compositional acrylonitrile mismatch between the matrix and the graft, insufficient or too high molecular weight of the graft coverage, high rubber level, high matrix molecular weight, and small rubber particle size (Chang, 1996). Large agglomerations of rubber would not provide good "lock and key" sites for adhesion.

Hardness of the butadiene rubber, determined by the degree of cross-linking, also had an effect on the shape of the rubber near the surface. Highly cross-linked, hard butadiene particles acted much like inorganic fillers in other polymer systems, retaining a rounder shape for improved adhesion, but more difficult to etch and also decreasing the strain hardening behavior (Takahashi, 1997).

In PC-ABS, the more PC there is in the blend, the fewer butadiene sites that will be present at the surface, so optimization of the sites becomes even more important. Lee et. al. found that in ABS rich blends, the dispersed PC phase in the continuous ABS phase was more elongated in the flow direction near the surface, and was spherical in the core (Lee, 1992). This finding correlates with our studies on the rubber (dispersed) phase in TPO blends in Chapter 3. The size of the dispersed PC domains decreased with decreasing amounts of PC in the blend. With more, elongated PC at the surface, there is less butadiene available for etching, resulting in poorer adhesion.

The size of the PC domains was also found to be affected by the amount of rubber in the ABS phase (Tan, 2006). Increasing the amount of rubber in ABS from 15% to 55% was found to increase the viscosity of the ABS dramatically. The effect of the viscosity changes in a 30/70 PC/ABS blend was demonstrated by Tan et. al. and showed that increasing the amount of rubber, and therefore the viscosity, of the ABS phase resulted in a change in size and shape of the PC domains (Tan, 2006). At 15% rubber in ABS, the PC domains were round and well dispersed. Increasing the rubber to 30% resulted in larger, more elongated PC domains, and finally at 55% rubber the PC domains become much smaller and irregular due to the large shearing effect (Tan, 2006). All of these various morphologies will impact adhesion performance.

To get the optimum butadiene sites, the stress at the surface needs to be minimized (Kato, 1967). This can be accomplished not only through material properties described above, but also through part and mold design, and processing conditions. Part design should minimize or eliminate sharp corners and deep recesses, and the recommended minimum wall thickness is 2.5 mm (Ellis, 1967). Mold design should avoid long flow lengths as well as provide adequate venting. A mold technique that can be used to improve adhesion is the mold surface effect (MSE), where grooves approximately 120-250 μm deep are carved in the mold wall in non-appearance areas. The MSE works by disrupting the flow in the melt front, reducing the skin orientation and rubber elongation, and promoting anisotropy (Kulich, 2003; Fritch, 2006).

Melt processing conditions can also affect the amount of stress at the surface. To minimize surface stress, it is recommended to run "hot and slow" by raising the mold and melt temperatures and reducing the injection speed within the recommended specifications of the material (Ellis, 1967). Surface stress is often

qualitatively assessed by immersing the part in glacial acidic acid, which will whiten surface stressed regions of the part (Ellis, 1967).

4.2.D Bulk Morphology

Residual, or molded-in, stress is a mechanical stress that is present in the material with no externally applied stress. Residual stresses can be flow induced microstresses (due to orientation) or non-isothermal cooling induced macrostresses (Pham, 1993; Kamal, 2002). The flow induced microstresses are due to orientation created during the filling and packing of an injection molded part, whereas thermally induced macrostresses are created during the cooling stage and result from the temperature gradient from the cooler wall to the warm core of the part.

Minimizing the molded-in stress of the polymer will improve the dimensional stability and reduce the stress between the metal and the polymer. Unfortunately, the low injection speeds that minimize surface stress (Ellis, 1967) increase the orientation in the bulk, which increases the molded-in stress and warping tendencies (Turner, 2002). Figure 4-4 shows the effect of injection speed and melt temperature on both surface stress and bulk stress. The surface stress was assessed by dipping the samples in glacial acetic acid for 1 minute and observing the amount of whitening. Molded-in stress was determined by the amount of shrinkage in the part after it had been stress relieved at 191°C for 2 hours. Low melt temperatures increase the amount of both surface and molded in stress, as demonstrated by the samples on the left which show more whitening and more shrinkage than the samples on the right. Faster fill times (injection speed) show more surface stress at both melt temperatures, but less molded-in stress.

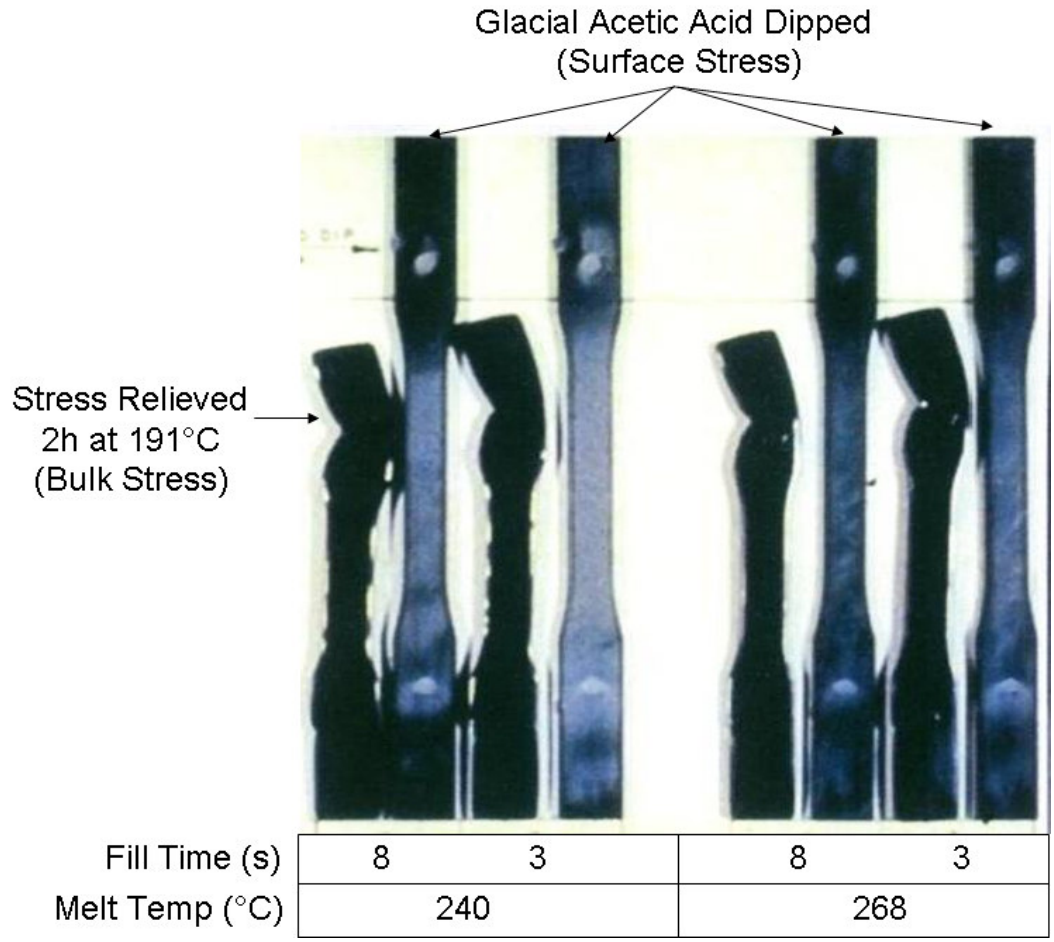

Figure 4-4: Effect of injection speed and melt temperature on surface and bulk stress (Turner, 2002)

Having less molded-in stress in parts that are molded at a faster injection rate is not intuitively obvious, since it would be assumed that faster rates would result in more orientation and therefore more molded-in stress. However, several authors have confirmed these findings, and theorize that the higher injection rate raises the temperature of the melt, allowing for more relaxation time, which is what decreases the molded-in stress (Siegmann, 1982; Chiu, 1987; Pham, 1993). Therefore, it can be concluded that minimizing the bulk and surface stresses are competing factors for processing conditions and the proper balance must be found for the best adhesion for each part.

4.2.E Adhesion

Similar to painted components, the adhesion between the polymer and metal layers is difficult to quantify. Qualitative methods to evaluate the adhesion strength include bend and saw tests to look for flaking or peeling as a result of stress from bending or saw blades (Standard Practice for Qualitative Adhesion Testing of Metallic Coatings, 2008), thermal cycling and looking for cracks or blisters (Electroplating, bright or low gloss decorative over ABS or PPO plastic - Exterior, 2006), and cross-hatch adhesion testing (Teixeira, 2005; Standard Practice for Qualitative Adhesion Testing of Metallic Coatings, 2008). A more quantitative way to assess adhesion is a pull test, in which the metal layer is scribed and an Instron is used to measure the force needed to remove it at a 90° angle (Ellis, 1967; Matsunaga, 1971; Villamizar, 1981).

As previously described in Chapter 3, Professor Martin's group at the University of Michigan has demonstrated a quantitative adhesion test for painted TPO that uses tensile forces generated by either placing the sample in tension, or using mandrel bend (elastica) testing (Figure 4-5) (Tang, 2001). This tensile stress produces a shear stress between the coating and substrate due to the difference in elastic moduli that can be calculated for a quantitative adhesion assessment. Metalized ABS parts with known areas of good and poor adhesion will be tested to determine if that method is also applicable to these systems.

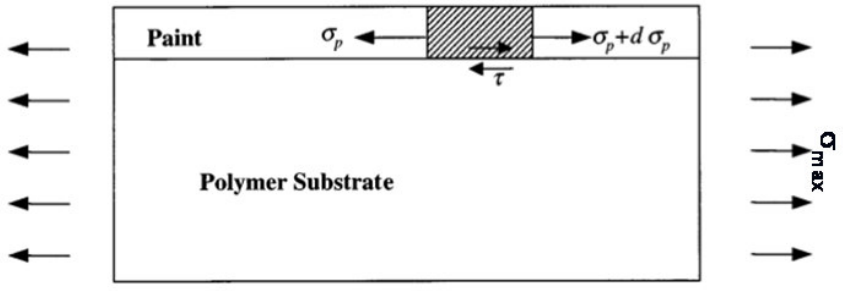

Figure 4-5: Using tension to create a shear stress at the paint/polymer interface for quantitative adhesion testing (Tang, 2001)

The shear strength of the interface (τ) can be calculated from the tensile strength of the paint (σ_{max}), the film thickness (h_p) and the crack spacing at saturation ($\bar{l}$) using Equation 4.1:

$$\tau = 1.337\, h_p \frac{\sigma_{\max}}{\bar{l}}$$

Equation 4.1

4.3 Experimental

To better understand the correlation between the processing conditions and the resulting surface morphology, bulk molded-in stress, and adhesion performance in the field, automotive grilles were processed with various conditions using an L8 DOE shown in Table 4-1. The processing variables examined for the DOE were injection speed, melt temperature and mold temperature. The material used for the DOE was the GE Sabic MG37 ABS. A control was also molded in the MG37 using the current manufacturing processing conditions and for comparison, a grille was molded in GE Sabic MC1300 PC/ABS. These conditions were compared to the current production conditions to determine if performance improvements could be made.

The effect of resin formulation was also examined by using the optimized processing condition with ABS material supplied from three different suppliers: Lanxess Lustran PG 298, Sabic MG37 and Samsung STAREX ABS MP-0160R. These particular resins were chosen for this study because they were all commercially available ABS resins of potential use for making these components in production; however they were suspected to have subtle variations in near-surface morphology that might influence coating adhesion.

Table 4-1: L8 DOE of processing conditions

Cell	Run Order	Injection Speed	Melt Temperature	Mold Temperature	Material
1	2	L	L	L	Sabic MG37
2	3	H	L	L	Sabic MG37
3	10	L	H	L	Sabic MG37
4	9	H	H	L	Sabic MG37
5	5	L	L	H	Sabic MG37
6	4	H	L	H	Sabic MG37
7	7	L	H	H	Sabic MG37
8	8	H	H	H	Sabic MG37
A	1	Current Production Values - Baseline			Sabic MG37
9	6	L	H	H	Sabic MC1300

	H	L
Injection Speed	+10%	-10%
Melt Temperature (°C)	277	249
Mold Temperature (°C)	82	38

4.3.A Molded-in Stress Measurements

Parts were strain gauged to measure molded in stress using Vishay Micro-Measurements general purpose strain gages. The strain gages were mounted to the parts using M Bond 200 adhesive in the upper corner (Figure 4-6). The part was placed in an oven and taken from room temperature to 100°C at a rate of 2° per minute and the strain was recorded every 2 minutes. It was held at 100°C for two hours and the strain was recorded every 5 minutes. The part was brought back to room temperature and the strain was recorded every 2 minutes. The final strain was recorded after 24 hours at room temperature.

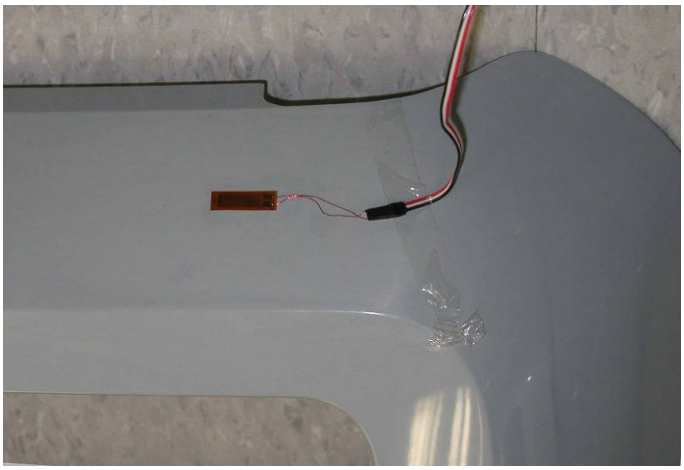

Figure 4-6: Strain gage location

4.3.B Glacial Acetic Acid Testing

Fifty minutes after the parts were molded they were dipped in room temperature glacial acetic acid for 30 seconds and photographed. Glacial acetic acid is used as an indicator of areas with high surface stress because the acid attacks the stressed areas and causes them to visibly whiten (Ellis, 1967; Standards and guidelines for electroplated plastics, 1984; Electroplating Fundamentals, 2008). The parts were photographed and the results were used to direct later testing.

4.3.C SEM Microstructure Evaluation

The surface microstructure of the samples was examined with a JEOL 6300F field emission microscope using a 20 kV beam. An Oxford ISIS Energy Dispersive X-ray Spectroscopy (EDS) system was used determine the elemental distributions. Polymer samples were carbon coated before analysis.

For the DOE, as-molded parts were removed from the process after the etching and neutralization step. Sections approximately 4 cm x 4 cm were removed from the part in two locations. First, an area that was not highlighted as an area of high stress by glacial acetic acid testing, but did include a radius, was evaluated

to look for the effect of geometry. Secondly, an area indicated by the glacial acetic acid testing to be a region of high surface stress was examined to compare it to the low stress area.

To understand the adhesion failures found in field returned samples, plated parts were prepared for SEM examination using two different methods. Areas with adhesion loss were removed, and the interface on the metal and polymer sides were both examined. The metal in these areas had already separated from the polymer.

In areas where the metal was still attached to the polymer, it was either physically removed pulling the metal off the substrate or chemically removing the metal layers using acid. The physical removal method allows us to examine the metal side to look at how much polymer is on the metal interface. Failure with little polymer on the metal tells us that the there was not a good mechanical interlock between the polymer and the metal. If there is polymer on the metal side, this indicates that the weakest point of the layered structure is within a polymer boundary layer.

The chemical removal method involved first removing the chrome layer with concentrated hydrochloric acid (HCl). Next, the nickel and copper layers were removed with a bath in a piranha solution of 20% sulfuric acid and 5% (30% concentrated) H_2O_2. When the metal was removed with the physical removal method, it caused ductile failure in the polymer, obscuring the etch structure, but by removing the metal layers chemically, there was no mechanical stress on the polymer surface leaving the etch structure intact. This method could not be used to examine the metal interface since it was chemically dissolved, so typically, both methods were used in conjunction.

4.3.D Adhesion Testing

The adhesion of the metal layers to the polymer substrate was measured in two different ways. A cross-hatch scribe test, similar to what is done on painted components was used. For this method, the area was to be tested wiped clean with isopropyl alcohol and sanded with 280 grit silicon carbide sandpaper. The area was then scribed with a carbide tip through the metal layers and into the substrate as shown in Figure 4-7 for a total of 128 triangles. Any loose debris was removed from the surface before applying 3M No. 898 tape. The tape was pressed on firmly and then removed rapidly within 90 +/- 30 s of application by pulling it back upon itself at as close to an angle of 180° to the panel as possible. The number of triangles removed was reported as a measure of adhesion in addition to any other observations about chipping, flaking or general poor adhesion. It should be noted, that aside from the alcohol wipe and sandpaper scuffing, this is the same method described in ASTM B 571 (Standard Practice for Qualitative Adhesion Testing of Metallic Coatings, 2008).

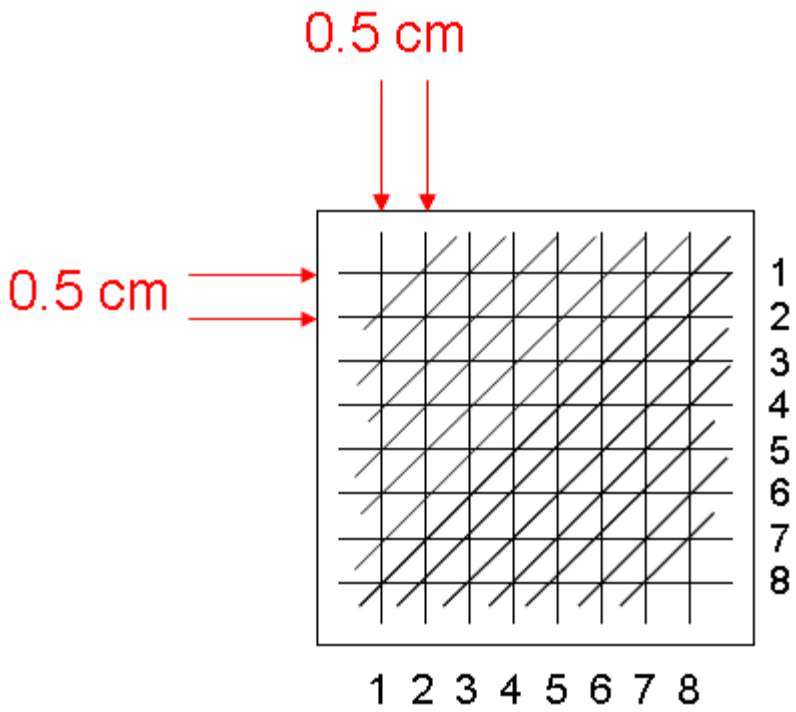

Figure 4-7: Diagram of scribe pattern for adhesion testing

Grilles with known areas of good and poor adhesion were prepared and analyzed by Brenda Vyletel of Professor Martin's group at University of Michigan. Samples were tested both in tension and using a mandrel bend. For both tests the samples were cut into 10 cm x 1 cm bars and the edges were polished to a 9 μm finish to minimize edge effects. The tensile samples were put in an Instron and pulled at a rate of 1 mm/min. The elastica samples were bent around a 16 mm diameter tube until fracture.

4.4 Results and Discussion

4.4.A Molded-in Stress Measurements

A typical strain measurement of ABS as a function of temperature for a 2 hour 100℃ thermal cycle is shown in Figure 4-8. Important regions of note on the graph are: 1) at what temperature the stress starts to relieve, which is the Heat

Deflection Temperature (HDT) and 2) the difference (delta) between the starting and ending strain value, which is a measure of the overall amount of molded-in stress.

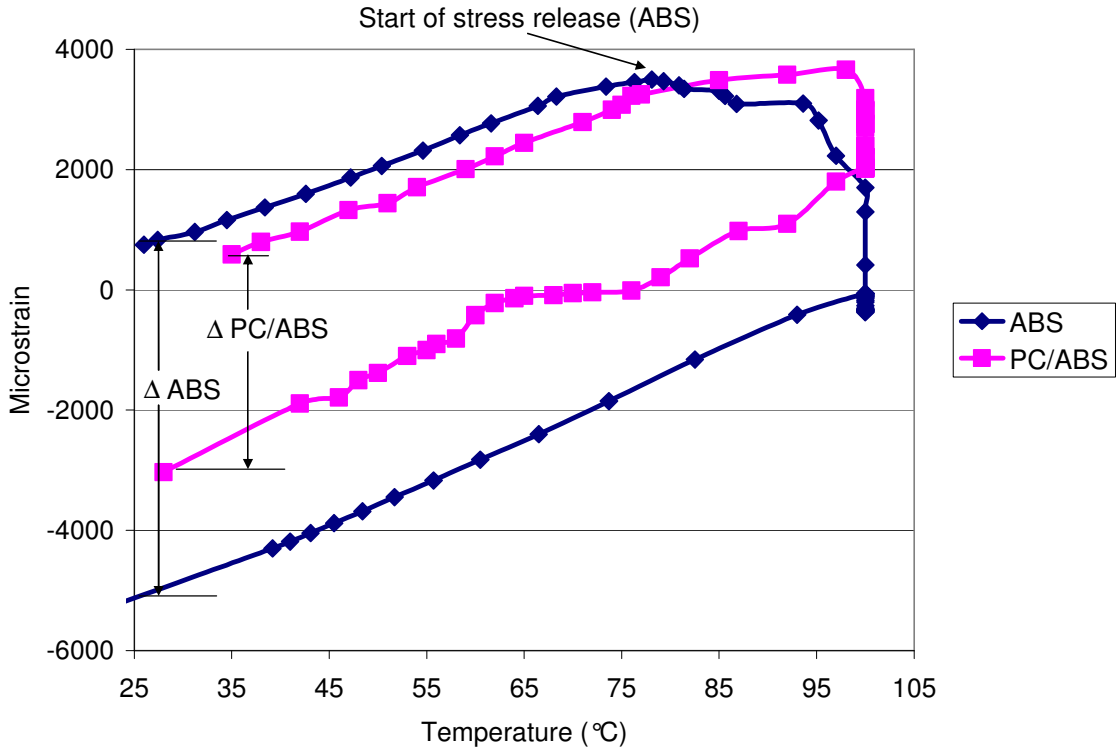

Figure 4-8: Typical strain vs. temperature measurement of molded-in stress

For the best in-service performance, it has been determined that the material should be able to withstand higher temperatures before the onset of stress relief and have the smallest delta for the best dimensional stability and least amount of stress between the coating and the substrate. The temperature at which the stress started to be relieved was not found to be dependent on molding conditions - only material formulation. The ABS materials start to relieve at ~80°C while the PC/ABS starts to relieve at ~90°C due to the improved thermal stability of the polycarbonate.

The measured deltas are shown in Figure 4-9. The cells are colored to correspond to the adhesion measurements (discussed later) where red = worst adhesion, green = best adhesion. The PC/ABS bar is textured for easy comparison. The current production condition (Cell A of the DOE) showed a large amount of molded in stress, more than any other condition during the trial, which was contributing to the high number of field returns.

It is noted that the sample with the best adhesion (Cell 7) had the most molded in stress, while the sample with the worst adhesion (Cell 6) had the least (of the ABS samples). This corresponds to the "hot and slow" molding condition providing the least surface stress (best adhesion) but also the most bulk orientation (high molded in stress) as discussed in the literature review (Turner, 2002). For the best overall performance, these two factors have to be balanced. The improvement in molded-in stress achieved by processing optimization of the ABS material is modest, however, compared to the ~75% reduction that can be achieved by using a PC/ABS blend. Due to the higher cost of the PC/ABS material, it must be determined on a part-by-part basis if this improvement in properties is required for adequate field performance.

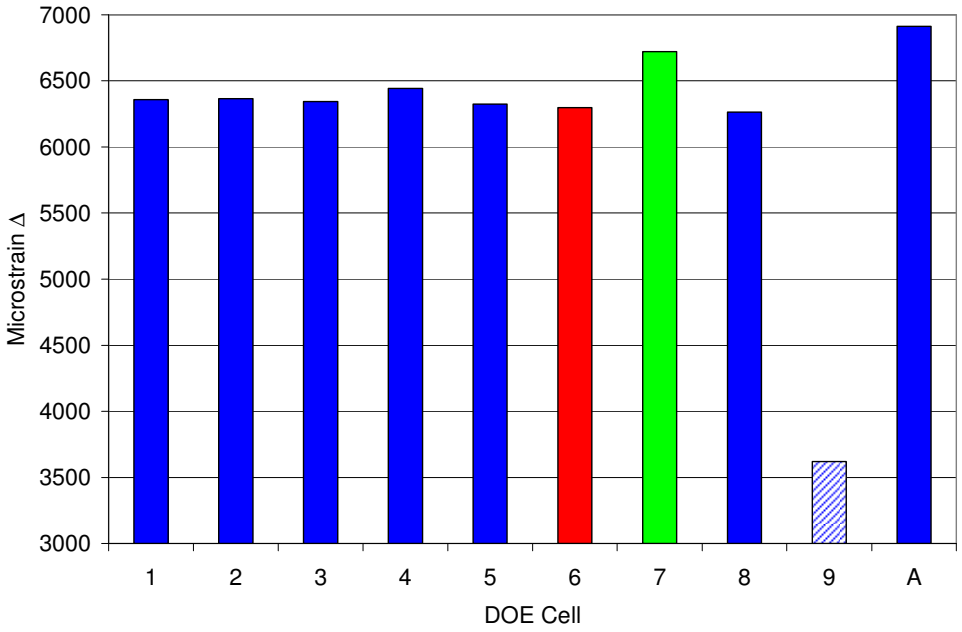

Figure 4-9: The Δ of molded in microstrain as a function of DOE cell number

ABS materials with different formulations from different suppliers were also evaluated for molded-in stress at the same molding conditions and the results are shown in Figure 4-10. There were differences between the three materials, even though they are all ABS. The Lanxess had the lowest HDT (83℃), while the Sabic (85℃) and Samsung ABS materials (87℃) were a few degrees higher. The Samsung ABS material also had the least amount of molded in stress (6200 microstrain compared to more than 7000 for Sabic and Lanxess). The increased thermal stability and lower amount of molded-in stress was found to improve adhesion performance in Ford durability testing.

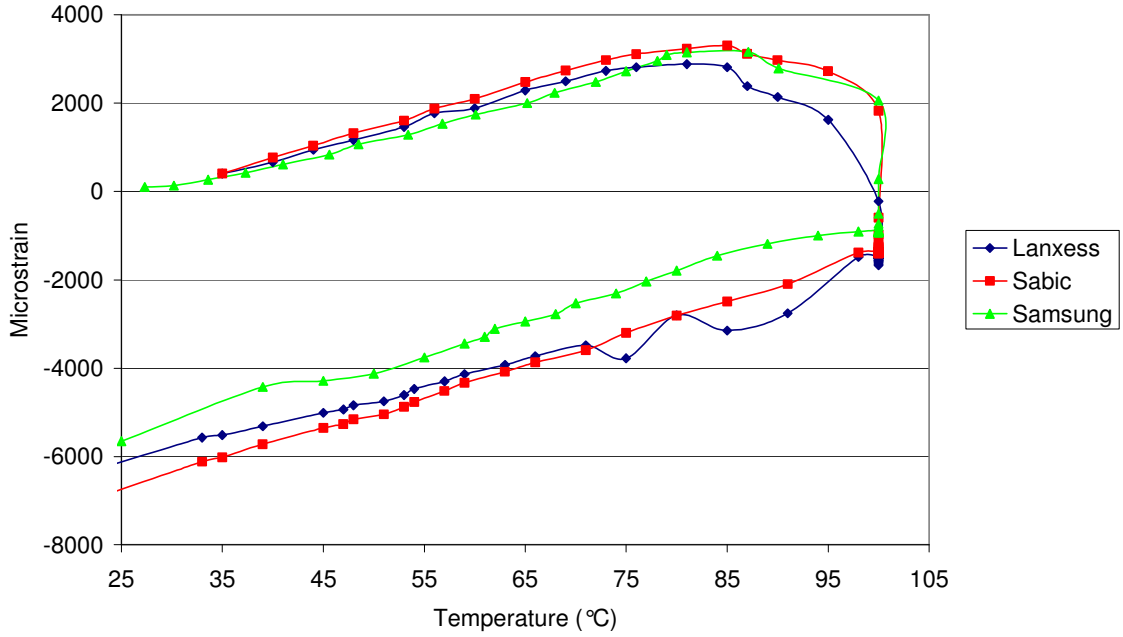

Figure 4-10: Molded-in stress comparison of ABS from 3 different suppliers

4.4.B Glacial Acetic Acid Testing

Molded grilles were dipped in glacial acetic acid and areas of whitening were documented as an indication of the amount of surface stress. The part molded with the current production molding conditions (Cell A of the DOE) showed whitening in the upper corner, at the bottom of the side opening and along the top of the grille, indicating high surface stress in those regions (Figure 4-11).

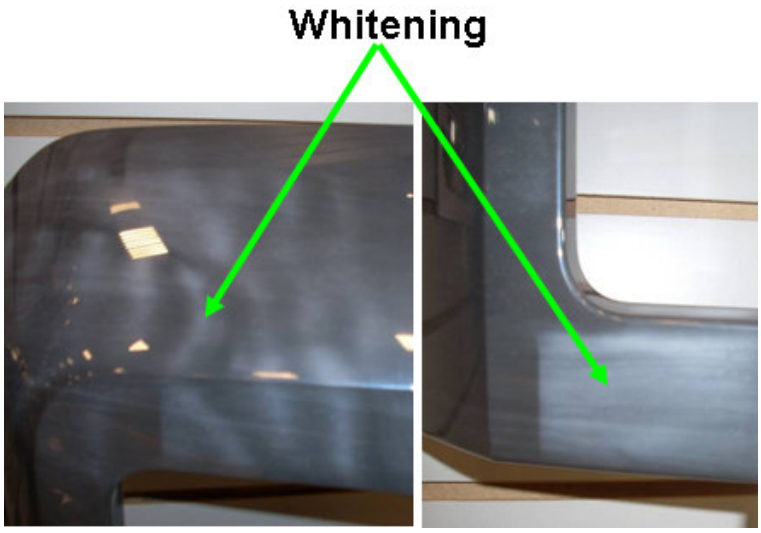

Figure 4-11: Pictures of grille molded using current production molding parameters after glacial acetic acid testing

Changing the molding parameters changed both the amount and location of the whitening. The conditions that were found to generate the highest amount of surface stress and most whitening were parts molded with low melt temperatures with high injections speeds, such as cells 2 and 6 of the DOE. Pictures of parts molded with these conditions are compared to those with lower surface stress (cells 3 and 7) in Figure 4-12 showing the greater amount of overall surface whitening in the high surface stress parts.

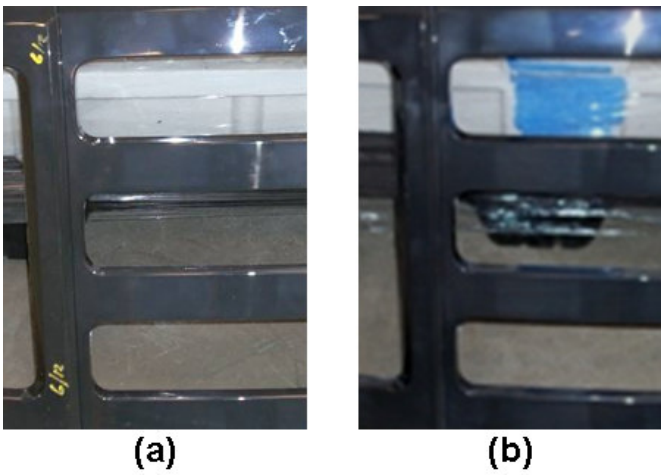

Figure 4-12: Picture of grille molded using (a) high surface stress inducing molding parameters and (b) low surface stress inducing molding parameters after glacial acetic acid testing

The DOE found that amount the surface stress in parts that were currently being produced could be reduced by increasing the melt temperature and decreasing the injection speed (Figure 4-13). While these molding conditions increased the bulk molded-in stress, as discussed above, the adhesion performance was improved (discussed later), indicating that the adhesion performance was more heavily influenced by surface morphology than bulk molded-in stress.

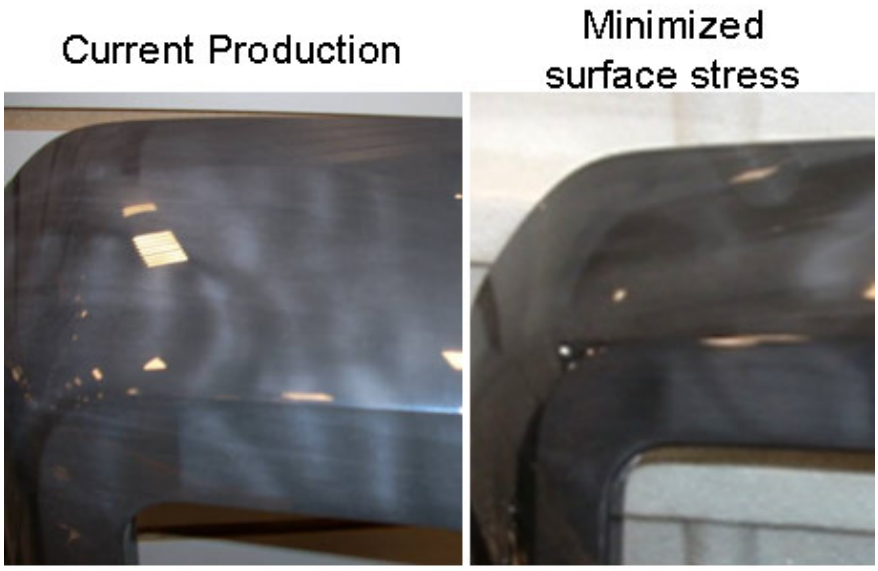

Figure 4-13: Picture of grille molded using low surface stress inducing molding parameters (hot melt temperature, slower injection speed) compared to the original production conditions after glacial acetic acid testing

The effect of different ABS formulations on the amount of surface stress was also investigated at a single molding condition. Results from the glacial acetic acid testing on the three supplied ABS materials are shown in Figure 4-14. It should be noted that glacial acetic acid testing was not conducted on the PC/ABS samples because there was not enough contrast with the whitening and the light color of the bulk resin. The Samsung ABS material was found to have the least amount of surface stress. The Lanxess ABS material had much more surface stress, even after processing optimization was completed, compared to the other materials.

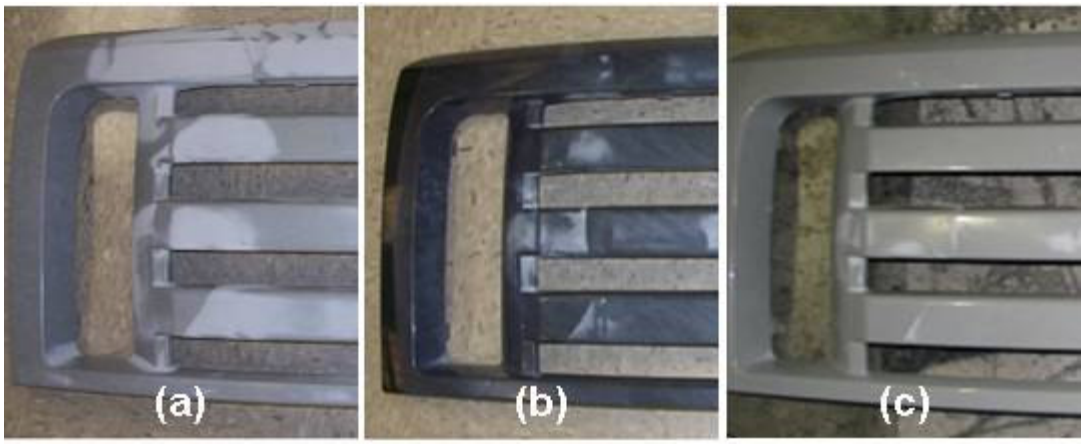

Figure 4-14: Effect of resin chemistry by supplier (a) Lanxess (b) Sabic and (c) Samsung on glacial acetic acid results

4.4.C SEM Microstructure Evaluation

To determine the effect of geometry on the surface morphology, all of the DOE samples were examined in a region indicated to be low in surface stress by the glacial acetic acid testing. Minimizing the effect of the surface stress on the morphology should allow the effect of the geometry on the morphology to be seen more clearly. Three areas on 6 cm x 4 cm samples that included a radius feature were examined: the top, which was the area closer to the top of the grille; the radius, which included the peak of the ~ 6 mm horizontal radius (Figure 4-15); the front, which was moving down from the radius along the front (vertical surface) of the grille.

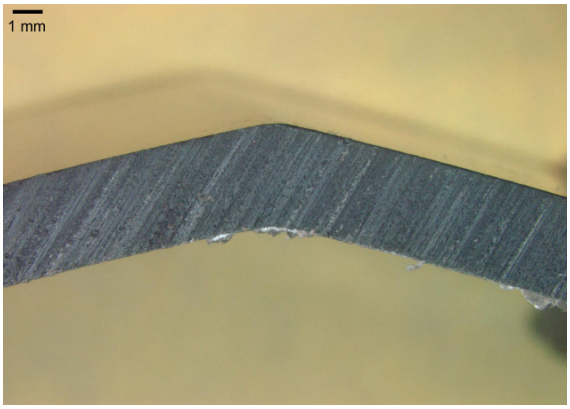

Figure 4-15: Cross-section of radius in low stress samples

There was no difference found in the etch patterns (and therefore rubber morphology at the surface) along the radius, indicating that the radius was not sufficiently sharp enough to cause additional surface stress (Figure 4-16) for any of the DOE conditions.

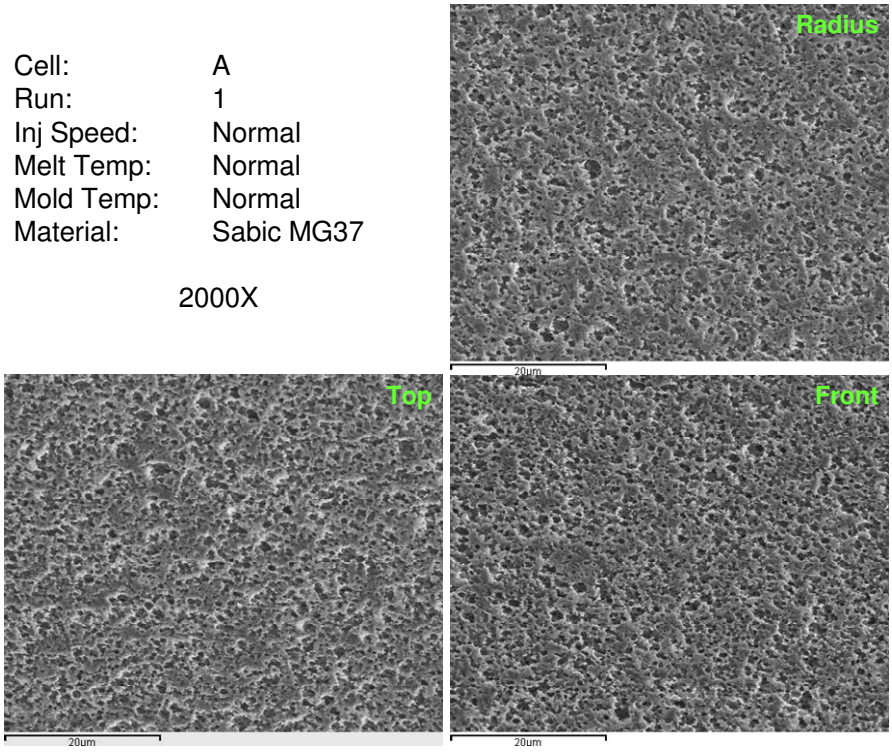

Figure 4-16: SEM results for the top, front and radius sections

To determine the effect of surface stress on the surface morphology, samples were examined in both high and low surface stress regions, as indicated by the glacial acetic acid testing. The etch microstructure is shown at two different magnifications in Figure 4-17 and Figure 4-18 for each of the processing conditions used in the DOE in a low surface stress region. In low surface stress regions, there is little difference seen in etch morphology as a function of molding conditions.

Regions that were shown to be high stress areas by glacial acetic acid testing were selected for further examination at certain molding conditions. The conditions selected were: current production (Cell A), best adhesion (Cell 7), worst adhesion (Cell 6) and PC/ABS (Cell 9). The results in those areas are shown in Figure 4-19 and Figure 4-20.

There were subtle differences found in the etch morphology as a function of processing conditions in high stress regions that could affect adhesion. At lower magnifications (Figure 4-19), the etch pattern of the current production (Cell A) sample and, to a greater extent, the worst adhesion (Cell 6) sample show evidence that there had been elongation of the rubber at the surface, due to the high surface stresses. The good adhesion (Cell 7) and PC/ABS samples showed a more rounded etch morphology, which provided a better "lock and key" surface structure for adhesion. This showed that areas of the part that had tendencies of higher surface stress due to part geometry and gating configurations were more sensitive to processing conditions that can produce additional stress at the surface.

In the higher magnification pictures (Figure 4-20), the samples with elongated rubber (Cell A, Cell 7) also showed less remaining SAN matrix at the surface. High surface stresses resulted in a faster acid attack during the etching process, the same principle behind the glacial acetic acid testing. Since all of these samples were in the etchant for the same amount of time, the condition of the matrix speaks to the amount of stress at the surface. If the matrix was attacked more aggressively due to high surface stress, this could have resulted in a weak boundary layer and poor adhesion.

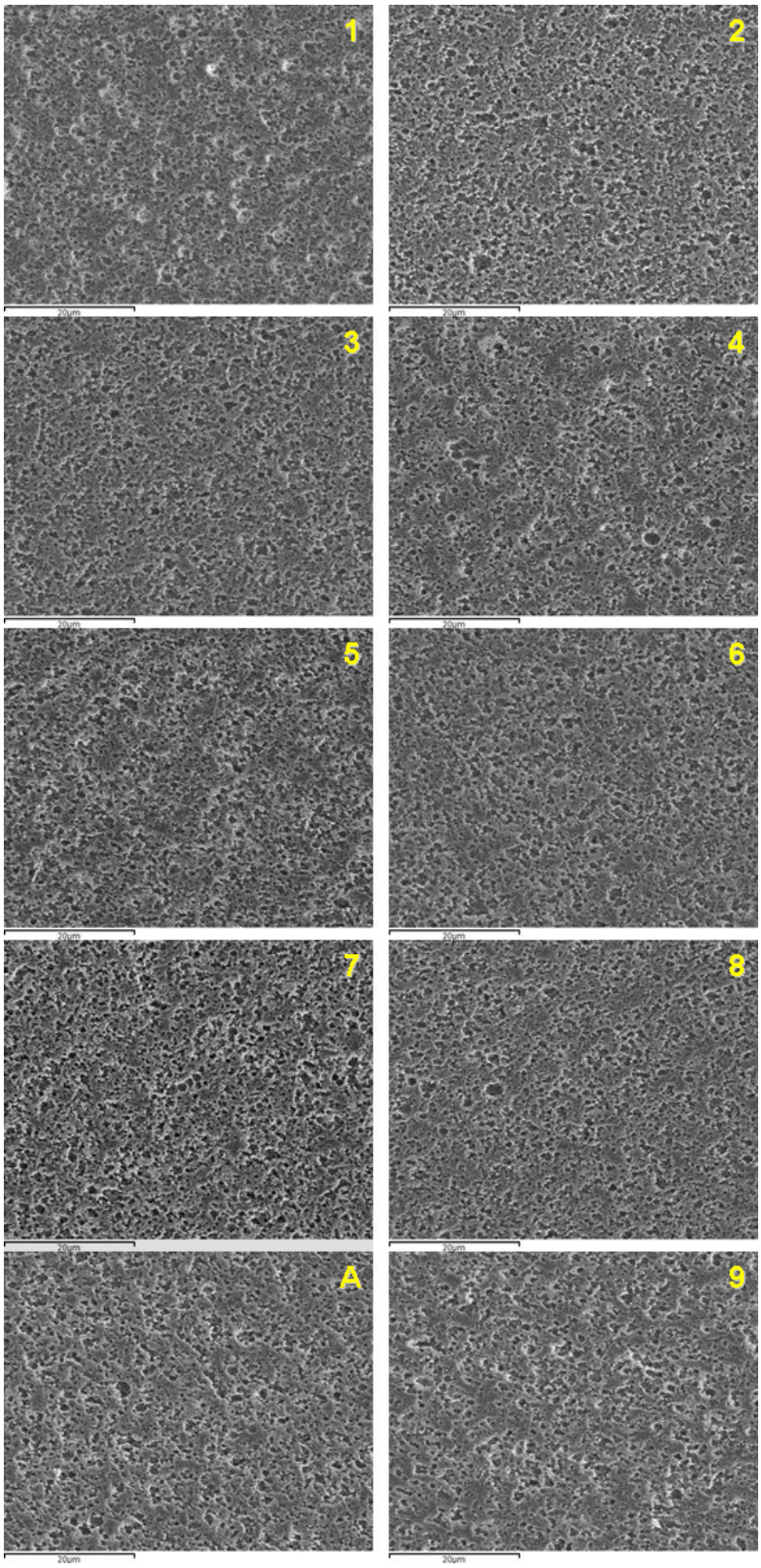

Figure 4-17: SEM of etch morphology as a function of molding conditions for each cell of the DOE (2,000X)

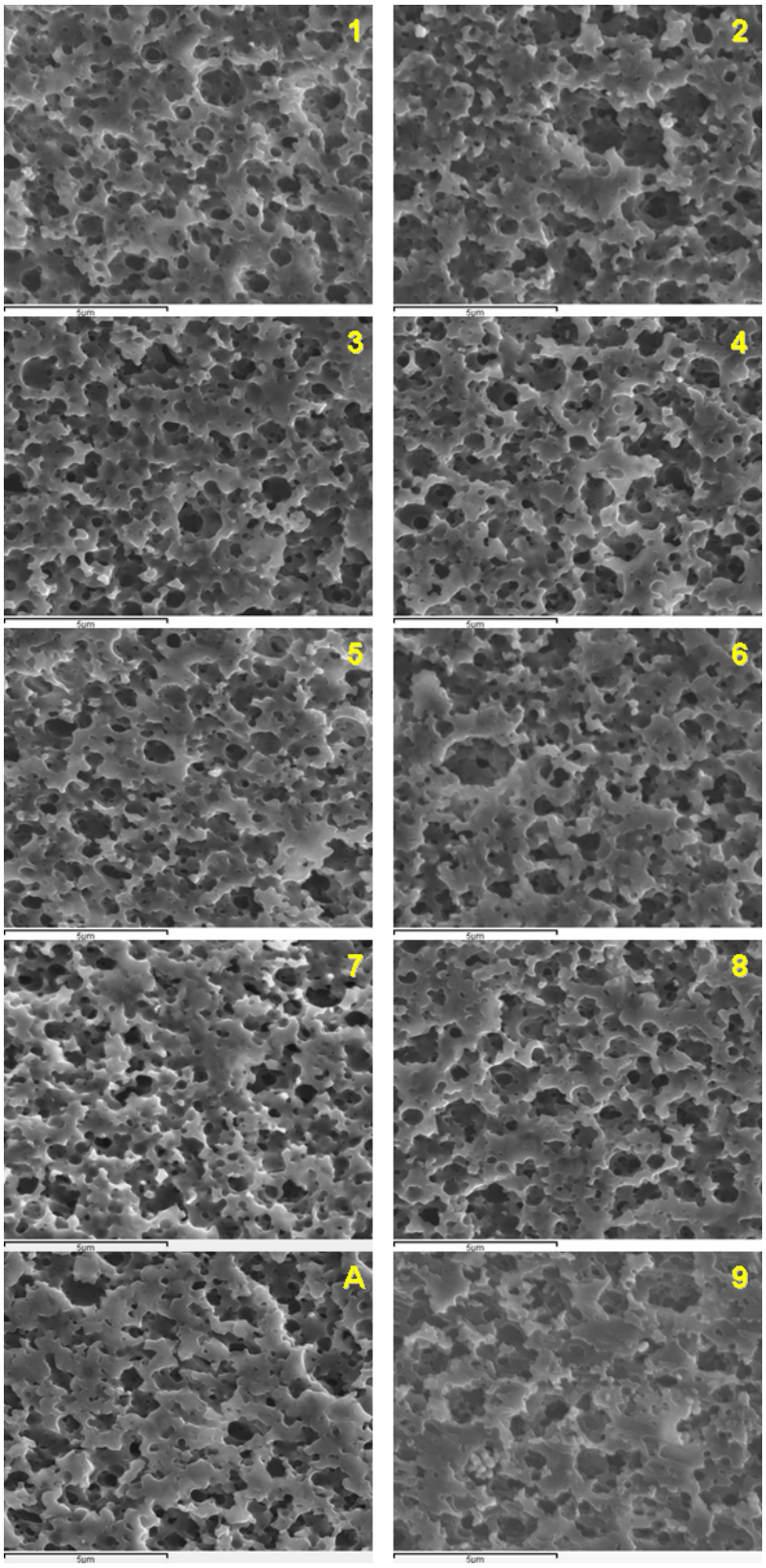

Figure 4-18: SEM of etch morphology as a function of molding conditions for each cell of the DOE (10,000X)

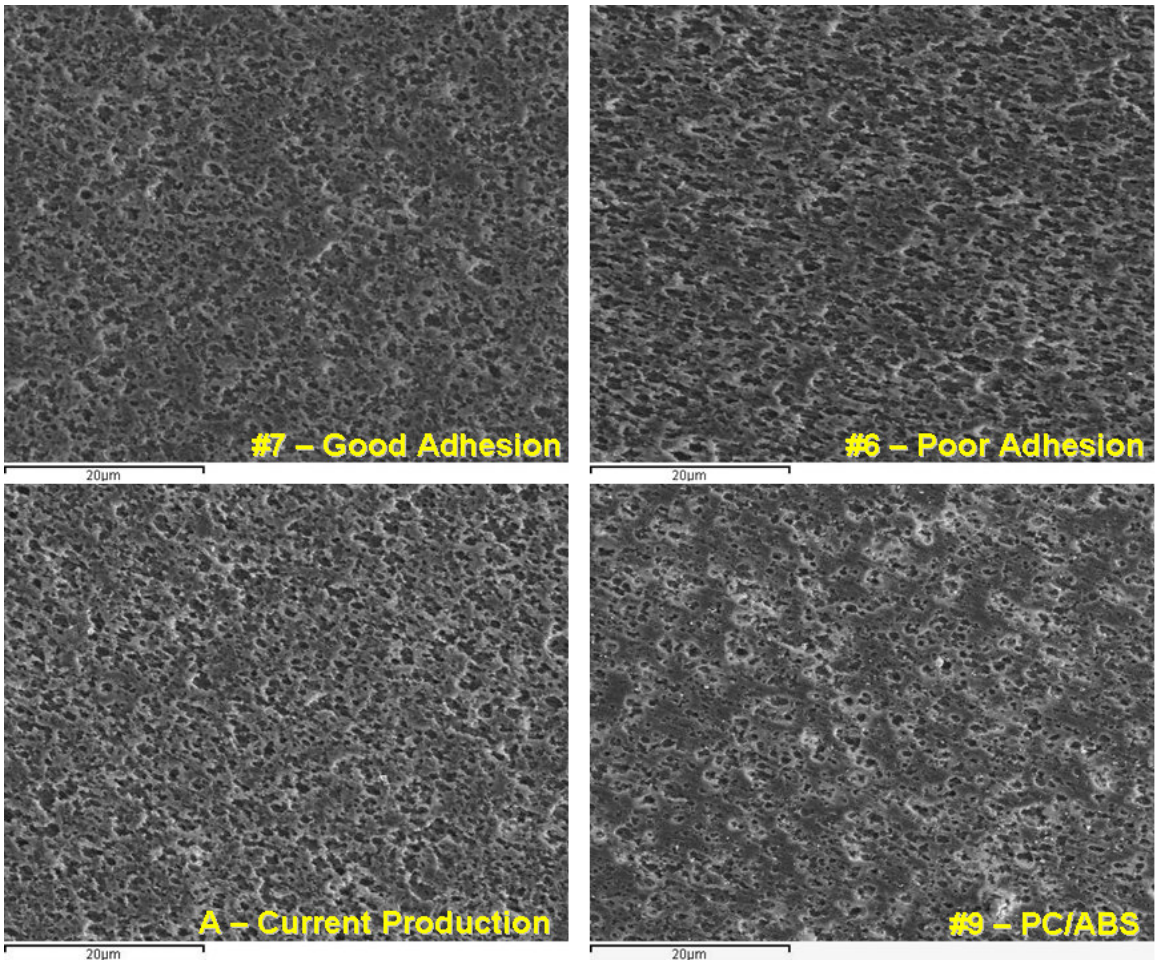

Figure 4-19: SEM of etch morphology in high stress region as a function of molding conditions (2,000X)

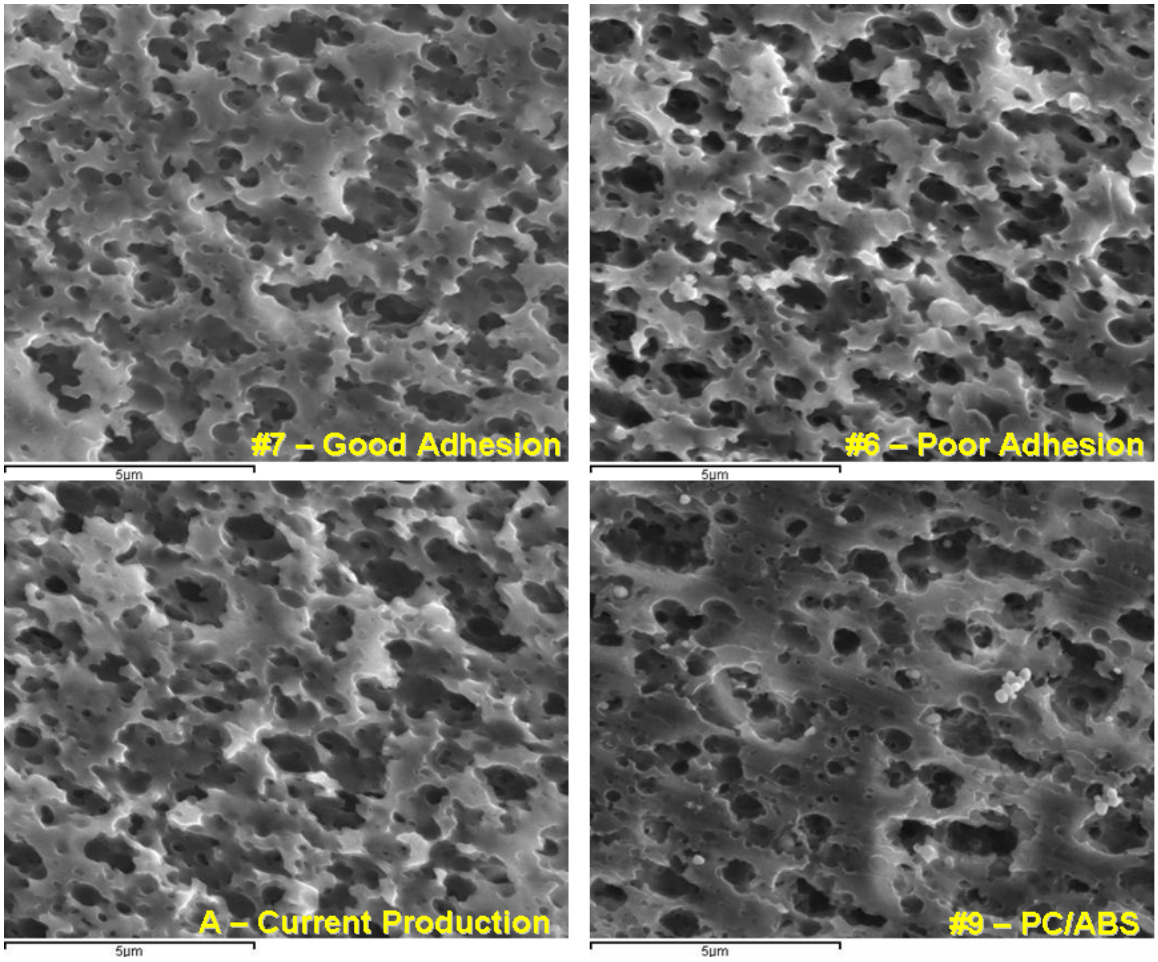

Figure 4-20: SEM of etch morphology in high stress region as a function of molding conditions (10,000X)

The materials evaluated were all ABS materials, but the surface morphology did vary by supplier under standard etch conditions as shown in Figure 4-21, which examines a high surface stress region as indicated by glacial acetic acid testing.

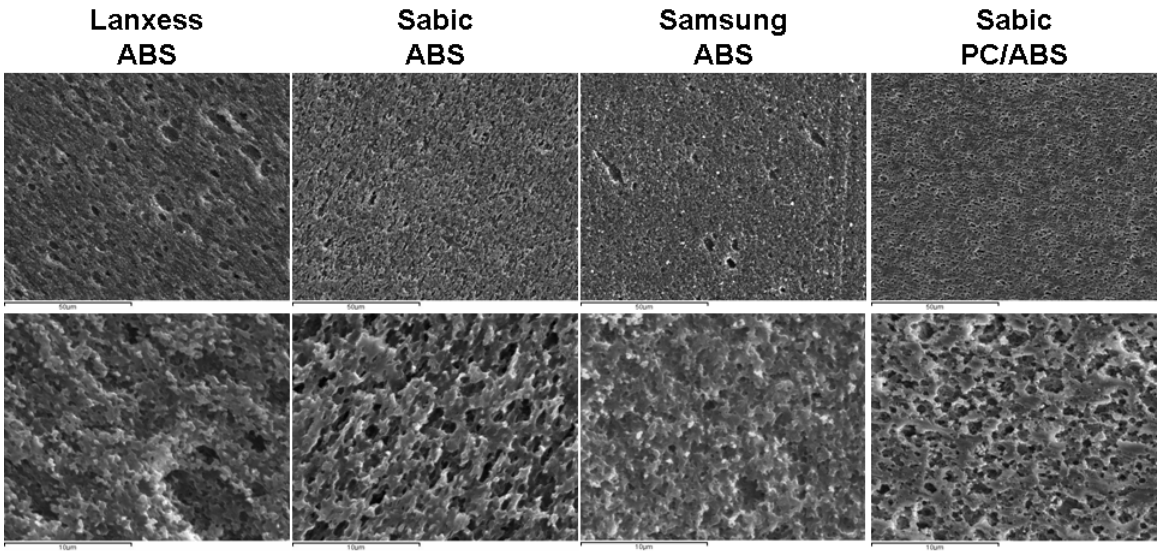

Figure 4-21: Comparison of etch structure as a function of material supplier

There are multiple factors driving the etched surface morphology that can all be varied by supplier. The number of "holes" as well as their size and distribution is directly related to the butadiene. The Lanxess ABS had a large etch size variation, compared to the Sabic and Samsung ABS materials. This could be due to the molecular weight distribution of the butadiene, compatibilizers used, mixing history, or a combination of those factors (Takahashi, 1997). The Sabic PC/ABS had fewer holes at the surface because the addition of the polycarbonate reduces the amount of ABS and therefore the amount of butadiene available.

The elongation of the etch pattern in the high stress areas was determined by both processing conditions and the viscosity ratio between the butadiene and the SAN matrix in ABS (Nysten, 1999; Yang, 1999; D'Orazio, 2001). If the processing conditions are held the same and the viscosity of the rubber is close to that of the matrix, the rubber can be more easily stretched along with the matrix in the high shear areas. The resulting etch structure looks "stretched out" in these regions, like the Lanxess and Sabic ABS material. If the viscosity ratio is very different with the rubber viscosity being much higher than the matrix, the

etch structure maintains its rounder shape in high stress areas, like the Samsung ABS. The addition of polycarbonate can also change the melt flow rheology enough to maintain round etch sites in high stress areas.

In addition to the amount of surface stress and resin composition, the etching process conditions such as bath temperature and time in the bath can also have an effect on the etch morphology and therefore, the adhesion. The etching parameters are typically much harder for the metal plater to change than resin molding parameters because they are often using the bath for many different types of parts, and changing the temperature of the bath or the line speed can take a long time to stabilize and cause problems for other parts of their operations.

Figure 4-22 shows the effect of etching parameters on the surface morphology in high and low stress regions. The standard etching time for this particular bath is 08:10 (min:sec) at 71°C. It should be noted that there is no quantitative measure of the quality of the etched surface used in the industry (Electroplating Fundamentals, 2008), so judgments of "over-etched" and "under-etched" are subjective. Typically, over-etching is indicated by a lack of intact resin at the surface and large, deep "holes". Under-etching is indicated by large, very smooth surfaces remaining and shallow "holes". Since we were seeing signs of over-etching in the higher stress regions of the parts analyzed above, lower temperatures and shorter times were tried.

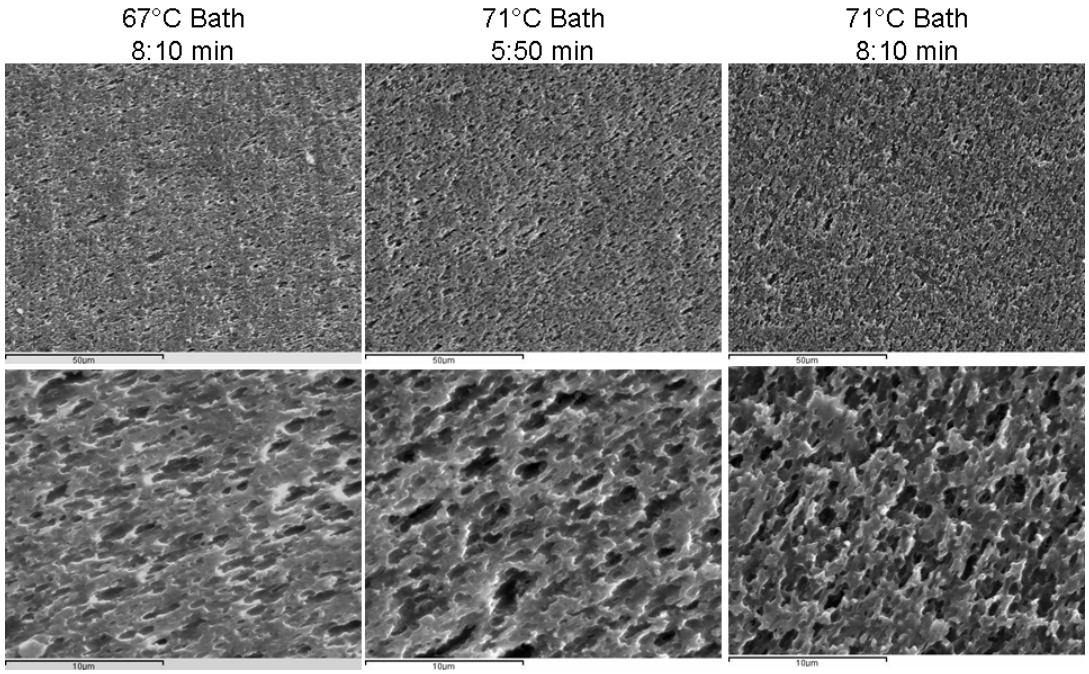

(a)

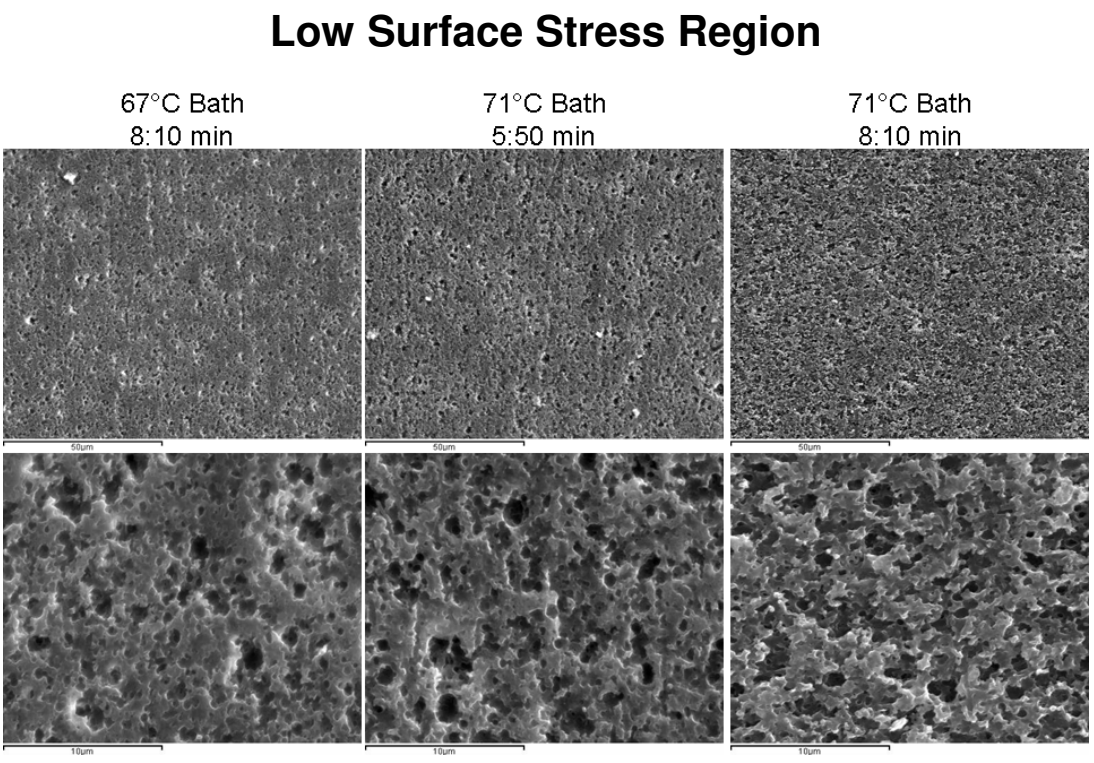

(b)

Figure 4-22: SEM images of effect of etch bath time and temperature in (a) high and (b) low surface stress areas as indicated by glacial acetic acid testing

As can be seen in the Figure 4-22, lowering the etch temperature seemed to have more of an effect on the etch structure than decreasing the etching time, indicating the etching process is thermodynamically driven. The etch pattern from the 67°C bath is under-etched. The etch pattern at the 05:50 minute etch at the standard 71°C temperature appears good in the high stress areas, but under etched in the low stress areas due to the shallow depth of the "holes" and the large amount of smooth surface area left. It can also be seen that due to the stress at the surface, the high surface stress areas are more affected by changes in the etch bath than samples in low stress regions.

In addition to the tendency for over-etching in high surface stress regions, adhesion problems would result from the elongated rubber in those areas which cannot be addressed by changing the etch conditions, but only through material choice and polymer processing conditions. Optimizing those variables to minimize the amount and variation of surface stress throughout the part addresses the root cause of poor adhesion, rather than trying to compensate after the fact by altering etching conditions.

4.4.D Adhesion

4.4.D.i Types of Adhesion Failures

Several root causes were found for adhesion failures between the metal and polymer substrate on chromed automotive components with field exposure, which typically presented as wormed or blistered metal, an example of which is shown in Figure 4-23.

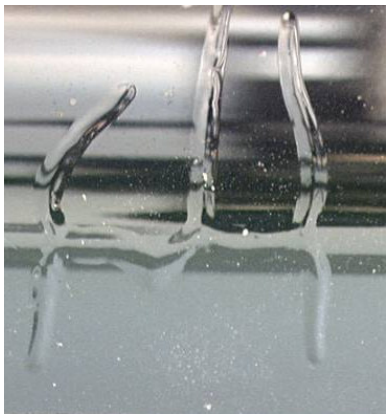

Figure 4-23: Typical appearance of metal-polymer adhesion loss due to field exposure

When the metal layers are physically removed in an area with good adhesion, there is a substantial amount of polymer on the back of the removed metal layer as shown in Figure 4-24. The SEI image shows regions where the electroless copper nodules can be seen along with regions that are still covered in polymer (Figure 4-24a). The compositional backscatter image (Figure 4-24b) confirms these finding, highlighting the heavier copper regions compared to the darker carbon polymer regions. The polymer side of the intentionally failed interface shows only the ductile failure of the polymer (Figure 4-25).

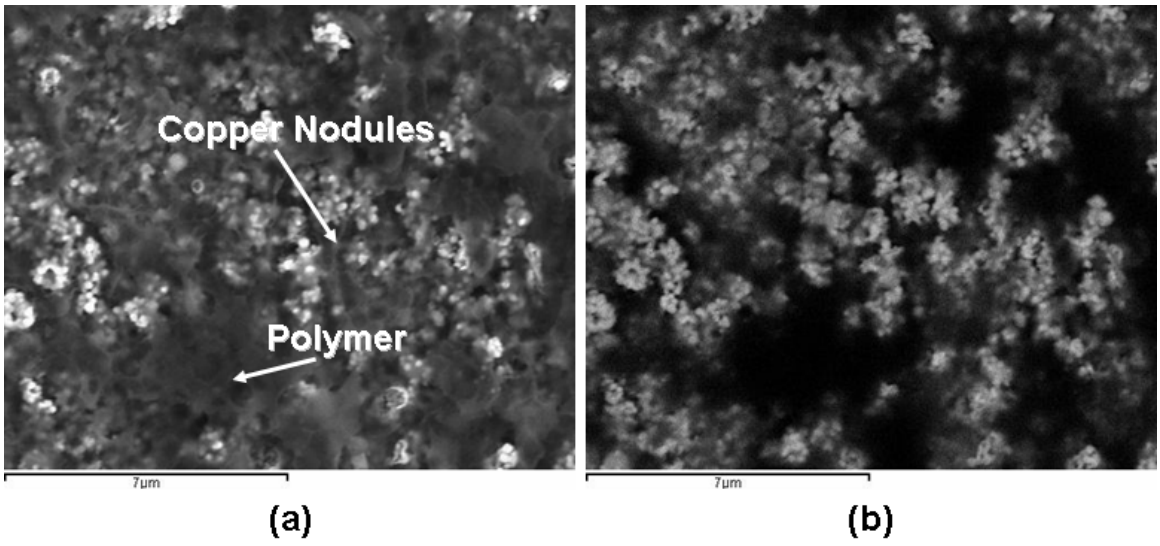

Figure 4-24: a) SEI and (b) BSE images of metal interface side of "good" adhesion site

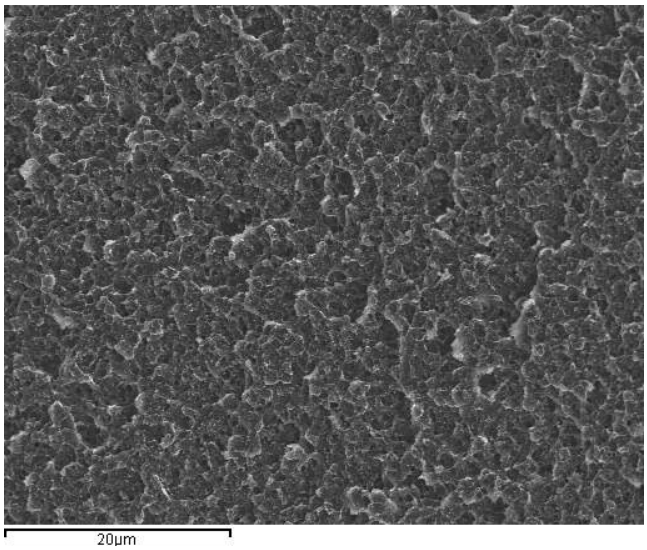

Figure 4-25: SEI Image of polymer interface of good adhesion site showing ductile failure

In areas with adhesion loss, the amount of polymer present on the back of the metal layer gives an indication of the cause of the failure. If there is an excessive amount or a skin of polymer on the back of the blistered metal interface, this indicates that there was a weak boundary layer created in the polymer due to over-etching. Figure 4-26 shows the polymer interface of a failed chromed PC/ABS component where the metal was removed chemically to leave remaining etch structures intact. The failed region shows that a boundary layer of polymer had been removed when the metal blistered. The nearby remaining etch structure is severely over-etched when compared to a typical etch structure for the same material in Figure 4-27. This failure is mostly likely a result of poor etch bath controls, not material choice or molding conditions.

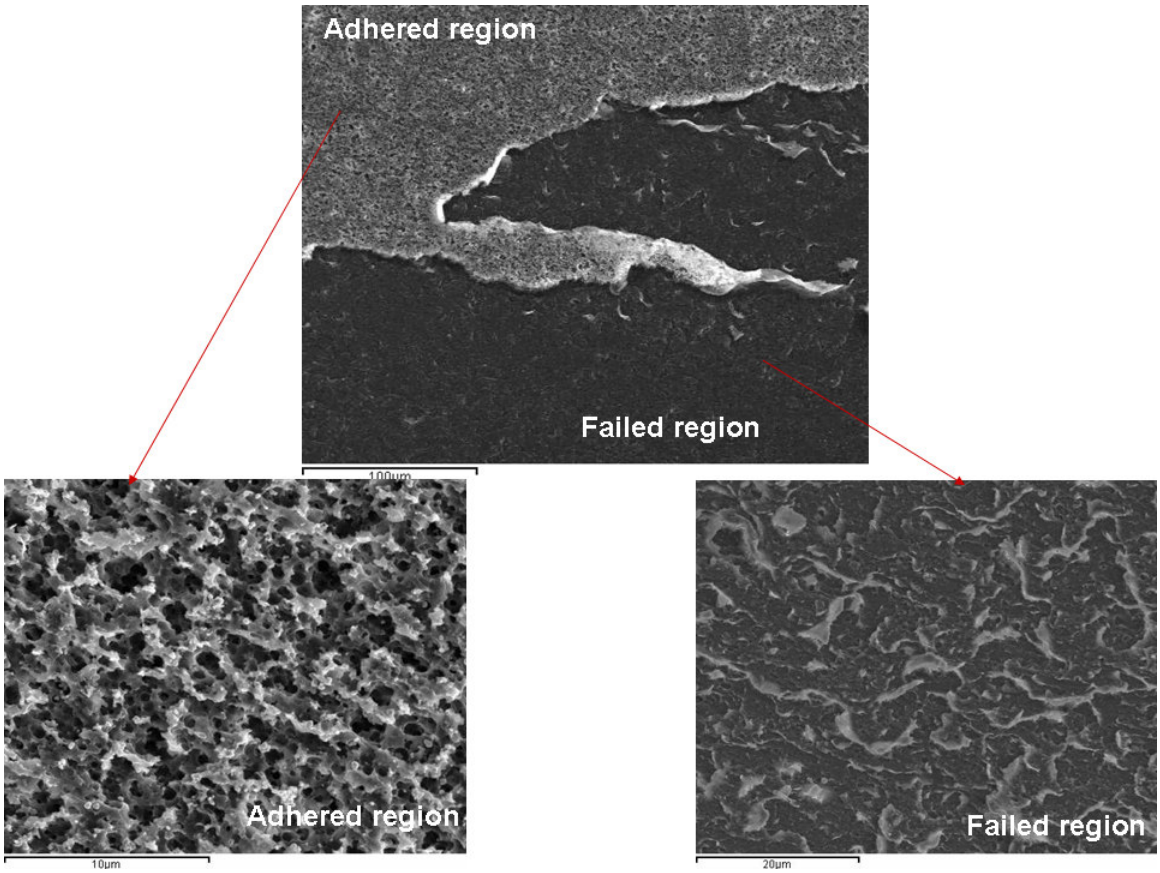

Figure 4-26: SEI image of failed PC/ABS interface with remaining metal chemically removed

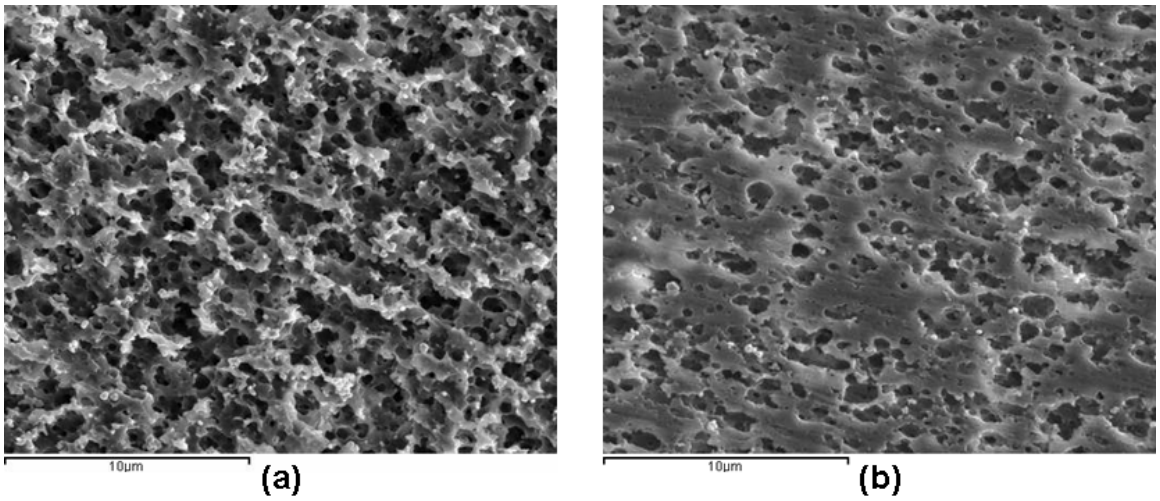

Figure 4-27: Comparison of (a) over-etched and (b) optimally etched structure for the same PC/ABS material

If there is little to no polymer remaining on the metal side of the failed interface (Figure 4-28), there could be a few possible root causes for the adhesion failure. One root cause is that either due to material choice (typically PC/ABS) or under-etch conditions, there are not enough sites on the polymer surface for a sufficient mechanical interlock (Figure 4-29).

Another possible root cause is that high surface stress due to either polymer processing and/or part geometry and gating is elongating the rubber at the surface. This results in elongated etch sites that do not provide the "lock and key" morphology necessary for good mechanical adhesion. Figure 4-30 shows an example of this from a failed sample where the metal has been physically removed. In the region where the metal was still adhered, there is ductile failure of the polymer, but in the region of adhesion loss, the etch structure is still intact, indicating that the metal layers lifted cleanly off with no damage to the polymer below. The remaining etch structure is highly elongated and would not provide a good "lock and key".

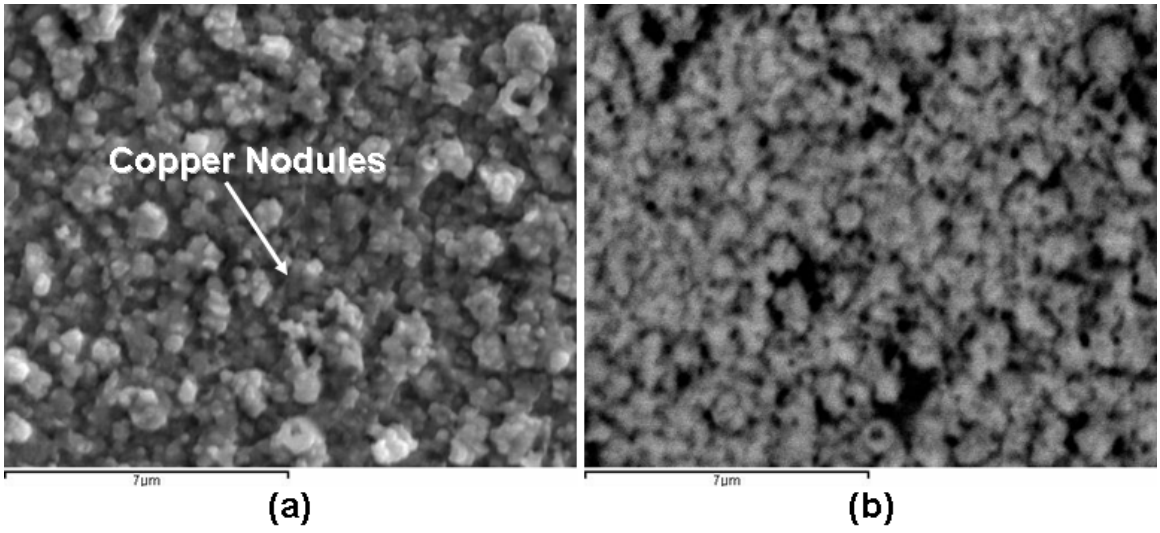

Figure 4-28: (a) SEI and (b) BSE images of failed metal interface with little to no polymer

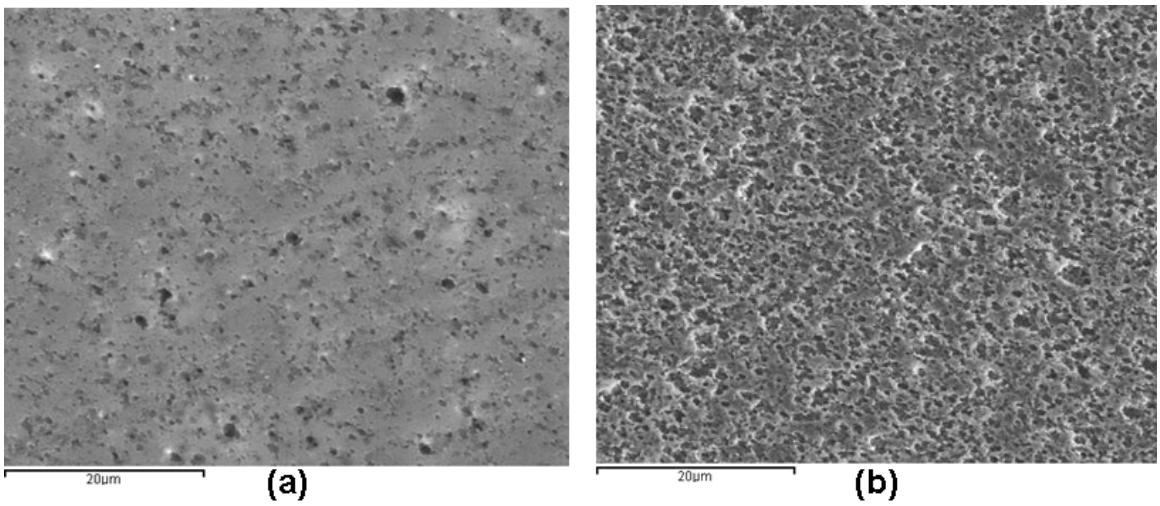

Figure 4-29: Comparison of (a) under-etched and (b) optimally etched structure for the same ABS material

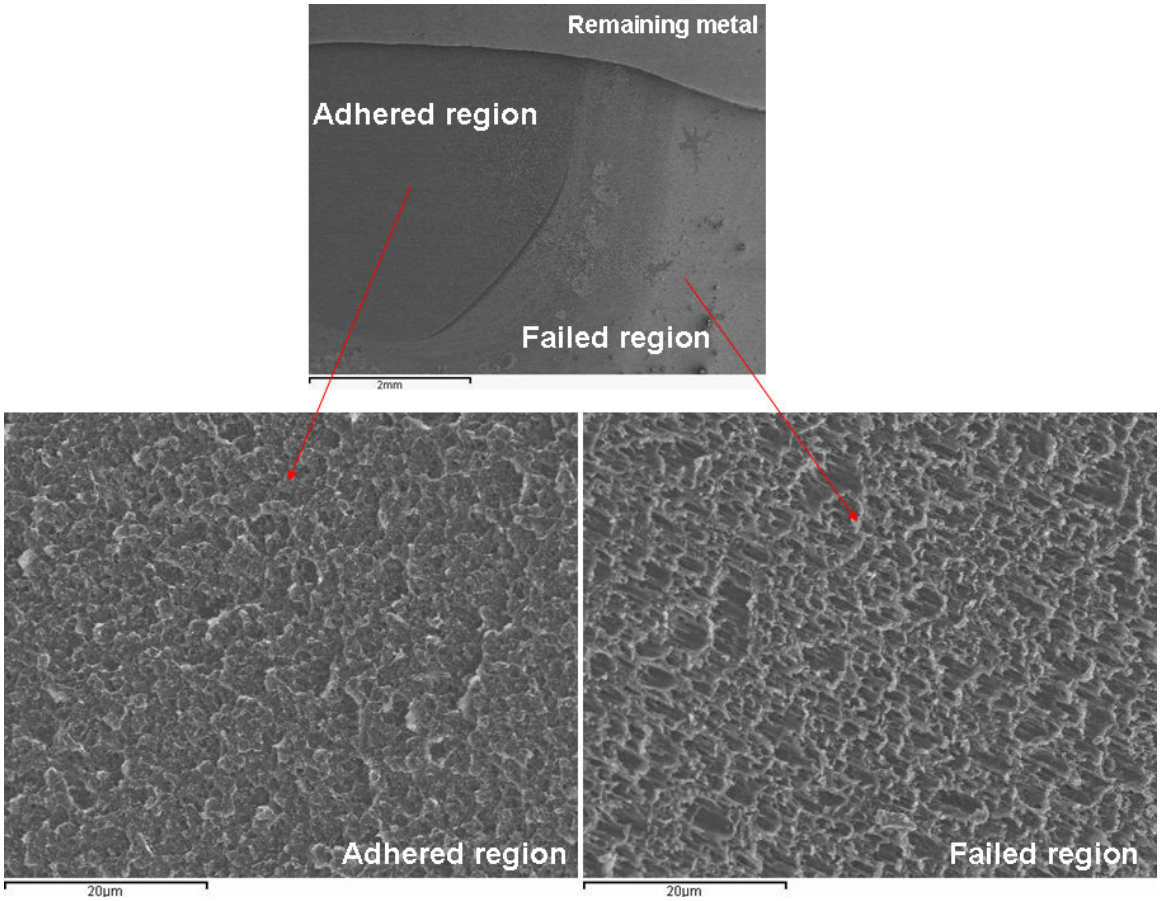

Figure 4-30: Polymer interface of failed sample with metal layer physically removed

4.4.D.ii Modified Cross-hatch Adhesion Testing Results

Five different regions of the grille were selected for cross-hatch adhesion testing from the results of the glacial acetic acid pictures including regions of high and low surface stress. The total percentage of removed triangles for these 5 areas is reported in Table 4-2.

Table 4-2: Cross-hatch adhesion testing results

DOE Cell								
1	2	3	4	6	7	8	A	9
29.7%	28.1%	14.7%	5.5%	36.1%	2.5%	14.4%	29.7%	0.5%

The best adhesion was found for cell 7 conditions (highlighted in green), while the worst was found for cell 6 (highlighted in red). This findings correlate well to known molding conditions that minimize surface stress, as discussed in previous sections. The dominating factor appears to be the melt temperature, with the higher melt temperatures resulting in better adhesion performance, but as discussed earlier, larger amounts of molded-in stress. The adhesion failures in the DOE parts were mostly found in the high surface stress areas and were all due to elongated rubber and over-etch conditions resulting from high surface stress.

4.4.D.iii Quantitative Adhesion Testing Results

Grille samples with known areas of good and poor adhesion were sectioned to see if the quantitative adhesion measurement developed by Professor Martin's group for painted TPO systems is applicable to metalized ABS systems. Samples were tested using both Instron tensile tests and mandrel bend (elastica) tests. Unfortunately, we could not generate reliable quantitative adhesion data

with either test method. This is probably due to a number of reasons, including the brittle nature of the ABS and metalized coating which resulted in sample failures around ~1% strain. This elongation at failure is much smaller than the >100% strain values that were achieved with the painted TPO systems. Due to the low sample elongations, cracking may not have been able to saturate before sample fracture, resulting in inaccurate calculations of the interfacial shear stress. Secondly, because we were using real world parts for this experiment, there was a large amount of variability in both the thickness of the substrate and the thickness of the metalized layers due to the grille geometry.

While quantitative results were not able to be confirmed, there were some general trends that were observed. In areas with good adhesion, there was generally no cracking or only fine cracking along the edges of the metalized layer (Figure 4-31a). In areas with moderate adhesion, the metalized layer cracked all the way across the sample, but it was very fine and closely spaced (Figure 4-31b). Areas of the grille known to have poor adhesion had cracks across the gage width of the sample that were spaced much further apart (Figure 4-31c). Again, while these general observations were made, either the sample size was too small or the geometry variability was too large to generate conclusive quantitative data. However, it may be possible to prove out this adhesion test method using controlled plaque testing, or a larger sample size.

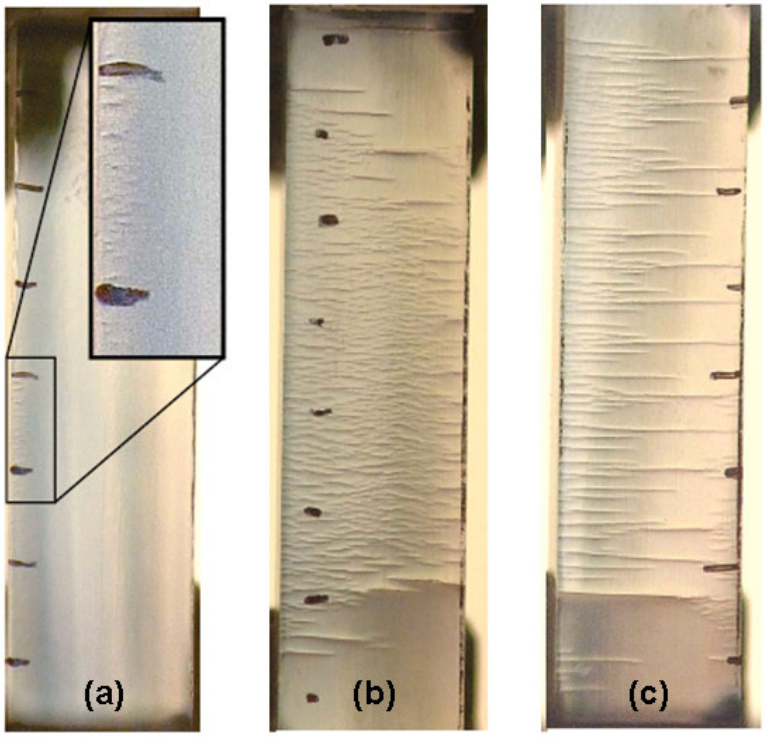

Figure 4-31: General trends of crack spacing observed during adhesion testing in areas of (a) good adhesion (b) moderate adhesion (c) poor adhesion

4.5 Conclusions

With the increasing size and number of metalized plastic components in the automotive industry, it is important to have a fundamental understanding of the effect of processing on the surface morphology of the polymer and adhesion mechanisms to be able to provide parts with long-term durability to the customer. Understanding the limitations of material, processing and geometry will provide both cost and time savings by providing design rules developed by this research.

To generate a greater understanding of molding processing effects on performance, an L8 DOE was conducted to determine the effect of injection speed, melt and mold temperature on the amount of molded-in stress and the

adhesion performance, which was characterized in numerous ways. The effect of resin composition on surface morphology, and therefore adhesion performance, was also studied by evaluating three different industrially available resins. While the formulation details are not made available from the three different suppliers, the resulting differences surface morphology and performance provided some insight to the compositional make-up. Additions of polycarbonate to the ABS blend and its effect on performance was also compared for reference. To understand the plating process, the effect of etching time and temperature on adhesion performance was studied.

The molding DOE found that there was no effect of the mold temperature on bulk molded-in stress, surface stress, or adhesion performance. Parts molded at high temperatures and slow injection speeds had the most molded-in bulk stress. Minimizing the bulk stress is important for durability because of the large thermal expansion mismatch between the polymer substrate and the metal coating. Conversely, the lower melt temperatures and faster injection conditions produced the least amount of molded-in stress. These findings correlated with those of other investigators, and it has been theorized that this is a result of higher temperatures being generated by the fast molding conditions allowing some relaxation of the bulk molded-in stress.

Slight differences in formulation due to different suppliers also produced variation in performance. The heat deflection temperature ranged from 83°C-87°C and the molded-in stress varied as much as 13% depending on the formulation of the ABS. The improvements in molded-in stress from part processing and ABS formulation changes were minor compared to ~75% improvement in molded-in stress achieved by adding polycarbonate to the blend. However, the benefit in properties must be balanced with the additional cost of the PC/ABS and determined if it is warranted by the design and/or intended use of the part.

Glacial acetic acid testing performed as an indicator of surface stress in the part and it was verified that areas whitened during this testing did have elongated rubber resulting from higher surface stress, due to molding conditions and/or part geometry. The whitened, high surface stress areas were also found to have poor adhesion compared to areas with less whitening. The DOE parts that had the highest amount of molded-in stress were actually had the lowest amount of surface stress (high melt temperature, slow injection speed). There was also a large variation in the amount of surface stress (whitening) based on variations resin formulation. These variations were better understood after during the microstructural examination of the surface morphology.

When the surface morphology of the DOE samples was examined, the areas indicated to have high amounts of surface stress by glacial acetic acid testing showed subtle differences in etch structure depending on molding conditions. Samples molded at high melt temperatures and slow injections speeds that were found to have high molded-in stress, yet lower surface stress and better adhesion, displayed optimum round rubber sites. Samples molded at lower melt temperatures and higher speeds had lower molded-in stress, but also had higher surface stress and more elongated rubber sites. Due to the high surface stress in these parts, the etching step more rapidly attacked and removed the SAN matrix, which also led to poorer adhesion performance.

The etched rubber sites providing the mechanical interlock for adhesion were found to vary tremendously based on resin supplier (formulation). Both the size distribution and the degree of elongation of the rubber at the surface molded at the same conditions were dependent on the formulation. Smaller size distributions and higher viscosity ratios between the rubber and the SAN matrix were found to improve adhesion performance.

While the effect of molding conditions was studied, the etch conditions were held constant at a nominal value, however etch conditions also have an important role in adhesion performance. Different etch bath exposure times and temperatures were investigated to determine the effect on surface morphology. It was found that the lowering the etch temperature had more of an effect on the etch structure than decreasing the etching time, indicating the etching process is thermodynamically driven. As expected, the areas with higher surface stress (which whitened during glacial acetic acid testing) etched faster at the same etch bath conditions compared to areas with lower surface stress. Etching parameters are typically much harder for the metal plater to change than resin molding parameters since they are often using the bath for many different types of parts, and changing the temperature of the bath or the line speed can take a long time to stabilize and could cause problems for their other parts. Therefore, the molding conditions should be optimized to produce the most uniform amount of surface stress on the part as possible to make the etching rate as even as possible. Also, changing etching conditions cannot improve the adhesion in regions that have elongated rubber due to high surface stress – this can only be addressed by molding processing or part/gate geometry changes.

A variety of plated ABS and PC/ABS failure modes and their root causes were discussed, and cross-hatch adhesion testing was conducted on parts examined for this study to confirm that a proper balance of bulk and surface molded in stress must be struck using molding conditions for optimum adhesion. The quantitative adhesion testing method used in Chapter 3 was also applied to these parts, but repeatable, quantitative adhesion data could not be acquired with either the tensile or mandrel bend test method. Due to the low sample elongations of the more brittle system of metalized ABS, cracking may not have been able to saturate before sample fracture, resulting in inaccurate calculations of the interfacial shear stress. Also, we were using real world parts for this

experiment, and there is a large amount of variability in the thickness of both the substrate and the metalized layers due to the grille geometry that was likely affecting the results. To truly determine the validity of the adhesion test with this material system, a controlled trial should be run using plaques, as was done with the painted TPO samples.

While the polymer substrate and the coating system (metalized ABS) is very different from the system examined in Chapter 3 (painted TPO), it was also found that the material composition and the processing conditions did affect the surface morphology and was reflected in changes in properties. Again, small changes in material formulation or processing conditions could have a large effect on the surface and resulting properties. These similar results for two very different material systems further demonstrates the difficult task ahead of gaining enough understanding the effect of all of these variables to be able to produce material models capable of accurately generating material property data.

4.6 References

Anis, N. (1994). "Mold and part design for plating on plastics." Plastics Design Forum **October**: 26-28.

Beacom, S. E. and R. G. Wedel (1970). "Scanning electron microscopy of plastic surfaces as related to metal deposition." Journal of Colloid and Interface Science **34**(3): 375-386.

Bucknall, C. B. (1977). Toughened Plastics. London, Applied Science Publishers, LTD.

Casale, A., A. Moroni, et al. (1975). ABS Resins: The Relation between Composition and Rheological Behavior. Copolymers, Polyblends, and Composites. WASHINGTON, D. C., AMERICAN CHEMICAL SOCIETY**:** 172-185.

Chang, M. C. O. and R. L. Nemeth (1996). "Rubber particle agglomeration phenomena in acrylonitrile-butadiene-styrene (ABS) polymers. I. Structure-property relationships study on rubber particle agglomeration and molded surface appearance." Journal of Applied Polymer Science **61**(6): 1003-1010.

Chiu, C. P. and M. C. Hsieh (1987). "The Correlation Between the Residual Stresses of ABS Terpolymers and Injection Molding Conditions." J. Eng. Mater. and Technol. **109**(2): 171-175.

Choi, H. J., S. H. Park, et al. (2000). "Effects of acrylonitrile content on PC/ABS alloy systems with a flame retardant." Journal of Applied Polymer Science **75**(3): 417-423.

Concise Encyclopedia of Plastics (2000). Springer - Verlag.

D'Orazio, L. and G. Cecchin (2001). "Isotactic polypropylene/ethylene-co-propylene blends: effects of composition on rheology, morphology and properties of injection moulded samples." Polymer **42**(6): 2675-2684.

Electroplating Fundamentals (2008). Presented at Ford Motor Company, Dearborn, MI, MacDermid.

ELECTROPLATING, BRIGHT OR LOW GLOSS DECORATIVE OVER ABS OR PPO PLASTIC - EXTERIOR (2006). WSB-M1P83-B2. Ford Motor Company.

Ellis, P. A. M. (1967). "The importance of moulding conditions to the quality of electroplated ABS plastics." Trans. J. Plastics. Inst. **June**: 537-542.

Fritch, L. W. (2006). Grooved Mold Improves Plate Adhesion, GE Plastics.

Kamal, M. R., R. A. Lai-Fook, et al. (2002). "Residual thermal stresses in injection moldings of thermoplastics: A theoretical and experimental study." Polymer Engineering & Science **42**(5): 1098-1114.

Kato, K. (1967). "ABS mouldings for electroplating--An electron microscope study." Polymer **8**: 33-39.

Kato, K. (1968a). "Electron microscope studies on the etching of ABS mouldings for electroplating." Polymer **9**: 419-424.

Kato, K. (1968b). "Moulding anisotropy in ABS polymers as revealed by electron microscopy." Polymer **9**: 225-232.

Kulich, D. M., S. K. Gaggar, et al. (2003). Acrylonitrile–Butadiene–Styrene (ABS) Polymers. Kirk-Othmer Encyclopedia of Chemical Technology John Wiley & Sons, Inc.

Lee, M. P., A. Hiltner, et al. (1992). "Phase morphology of injection-moulded polycarbonate/acrylonitrile-butadiene-styrene blends." Polymer **33**(4): 685-697.

Li, L., T. Masuda, et al. (1990). "Elongational flow behavior of ABS polymer melts." Journal of Rheology **34**(1): 103-116.

Matsunaga, M. and Y. Hagiuda (1971). "Mechanical properties of electroplated ABS plastics." Metal Finishing **69**(4): 36-40.

Nielsen, S. (1985). "Achieving quality finishes with electroplated plastic." Engineers' Digest **June**: 22-27.

Nysten, B., A. Ghanem, et al. (1999). "Influence of EP/PP viscosity ratio on the surface morphology and elasticity of injection moulded PP/EP." Polymer International **48**(4): 334-338.

Pham, H. T., C. P. Bosnyak, et al. (1993). "Residual stresses in injection molded polycarbonate rectangular bars." Polymer Engineering & Science **33**(24): 1634-1643.

Polymer Blends Handbook, Volumes 1-2 (2002). Springer - Verlag.

Rose, W. (1961). "Fluid-Fluid Interfaces in Steady Motion." Nature **191**(4785): 242-243.

Siegmann, A., A. Buchman, et al. (1982). "Residual stresses in polymers III: The influence of injection-molding process conditions." Polymer Engineering & Science **22**(9): 560-568.

Standard Practice for Qualitative Adhesion Testing of Metallic Coatings (2008). ASTM Standard B 571, ASTM. **ASTM Standard B 571**.

Standards and guidelines for electroplated plastics (1984). Englewood Cliffs, N.J., Prentice-Hall.

Tadmor, Z. (1974). "Molecular orientation in injection molding." Journal of Applied Polymer Science **18**(6): 1753-1772.

Takahashi, T., W. Wu, et al. (1997). "Elongational viscosity of ABS polymer melts with soft or hard butadiene particles." Journal of Non-Newtonian Fluid Mechanics **68**(2-3): 259-269.

Tan, Z. Y., X. F. Xu, et al. (2006). "Influence of rubber content in ABS in wide range on the mechanical properties and morphology of PC/ABS blends with different composition." Polymer Engineering & Science **46**(10): 1476-1484.

Tang, H., B. Foran, et al. (2001). "Quantitative measurement of adhesion between polypropylene blends and paints by tensile mechanical testing." Polymer Engineering & Science **41**(3): 440-448.

Teixeira, L. A. C. and M. C. Santini (2005). "Surface conditioning of ABS for metallization without the use of chromium baths." Journal of Materials Processing Technology **170**(1-2): 37-41.

Turner, R. (2002). Molding Parameters for Electroplated Parts. The Promotion of Chrome Plated Plastics for Automotive Plating on Plastics Committee, May 22, 2002.

Utracki, L. A. (1998). Commercial Polymer Blends, Springer - Verlag.

Utracki, L. A. (2002). Polymer Blends Handbook, Volumes 1-2, Springer - Verlag.

Villamizar, C. A., J. Rojas, et al. (1981). "Chemical Etching Versus Plasma Etching in Electroplating ABS Resin Surfaces." Metal Finishing **79**(3): 27-33.

Yang, K., S.-H. Lee, et al. (1999). "Effects of viscosity ratio and compatibilizers on the morphology and mechanical properties of polycarbonate/acrylonitrile-butadiene-styrene blends." Polymer Engineering & Science **39**(9): 1667-1677.

Yen, P.-C. (1995). "Improved ABS plastic activating treatment for electroless copper plating." Polymer Communications **36**(17): 3399-3400.

Chapter 5

Summary

This thesis is concerned with the effect of processing variables, resin formulation and mold material on the morphology of industrially relevant polymers in parts molded on large presses with fully developed flow lengths. The resulting mechanical properties and adhesion performance were all found to be affected by the resulting morphology. Adhesion performance is especially important considering more than 30% of polymers are coated in some fashion (Ryntz, 2005).

In the case of painted TPO (a chemically bonded system), changes in the near-surface rubber morphology and surface chemistry based on material and processing conditions used in this work had no significant effect on the adhesion performance. For the mechanically bonded metal plated ABS system, the adhesion performance was found to be very dependent on the surface rubber morphology, which varied widely with material and processing conditions.

One of the most important findings was that the use of forged aluminum alloys for the injection molding tooling had no significant effect on the surface morphology or adhesion performance of either neat polypropylene or the two TPO formulations examined in this work. This was surprising given the nearly five-fold increase in heat transfer coefficient of the aluminum compared to traditional tool steel. As reported in the literature (Zironi, 2005; Bank, 2008), the parts molded in

this study using aluminum tooling cooled faster and provided opportunity for decreasing the cycle time by keeping the mold temperature about 15-20 degrees cooler for the aluminum tool (Figure 5-1).

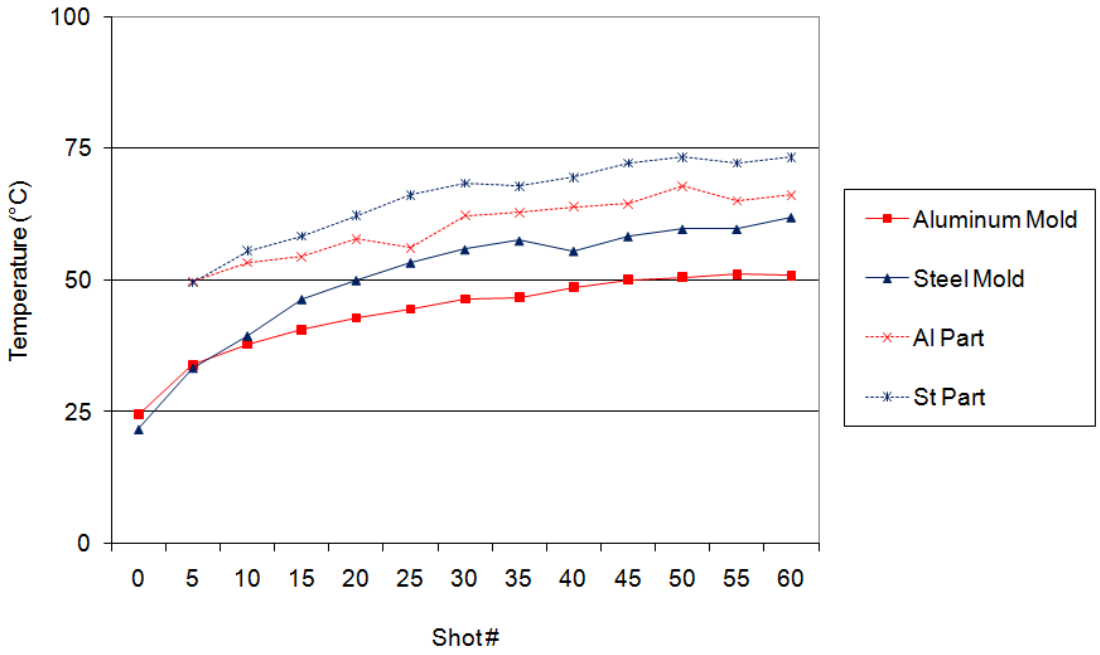

Figure 5-1: Mold and part temperatures of i-PP plaques as a function of shot number

To better understand this finding, Equation 5-1, which approximates the temperature of an infinite plate as a function of distance from the mid-plane (y) and time (t), was used to understand the melt temperature during cooling (Stelson, 2003). For these estimations, it is assumed that there is perfect thermal contact between the polymer and mold, and constant thermal diffusivity of the cooling polymer. The mold temperature is assumed to remain constant at the steady-state values found in the experimentation (64℃ for the steel mold and 52℃ for the aluminum mold).

$$T(y,t) = \frac{4(T_i - T_f)}{\pi} e^{-\left(\frac{\pi^2 \alpha t}{a^2}\right)} \cos\frac{\pi y}{a} + T_f \qquad \textbf{Equation 5-1}$$

Where T_i is the initial melt temperature, T_f is the mold temperature, a is the part thickness, and α is the thermal diffusivity of the polymer (m^2/s).

For the case of i-PP, the melt temperature is 221°C, the part thickness is 3.5 mm, and the thermal diffusivity of polypropylene was taken to be 1.26×10^{-7} m^2/s (Zhang, 2002). The mid-plane temperature (y=0) of the part is shown as a function of time in Figure 5-2. If an ejection temperature of 115°C is assumed (Nylund, 2005), the cooling time for the steel molded sample is 13.5 s and the aluminum molded sample is 12.1 s, a savings of ~10%, which agrees with the experimental results as well as reported findings (Zironi, 2005; Bank, 2008; Miel, 2009, 2009) and shows the approximation in Equation 5-1 is valid.

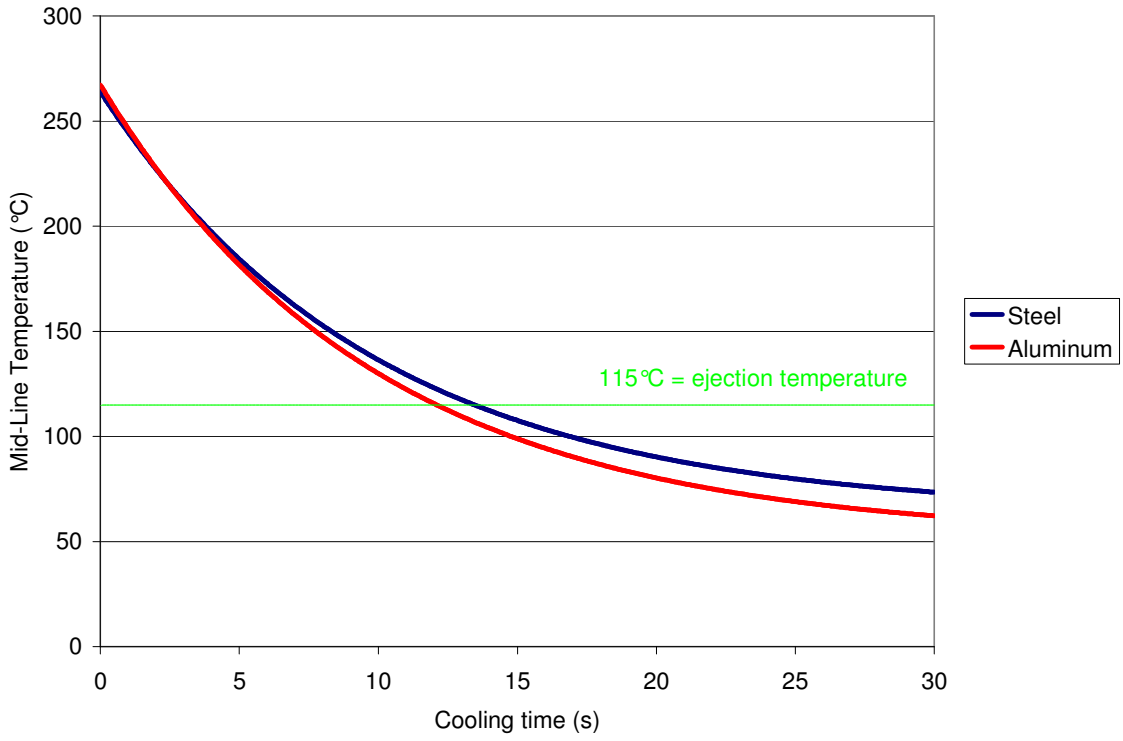

Figure 5-2: Approximated mid-plane temperature as a function of cooling time for aluminum and steel molded plaques

To understand the difference of the mold material on the temperature profile of the part, the temperature as a function of distance from the mid-plane at three different cooling times (1, 5 and 10 seconds) was calculated using equation 5-1. As can be seen in Figure 5-3, the difference in temperature between the aluminum and steel molded sample within the first 200 mm from the mold wall is only ~10°C. This difference, combined with the rapid nucleation and crystallization occurring at the surface due to the high shear rates is likely responsible for the lack of effect of cooling time on surface morphology (Kumaraswamy, 1999; Kumaraswamy, 2000; Kornfield, 2002; Kumaraswamy, 2002; Janeschitz-Kriegl, 2005).

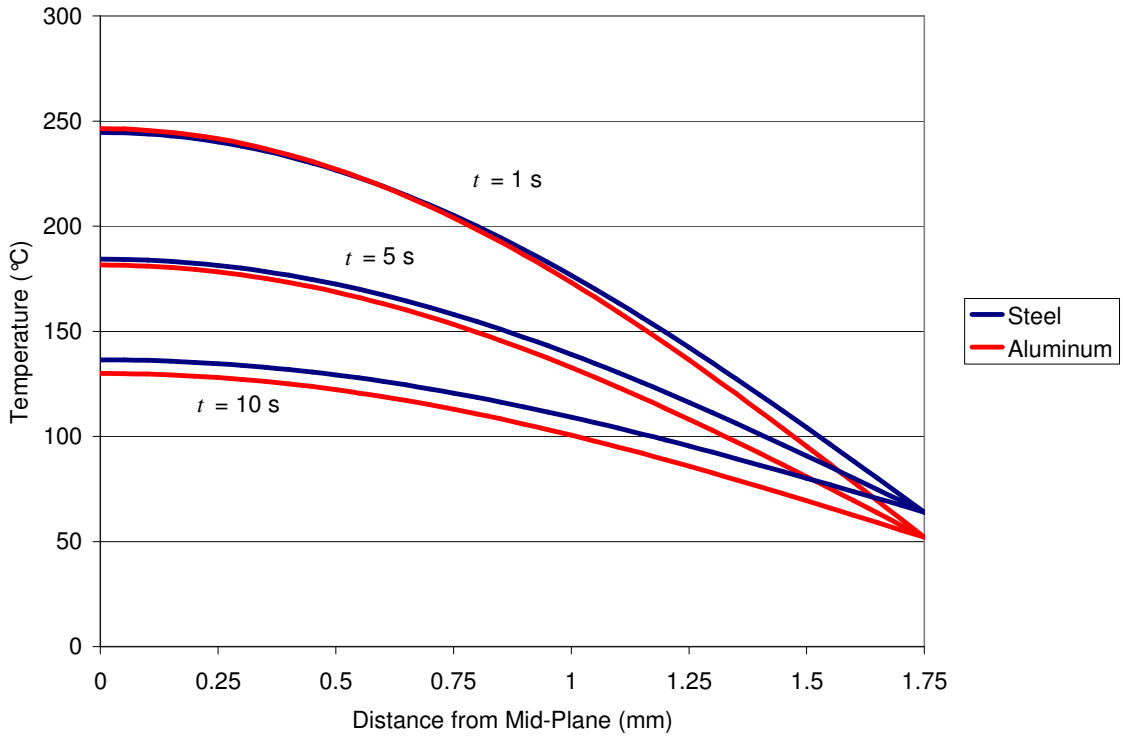

Figure 5-3: Temperature profile from mid-plane to mold wall for aluminum and steel molded plaques at cooling times of 1 s, 5 s, and 10 s

The effect of cooling rate will likely have more of an effect on the behavior of the more slowly cooled core, and literature results have shown the overall faster, more isothermal cooling in parts molded with aluminum tooling does result in less

molded-in stress and warping (Zironi, 2005; Bank, 2008). The technique developed in this work to measure molded-in stress in the shear zone by combining optical profilometry with a hot stage could be expanded on to provide a new method to measure molded-in stress that offers the possibility for higher resolution and minimizes the possibility of damage compared to previous bulk or layer removal techniques. This information could be used in the future to help further understanding of the role of material and processing on molded-in stress and dimensional tolerance.

While the surface rubber morphology was not changed by the cooling rate, the surface chemistry was found to be affected, as a function of material. XPS of the surface of the aluminum and steel molded compounded TPO showed a significant (~2.5 at%) amount of nitrogen concentrated at the surface of the aluminum-molded sample that was not present on the steel-molded sample, nor in the bulk of either sample. This correlated with the TEM and EDS data which showed a thin (~0.7 μm), more heavily ruthenium stained (therefore less crystalline) layer at the surface of the aluminum-molded sample that was not found on the steel molded sample.

This was an important finding, because even though it may not have had an effect on the adhesion performance in this particular case, the faster cooling rate of the aluminum tools does appear to be trapping a lower molecular weight additive (most likely a Hindered Amine Light Stabilizer (HALS) UV stabilizer present in the formulation) at the surface due to immiscibility and the fountain flow phenomenon. This suggests the possibility for designing new TPO formulations for use in aluminum tools to provide a custom surface by utilizing processing and additive selection. One possible application would be increasing surface energy for improved adhesion, possibly eliminating adhesion promoter or flame treatments. This would be a huge cost and energy savings opportunity for

painted components, however, a robust study would need to be conducted to understand the impact of molding conditions and geometry on the quality of the surface. This could be a topic of future work, and also serves as a warning that an additive that may have unintended negative effects on adhesion (such as an internal mold release) could be trapped at the surface depending on resin formulation. With this type of aluminum tooling just starting to make its way into the industry, the effect on the surface must be a factor in choosing materials and applications for future use, especially for coated components.

Chapter 2 evaluated the effect of injection speed, geometry and cooling rate on the morphology and properties of neat polypropylene. Polypropylene is not typically used in industry without some modifications such as fillers, additives, or dyes, which can have a large effect on properties. However, neat polypropylene is more easily studied with optical microscopy, and there is a large volume of available research on it for comparison. This work focused on the effect of long flow lengths (300 mm) and processing conditions that are more representative of mass manufacturing, rather than research applications, which makes it unique from the current literature. The intent and main accomplishment was to develop the protocol and techniques to evaluate the effect of processing on morphology and properties that would be used in future chapters including microscopy techniques, XPS, and molded-in stress measurements.

The physical distance from the gate was found to dramatically affect the microstructure of neat i-PP, with the shear zone decreasing non-linearly from 300 μm to zero. The shear zone was found to have localized wrinkling of the cross-sections taken perpendicular to the flow, but not parallel to flow. This same wrinkling was also found by Phillips et. al., but they did not propose any explanation of this behavior (Phillips, 1994). A new technique developed in this work, combining optical profilometry with a heated stage, determined this

wrinkling to be due to a large amount of molded-in stress due to the shish-kabob orientation of polypropylene crystallites in the shear zone.

This orientation in the shear zone was also found to have an effect on the impact properties, which are very sensitive to near surface morphology, as was also found by other authors (Schrauwen, 2004). This was not surprising given the role of the shear zone in crack propagation (Karger-Kocsis, 1989). A future work may expand on this, and incorporate the change in the shear zone size as a function of distance from the gate in simulation work to improve predictions of shrink and impact properties.

The molded-in stress that was found in the shear zone of the i-PP was found to be significantly reduced in the TPO materials studied in Chapter 3. The addition of rubber for the reactor grade TPO resulted in only small amounts of localized wrinkling in optical microcopy samples taken perpendicular to the flow due to the increased nucleation rate from the rubber addition (Karger - Kocsis, 1979). The wrinkling and amount of molded-in stress in the shear zone was further reduced with the addition of talc in the compounded TPO, which increases the nucleation rate further (Fujiyama, 1991; Velasco, 1996).

At the faster injection speeds representative of mass production, there was no effect of the mold material on the rubber morphology of the compounded TPO material, but the reactor grade material was found to have larger, lower aspect-ratio rubber domains in the steel molded samples. This is likely due to the "freezing" of the highly elongated rubber during fountain flow on the more quickly cooled aluminum molded samples, while the rubber in the more slowly cooled steel molded is able to relax. This difference was not seen in the compounded material, likely due to the faster nucleation rates from the talc present in that

formulation that was not present in the reactor grade. This small variation in surface morphology did not have a measureable effect on the adhesion behavior of the reactor-grade TPO using either cross-hatch adhesion technique or the qualitative interfacial shear strength measurement technique.

The effect of processing conditions on surface morphology and adhesion of electroplated ABS was studied in Chapter 4. Because the adhesion of the metalized layer is dependent on the shape and distribution of the rubber at the surface that is etched out, this system is much more sensitive to surface morphology than chemically bonded systems, such as painted TPO. The shape of the rubber at the surface was optimized for adhesion when the surface stress was the lowest, with processing conditions that used a high melt temperature and low injection speed. Samples generated with high surface stress had elongated rubber that did not provide a good "lock and key" effect for mechanical adhesion. The surface also etched at a faster rate than lower surface stress samples, leaving less of the matrix intact.

The contribution of the surface morphology to the adhesion of electroplated ABS materials must also be balanced by the effect of bulk molded-in stress. There is a high mismatch in thermal expansion and mechanical properties between the polymer and metalized layers, and relief of excess molded-in stress during thermal cycling or impact events has been demonstrated to cause adhesion loss. Our findings, that colder melt temperatures and faster injection speeds minimized bulk molded-in stress correlated with that of previous authors, though it is seemingly counter-intuitive. It has been theorized that this could be due to the faster injection speeds raising the temperature of the melt to allow bulk relaxation (Siegmann, 1982; Chiu, 1987; Pham, 1993). It could also be due to better packing and more isothermal cooling that occurs in the more quickly injected parts.

The major conclusion for metal plated ABS systems is that the material formulation and the processing conditions play a large role in adhesion, and the effects must be understood to assure good performance. The evaluation of both surface and bulk stress as outlined in Chapter 4 lays the foundation for the improvement of future designs and provides guidelines for understanding various failure mechanisms and how to resolve them.

This thesis establishes a protocol for examining the effect of injection molding processing conditions and mold materials on a variety of semi-crystalline and amorphous polymers. Multiple techniques were developed and used to evaluate the surface morphology and chemistry, bulk and surface stress, and the interactions of those factors with adhesion and mechanical properties. For example, optical microscopy was found to be most informative method to determine the morphology of neat polypropylene, while the two TPO formulations required AFM, and the three ABS formulations were best studied with SEM. Correlations between the morphology and adhesion performance, mechanical properties and molded-in stress that were determined in this thesis can be used in the future to optimize material formulations and processing conditions for given applications, as well as improve upon current modeling predictions for the shrink and mechanical behavior of injection modeled polymers. Surface chemistry, as studied with XPS, was found to be very dependent on material composition as well as processing conditions. It was found that additives, which make up a very small fraction of the bulk, can be concentrated preferentially on the surface, depending on formulation, processing conditions and mold material. This finding could be used in the future to create "designer" surfaces, affecting a multitude of surface-sensitive properties such as adhesion, conductivity, scratch and mar, chemical/environmental sensitivity and gloss. Following the protocols and methodologies developed in this thesis can improve the quality of injection molded parts and performance, and help implement new designs more quickly and cost effectively.

5.1 References

Bank, D., D. Klafhen, et al. (2008). "Why Plastic Flows Better in Aluminum Injection Molds." from http://www.alcoa.com/mold/en/pdf/spiral_report.pdf.

Chiu, C. P. and M. C. Hsieh (1987). "The Correlation Between the Residual Stresses of ABS Terpolymers and Injection Molding Conditions." J. Eng. Mater. and Technol. **109**(2): 171-175.

Fujiyama, M. and T. Wakino (1991). "Crystal orientation in injection molding of talc-filled polypropylene." Journal of Applied Polymer Science **42**(1): 9-20.

Janeschitz-Kriegl, H. and E. Ratajski (2005). "Kinetics of polymer crystallization under processing conditions: transformation of dormant nuclei by the action of flow." Polymer **46**(11): 3856-3870.

Karger-Kocsis, J. and K. Friedrich (1989). "Effect of skin-core morphology on fatigue crack propagation in injection moulded polypropylene homopolymer." International Journal of Fatigue **11**(3): 161-168.

Karger-Kocsis, J., A. Kallo, et al. (1979). "Morphological study on the effect of elastomeric impact modifiers in polypropylene systems." Polymer **20**(1): 37-43.

Kornfield, J. A., G. Kumaraswamy, et al. (2002). "Recent Advances in Understanding Flow Effects on Polymer Crystallization." Ind. Eng. Chem. Res. **41**(25): 6383-6392.

Kumaraswamy, G., A. M. Issaian, et al. (1999). "Shear-Enhanced Crystallization in Isotactic Polypropylene. 1. Correspondence between in Situ Rheo-Optics and ex Situ Structure Determination." Macromolecules **32**(22): 7537-7547.

Kumaraswamy, G., J. A. Kornfield, et al. (2002). "Shear-Enhanced Crystallization in Isotactic Polypropylene. 3. Evidence for a Kinetic Pathway to Nucleation." Macromolecules **35**(5): 1762-1769.

Kumaraswamy, G., R. K. Verma, et al. (2000). "Shear-enhanced crystallization in isotactic polypropylenePart 2. Analysis of the formation of the oriented “skin&rdquo." Polymer **41**(25): 8931-8940.

Miel, R. (2009, April 29, 2009). "Honda hits gold with aluminum molds " Plastics News, from http://plasticsnews.com/toolbox/printer.html?id=1240847756.

Miel, R. (2009, April 29, 2009). "Metal's Monetary Magnetism." Plastics News, from http://plasticsnews.com/toolbox/printer.html?id=1240847951.

Nylund, C. and K. Meinander (2005). "The influence of heat transfer coefficient on cooling time in injection molding." Heat and Mass Transfer **41**(5): 428-431.

Pham, H. T., C. P. Bosnyak, et al. (1993). "Residual stresses in injection molded polycarbonate rectangular bars." Polymer Engineering & Science **33**(24): 1634-1643.

Phillips, R., G. Herbert, et al. (1994). "High modulus polypropylene: Effect of polymer and processing variables on morphology and properties." Polymer Engineering & Science **34**(23): 1731-1743.

Ryntz, R. A. (2005). "Attaining Durable Painted Plastic Components." JCT Research **2**(5): 351-360.

Schrauwen, B., L. Breemen, et al. (2004). "Structure, Deformation, and Failure of Flow-Oriented Semicrystalline Polymers." Macromolecules **37**(23): 8618-8633.

Siegmann, A., A. Buchman, et al. (1982). "Residual stresses in polymers III: The influence of injection-molding process conditions." Polymer Engineering & Science **22**(9): 560-568.

Stelson, K. (2003). "Calculating cooling times for polymer injection moulding." Proceedings of the Institution of Mechanical Engineers, Part B: Journal of Engineering Manufacture **217**(5): 709-713.

Velasco, J.I., J.A.D. Saja, et al. (1996). "Crystallization behavior of polypropylene filled with surface-modified talc." Journal of Applied Polymer Science **61**(1): 125-132.

Zhang, X., W. Hendro, et al. (2002). "Measurements of the Thermal Conductivity and Thermal Diffusivity of Polymer Melts with the Short-Hot-Wire Method." International Journal of Thermophysics **23**(4): 1077-1090.

Zironi, C. (2005). "Competitive Advantages of Aluminum Molds for Injection Molding Applications: Process Simulation Used to Evaluate Cycle Times." Flowfront Magazine, April 2005, from http://www.flowfront.com/1004/articles/articles_ff08_0405/design2.htm.